Odd Transport Phenomena in Active Matter

by

Cory M. Hargus

A dissertation submitted in partial satisfaction of the

requirements for the degree of

Doctor of Philosophy

in

Chemical Engineering

in the

Graduate Division

of the

University of California, Berkeley

Committee in charge:

Professor Kranthi K. Mandadapu, Chair
Professor Clayton J. Radke
Professor David T. Limmer

Fall 2022

Odd Transport Phenomena in Active Matter

Abstract

Odd Transport Phenomena in Active Matter

by

Cory M. Hargus

Doctor of Philosophy in Chemical Engineering

University of California, Berkeley

Professor Kranthi K. Mandadapu, Chair

The familiar macroscopic properties of matter emerge out of complex dynamics occurring at the molecular scale. Establishing this connection between microscopic and macroscopic behaviors is the principal task of statistical mechanics. But collective phenomena can emerge out of individual motion and interactions in a much broader class of systems than those with which statistical mechanics has traditionally been concerned, including systems composed of particles that move under their own power by consuming energy from their environment. Known as active matter, such systems can exhibit novel phase and transport behavior with both surprising similarities and striking differences compared to ordinary matter. In this dissertation, I present contributions to the development of a revised statistical mechanical framework describing the emergence of linear transport phenomena in active matter. In particular, odd transport phenomena, in which fluxes arise in the direction perpendicular to thermodynamic driving forces, are shown to be a consequence of chirality in the microscopic fluctuations, characterized by the breaking of time-reversal and parity symmetries. The main results presented in this dissertation consist of the derivations of Green-Kubo relations connecting microscopic symmetries to macroscopic odd transport, together with numerical validation of these relations through molecular dynamics simulations of active model systems. Through this lens, odd diffusion and odd viscosity are introduced and developed. I conclude by presenting a general framework for deriving Green-Kubo relations for odd transport coefficients in active matter. Taken as a whole, these results provide a fruitful extension of existing statistical mechanics concepts, facilitating an understanding of the microscopic origins of odd transport phenomena and indicating the physical contexts in which new types of odd transport can be expected.

To the memory of my grandfather, Louis Kingma.

Contents

List of Figures

List of Tables

Acknowledgments

It is with tremendous gratitude and tenderness that I reflect on my time at Berkeley, and the many people who have made it so meaningful. I arrived in 2018 with only a vague sense of my own research interests, but I was quickly drawn in by Kranthi Mandadapu's ferocious intellectual energy, and his gusto for a good debate. Kranthi has challenged me to become an independent researcher, while backing me up when I most needed it. I'm grateful for everything I've learned from him, both scientifically and personally. I also thank the other members of my committee — David Limmer, Clay Radke, and Carlo Carraro — who have all provided keen insights at critical moments in my research trajectory.

I wouldn't have ended up in Kranthi's group if it hadn't been for the encouragement of Katie Klymko. More than a collaborator, she has been a friend and an unpaceable running buddy from the beginning. Jeff Epstein got me interested in the topic of odd transport, and changed how I think about the epistomology of science by asking bizarrely incisive questions like "what does 'what does quantum information mean?' mean?" I've been very fortunate to work with Vida Jamali, who has been a brilliant, energetic, and empathetic collaborator. Many thanks to Yannick Omar, Zach Lipel, Alison Lui, Ahmad Alkadri, Alhad Deshpande, and Joshua Fernandes for making Gilman 2 feel less like a basement and more like a home. I've benefited greatly from the experience and friendship of Clay Batton, Amaresh Sahu, Dimitrios Fraggedakis, Joel Tchoufag, Kara Fong, and in particular Muhammad Hasyim, who always manages to put everyone in a good mood.

My deepest gratitude goes to Ahmad Omar, from whom I have learned a great deal about soft matter, and still more about matters of the heart. It was through chatting about active matter that I got to know Ahmad, but over time he has become one of my closest friends. I would also like to express my gratitude to Adrianne Zhong, Benjamin Kuznets-Speck, Nivedina Sarma, and the rest of the rotating cast of the non-equilibrium journal club for many fun and free-ranging conversations, and especially to Adri for being a source of inspiration and connection on topics ranging from optimal control theory to Brazilian tropicalia. Special thanks to Helen Bergstrom, Adrian Davey, Jeremy Adams, and Anthony Abel for leading a truly transformational seminar, where we held up a radical lens to our own pedagogies, scientific practices and epistemological systems. I'd like to recognize the hard work of Dustin Wallace, JohnMatthew Garcia, and Conan Minihan, who I had the pleasure of working with through the Berkeley Underground Scholars and NavCal programs.

As I get older, I find myself more and more appreciative of my incredible siblings. My sister Kelley moved to the Bay Area just months after I did, and has been a kindhearted companion through many highs and lows. My younger brother Connor is an inspiration for how he walks off the beaten path with such deliberateness and calm confidence. And my older brother Kyle has been my role model all my life, and is still one of the most sincere and culturally literate people I know. My dad, Brian, has always been my partner, and it's from him that I learned to value curiosity and kindness. And of course so much of who I am comes from my mom, Sheri, whose avid work ethic is tempered by an equal devotion to mindfulness.

I couldn't have asked for better podmates than Fiona McBride, Helen Bergstrom, and Oded Ritov with whom to weather the most frightening and disruptive early stages of the pandemic. My time in the Bay Area has been made immeasurably sweeter by the presence of friends like Jared Moffat, Rebecca McGoldrick, Tito Rinaldo, Allegra Chen-Carrel, David Wood, Allison Eckert, Andy Horng, Ethan Richman, Rob and Lara Crystal-Ornelas, Yasmine Azzaoui, Lindsay Sovern, Dipti Jasrasaria, Will Burton, Will Poole, Alois Cerbu, and Ayah Hassan. Finally, it is the immense love, care, and friendship I've shared with Ana Cecilia Alvarez that have truly defined this period of my life. To Ana, for everything we have been and become together, I owe more gratitude than I can name.

As I write this, I am sitting at my desk in Oakland. The brilliant red leaves of the Japanese maple outside my window are catching the morning light, while oxalis sprouts insistently from the moist earth below. The rainy season is finally here; that dizzy time of year in the Bay Area when fall and spring seem to happen at once. It's difficult to say goodbye to a place and a time that has given me so much meaning. As new chapters open, I'll be carrying this one deep within my heart.

Chapter 1

Introduction

> *. . . it will be shown that according to the molecular-kinetic theory of heat, bodies of microscopically-visible size suspended in a liquid will perform movements of such magnitude that they can be easily observed in a microscope, on account of the molecular motions of heat. It is possible that the movements to be discussed here are identical with the so-called "Brownian molecular motion"; however, the information available to me regarding the latter is so lacking in precision, that I can form no judgment in the matter.*
>
> – Albert Einstein [1, 2]

Linear transport phenomena are behind many everyday occurrences. Indeed, over breakfast one might contemplate the diffusion of tea into hot water, the flow of heat from hot to cold, and the resistance of a fluid to being stirred. Mathematicians such as Isaac Newton, Joseph Fourier, and Adolf Fick developed an empirical framework describing these phenomena centuries before they were discovered to arise as a consequence of random fluctuations occurring on the molecular scale. It was Albert Einstein who, at the beginning of the twentieth century, first made the connection between random Brownian motion of individual solute particles and diffusion from high to low concentration in a solution.

Until that point, Brownian motion — which had been observed microscopically for tiny particles of pollen or other substances immersed in a fluid — was regarded as somewhat of a curiosity. But as Einstein realized, Brownian motion was in fact a manifestation of a deep and non-intuitive truth; namely, that heat is a macroscopic expression of random microscopic motion. The quotation that opens this chapter, taken from Einstein's dissertation, shows the extent to which his theory of diffusion (which would be validated a few years later by the experiments of Jean Perrin) was based much more on physical reasoning than on the availability of reliable accounts of Brownian motion.

Einstein's results proved definitively that matter is made up of atoms, and even provided an estimate of their size. But his work on diffusion also contained the seed of a concept that would become central to the emerging field of non-equilibrium statistical mechanics: not only do atoms continue to move even in equilibrium systems, which appear macroscopically

to be at rest, but in fact this random equilibrium motion *precisely* encodes the response of the system to perturbations out of equilibrium.

From the macroscopic perspective of Newton, Fourier, and Fick, there is no fundamental reason why quantities like momentum, heat, and mass should only flow parallel to gradients (in velocity, temperature, and concentration, respectively) and not also in the perpendicular direction. Yet, as the study of transport phenomena developed, such perpendicular flows were never observed, except as a consequence of material anisotropy, for instance when examining dispersion in porous media. In such anisotropic cases, the perpendicular flow is driven by off-diagonal but symmetric elements of the tensor of transport coefficients (the viscosity, thermal conductivity, and diffusivity, respectively). But these elements can always be made to vanish by rotating the reference frame into the eigenbasis of the transport tensor. In contrast, an antisymmetric (or "odd") component of the transport tensor would always drive perpendicular flows, regardless of orientation.

Most likely no one was bothered that such nonvanishing perpendicular flows hadn't been observed; why worry about something that seemed not to exist? Nonetheless, an explanation arrived in 1931 when Lars Onsager, building on the work of Einstein and others [1–4], proved his famous reciprocal relations [5, 6]. These relations showed that certain macroscopic transport symmetries arise as a direct consequence of time-reversal symmetry of the underlying microscopic dynamics; in other words, the fact that at equilibrium these dynamics appear equally probable when reversed. Onsager's results proved that for perpendicular flows to exist, quantities which are ordinarily even under time reversal would have to somehow become odd. These perpendicular flows earn the appropriate name *odd transport phenomena*, and their connection to microscopic time-reversal symmetry will be a major theme of this dissertation.

In ordinary matter, made up of atoms and molecules that move and interact subject to energy-conserving dynamics, odd transport phenomena can in fact be observed, but only in limited contexts, often involving charged particles moving through a magnetic field, as in the Hall effect [7–9]. But in recent decades, a broader class of systems termed "active matter" has attracted increasing attention. Active matter refers to systems composed of particles which consume and dissipate energy to propel themselves through their environment. These systems of particles can be biological, such as networks of molecular motors [10–12], colonies of bacteria [13–15], and even flocks social animals such as birds, fish and sheep [16, 17], or they can be synthetic, consisting for example of self-propelled colloidal particles [18–22] or vibrated granular materials [23, 24]. Despite the enormous range of lengthscales and timescales spanned by such systems, they exhibit many of the same emergent phenomena as ordinary matter, with phase transitions providing a noteworthy example [25, 26]. And, of greatest significance for this dissertation, self-propulsive forces allow active matter to break time-reversal symmetry, and thus to exhibit a rich array of odd transport behaviors, many of which are at this time only just beginning to be investigated [27–46].

But although active matter can exhibit odd transport phenomena, Onsager's arguments connecting microscopic time-reversal symmetry to macroscopic transport symmetries are no longer sufficient. The transport behavior of ordinary matter driven out of equilibrium

from the boundaries is well-understood within the framework of linear irreversible thermodynamics [47–49]. No such unifying framework exists, however, for active matter. Moreover, Onsager obtained his reciprocal relations through the assumption that microscopic fluctuations on average relax towards steady state according to the macroscopic transport equations. This is known as Onsager's regression hypothesis. Due to the perpendicular nature of odd transport, however, they do not contribute to the bulk relaxation, and thus are invisible from the perspective of the regression hypothesis. Nonetheless, in the following chapters it will be shown that certain core ideas from Onsager's theory can still be used to forge a rigorous connection between microscopic fluctuations and macroscopic transport in active matter. This connection takes the form of Green-Kubo relations, which will be shown to provide both an understanding of the symmetry properties analogous to Onsager's reciprocal relations, as well as a quantitative means of predicting transport coefficients from steady-state fluctuations, which can be verified in numerical simulations of model active matter systems.

Broadly speaking, there exist two categories of transport phenomena. In the first category, transport is driven by a mechanical perturbation coupling directly to the microscopic dynamics. An example is the mobility of particles relative to their surrounding medium in response to an imposed external field. Mechanical transport coefficients are encoded in the statistics of microscopic fluctuations by fluctuation-dissipation relations, a major result of linear response theory [50, 51] More recently, such relations have been derived and verified even for inherently non-equilibrium systems such as active matter [40, 52–58]. In the second category, transport is driven by spatial inhomogeneities established through the boundary conditions, while the microscopic dynamics remain unperturbed. An example is the diffusion of particles in response to concentration gradients. As described above, such boundary-driven (or "thermal") transport coefficients are encoded in microscopic fluctuations by Green-Kubo relations.

In the standard context of systems perturbed away from equilibrium, a third type of connection exists between boundary-driven transport coefficients and corresponding mechanical transport coefficients. These are known as Einstein relations, and emerge as a requirement of linear response theory. Indeed, the relationship between mobility and diffusivity was a central result in Einstein's work on diffusion. Thus for equilibrium systems there exists a tripartite structure between (A) the microscopic fluctuations, (B) the response to mechanical perturbations from equilibrium, and (C) the response to boundary-driven perturbations from equilibrium. Namely, (A) is connected by (B) by linear response relations, (A) is connected to (C) by Green-Kubo relations, and (B) is connected to (C) by Einstein relations. However, as will be demonstrated in the next chapter, though the first two connections can be established independently even in inherently non-equilibrium systems such as active matter, the third — that is, the Einstein relations — need not exist in such systems except under special circumstances.

In Chapter 2, I introduce the concept of odd diffusivity, which generates diffusive fluxes perpendicular to concentration gradients, and derive Green-Kubo relations connecting the odd diffusivity to microscopic chiral random motion. This derivation follows that of Einstein, in the sense that the complete macroscopic diffusion equations are obtained by considering

the random motion of a single particle, and the Green-Kubo relations emerge in the process. Chapter 3 contains a molecular dynamics study of odd viscosity, which couples shear flow to normal stresses, in a model chiral active fluid. Green-Kubo relations are presented and verified through comparison to independent simulations of the same model fluid sheared from the boundaries. Finally, in Chapter 4 I develop a general derivation for Green-Kubo relations in odd active systems, leading to reciprocal relations paralleling those of Onsager and revealing more broadly the role of time-reversal symmetry breaking in odd transport.

Chapter 2

Odd Diffusion

Eadem mutata resurgo.
– inscription on Jakob Bernoulli's tombstone

2.1 Introduction

Dilute diffusion represents perhaps the simplest context for odd transport, because the macroscopic fluxes and gradients depend only on the dynamics of a single particle. In this chapter, we introduce the concept of odd diffusion, illustrating the connection between chiral random motion of individual particles and the macroscopic emergence of fluxes perpendicular to concentration gradients. In two-dimensional active matter, chiral random motion can arise in a number of ways, for instance through self-propulsion of a particle with a steering bias or through collisions of a passive particle with active spinners. Chiral active matter may be synthetic, as in the case of active colloids [28, 59–61], or biological, as in the case of certain bacteria, algae, and spermatozoa [62–64]. Drawing from previous work published as *Phys. Rev. Lett.* 127(17), 178001 (2021), we show in this chapter that odd diffusion is a general feature of chiral active matter.

In dilute solutions, Fick's law posits the linear constitutive relation

$$\boldsymbol{J} = -\mathbf{D} \cdot \boldsymbol{\nabla} C \tag{2.1}$$

between the diffusive flux $\boldsymbol{J}$ and the concentration gradient $\boldsymbol{\nabla} C$, with $\mathbf{D}$ being a rank-two diffusivity tensor. In general $\mathbf{D}$ may contain both a symmetric and antisymmetric part. We term the latter the odd diffusivity, and will show it to emerge as a consequence of breaking time-reversal and parity symmetries at the level of microscopic fluctuations.

For simplicity, we examine odd diffusivity in two-dimensional isotropic systems. Physically, this could correspond to diffusion on a surface or, for example, in the xy-plane of a three-dimensional space, where isotropy maintained in that but broken along the z-axis. In

such contexts, the diffusivity tensor takes the form

$$D_{ij} = D_{\parallel}\delta_{ij} - D_{\perp}\epsilon_{ij} = \begin{bmatrix} D_{\parallel} & -D_{\perp} \\ D_{\perp} & D_{\parallel} \end{bmatrix} . \tag{2.2}$$

Here, $\delta_{ij} = \delta_{ji}$ is the symmetric Kronecker delta and $\epsilon_{ij} = -\epsilon_{ji}$ is the antisymmetric Levi-Civita permutation tensor. $D_{\parallel}$ is the ordinary isotropic diffusivity coefficient driving flux from regions of high to low concentration while $D_{\perp}$ is the odd diffusivity driving flux in the perpendicular direction (as in Figure 2.1a). Combining (4.29) and (4.39) with the continuity equation $\partial_t C = -\boldsymbol{\nabla} \cdot \boldsymbol{J}$ yields the diffusion equation

$$\partial_t C = D_{\parallel}\nabla^2 C \,, \tag{2.3}$$

which is unaffected by the divergence-free fluxes produced by $D_{\perp}$. Thus, while $D_{\perp}$ may influence C in the presence of boundary conditions involving fluxes (*e.g.* impermeable obstacles, see Appendix A), $D_{\perp}$ cannot affect C for boundary conditions involving solely the concentration.

Past studies of odd diffusivity have generally been limited to equilibrium systems, most commonly systems of charged particles in magnetic fields. Such systems acquire an antisymmetric component of both the diffusivity tensor and the mobility tensor, which describes the current response to an electric field. This is the basis of the Hall effect, and has consequences for the transport of confined plasmas and cosmic rays [7, 8, 65–70]. Odd diffusivity has also been recognized in certain mathematical models of chiral random walks [71, 72], and in convection-diffusion processes in chiral porous media [73].

In this chapter we suggest a unifying framework within which to understand these phenomena, which extends beyond equilibrium. We begin by asking: given that the existence of odd diffusivity is compatible with the macroscopic theory of diffusion, what microscopic conditions are necessary for it to appear? Through deriving a Green-Kubo relation for the odd diffusivity, we will show that it emerges in systems breaking time-reversal and parity symmetries, as characterized by chiral random motion of particle trajectories. Odd diffusivity is thus characteristic of a broad range of diffusive processes, and of particular interest for out-of-equilibrium systems such as chiral active matter, where time-reversal symmetry can be broken by microscopic driving forces. We validate the derived Green-Kubo relations exactly for a model chiral random walk and numerically in active matter simulations, demonstrating good agreement with direct measurements of the flux in response to an imposed concentration gradient.

2.2 Green-Kubo relations

We now proceed to obtain Green-Kubo relations for D_{ij}. We follow an approach similar in spirit to the celebrated work of Einstein, Smoluchowski and others [1, 3], which connected molecular-scale Brownian motion with the macroscopic diffusion equation (2.3), and we will

rely on similar arguments about the separation of timescales. However, because the odd diffusivity $D_\perp$ does not contribute to equation (2.3), such an approach can yield no information about $D_\perp$. The same is true when taking as a starting point the Onsager regression hypothesis [5, 6, 74], itself formulated upon equation (2.3), as will be discussed in the following chapters. Accordingly, rather than considering the time evolution of the concentration *via* the diffusion equation (2.3), we will instead directly examine the microscopic basis of the fluxes appearing in the constitutive law (4.29), similar to the route taken in linear response theory [51]. In doing so, however, we will not require any linear response relation between the diffusivity and the mobility.

We begin by considering a dilute solution of particles undergoing random motion, *e.g.* due to collisions with a solvent bath. Let $f(\boldsymbol{r},\boldsymbol{v},t)$ indicate the probability density of finding a particle at position $\boldsymbol{r}$ with velocity $\boldsymbol{v}$ at time t. The local, instantaneous flux $\boldsymbol{J}(\boldsymbol{r},t)$ is then defined as

$$\boldsymbol{J}(\boldsymbol{r},t) = \int d\boldsymbol{v}\ f(\boldsymbol{r},\boldsymbol{v},t)\boldsymbol{v}\,. \tag{2.4}$$

Let us now consider the subensemble of all single-particle trajectories compatible with the conditions $\boldsymbol{r}^\alpha(t)=\boldsymbol{r}$ and $\boldsymbol{v}^\alpha(t)=\boldsymbol{v}$, where α is an index over trajectories. As particles cannot be created or destroyed, continuity requires that

$$f(\boldsymbol{r},\boldsymbol{v},t) = \big\langle f\big(\boldsymbol{r}^\alpha(t-\tau),\boldsymbol{v}^\alpha(t-\tau),t-\tau\big)\big\rangle_{\substack{\boldsymbol{r}^\alpha(t)=\boldsymbol{r}\\ \boldsymbol{v}^\alpha(t)=\boldsymbol{v}}}\,, \tag{2.5}$$

where $\big\langle\,\cdot\,\big\rangle_{\substack{\boldsymbol{r}^\alpha(t)=\boldsymbol{r}\\ \boldsymbol{v}^\alpha(t)=\boldsymbol{v}}}$ denotes an average over all trajectories leading into point $\boldsymbol{r}$ with velocity $\boldsymbol{v}$ at time t. Equation (2.5) is a restatement in trajectory-ensemble notation of the standard Chapman-Kolmogorov equation $f(\boldsymbol{r},\boldsymbol{v},t) = \iint d\boldsymbol{r}'d\boldsymbol{v}'\Pi(\boldsymbol{r},\boldsymbol{v},t|\boldsymbol{r}',\boldsymbol{v}',t-\tau)f(\boldsymbol{r}',\boldsymbol{v}',t-\tau)$, where $\Pi(\boldsymbol{r},\boldsymbol{v},t|\boldsymbol{r}',\boldsymbol{v}',t-\tau)$ indicates the transition probability density of the particle arriving at the (r,v) at time t given that it was previously in the state $(\boldsymbol{r}',\boldsymbol{v}')$ at time $t-\tau$.

Suppose there exists a correlation timescale τ_c, such that for $\tau \gg \tau_c$ a particle's velocity $\boldsymbol{v}^\alpha(t)$ is uncorrelated with its earlier value $\boldsymbol{v}^\alpha(t-\tau)$ and thus becomes distributed according to the unconditional probability density function $\phi(\boldsymbol{v})$, which we assume to be independent of t (stationary) and $\boldsymbol{r}$ (translationally invariant). Then, for $\tau \gg \tau_c$, equation (2.5) factorizes to

$$f(\boldsymbol{r},\boldsymbol{v},t) = \phi(\boldsymbol{v})\langle C\big(\boldsymbol{r}^\alpha(t-\tau),t-\tau\big)\rangle_{\substack{\boldsymbol{r}^\alpha(t)=\boldsymbol{r}\\ \boldsymbol{v}^\alpha(t)=\boldsymbol{v}}}\,, \tag{2.6}$$

where the concentration $C(\boldsymbol{r},t) = \int d\boldsymbol{v}\ f(\boldsymbol{r},\boldsymbol{v},t)$.

Let the timescale over which the system relaxes from a state of nonuniform concentration be denoted τ_r, *e.g.* $\tau_r \approx L^2/D_\parallel$, for the macroscopic length L describing the variation in $C(\boldsymbol{r},t)$. We now assume that τ may be chosen to satisfy the separation of timescales

$$\tau_c \ll \tau \ll \tau_r\,, \tag{2.7}$$

following Einstein, Smoluchowski, Kubo and others [1, 3, 30, 74, 75]. With these assumptions, the subensemble-averaged concentration appearing in equation (2.6) may be approxi-

mated by expanding about $\boldsymbol{r}$ to first order and about t to zeroth order

$$\begin{aligned}&\left\langle C\big(\boldsymbol{r}^\alpha(t-\tau),t-\tau\big)\right\rangle_{\substack{\boldsymbol{r}^\alpha(t)=\boldsymbol{r}\\ \boldsymbol{v}^\alpha(t)=\boldsymbol{v}}}\\ &\approx C(\boldsymbol{r},t)+\big\langle \boldsymbol{r}^\alpha(t-\tau)-\boldsymbol{r}^\alpha(t)\big\rangle_{\substack{\boldsymbol{r}^\alpha(t)=\boldsymbol{r}\\ \boldsymbol{v}^\alpha(t)=\boldsymbol{v}}}\cdot\boldsymbol{\nabla}C(\boldsymbol{r},t)\,.\end{aligned} \tag{2.8}$$

Noting the relationship between a particle's displacement and its velocity

$$\boldsymbol{r}^\alpha(t-\tau)-\boldsymbol{r}^\alpha(t)=-\int_0^\tau dt'\ \boldsymbol{v}^\alpha(t-t') \tag{2.9}$$

and inserting the results of equations (2.6)-(2.9) into equation (2.4) yields

$$\begin{aligned}\boldsymbol{J}(\boldsymbol{r},t)&=\int d\boldsymbol{v}\ \phi(\boldsymbol{v})\boldsymbol{v}\ \times\\ &\quad\left[C(\boldsymbol{r},t)-\int_0^\tau dt'\ \big\langle\boldsymbol{v}^\alpha(t-t')\big\rangle_{\substack{\boldsymbol{r}^\alpha(t)=\boldsymbol{r}\\ \boldsymbol{v}^\alpha(t)=\boldsymbol{v}}}\cdot\boldsymbol{\nabla}C(\boldsymbol{r},t)\right]\\ &=-\int_0^\tau dt'\ \langle\boldsymbol{v}(t)\otimes\boldsymbol{v}(t-t')\rangle\cdot\boldsymbol{\nabla}C(\boldsymbol{r},t)\,,\end{aligned} \tag{2.10}$$

with $\otimes$ indicating the dyadic product. The convective term proportional to $C(\boldsymbol{r},t)$ vanishes under the assumption that $\phi(\boldsymbol{v})$ is unbiased, *i.e.* $\int d\boldsymbol{v}\,\phi(\boldsymbol{v})\boldsymbol{v}=0$. The second equality in (2.10) follows from the definition of the conditional expectation. The condition $\boldsymbol{r}^\alpha(t)=\boldsymbol{r}$ has been dropped due to the assumption of translational invariance; consequently, the average in the final expression is taken over all trajectories. Comparing with the constitutive relation (4.29), we conclude

$$D_{ij}=\int_0^\tau dt'\ \langle v_i(t)v_j(t-t')\rangle\,. \tag{2.11}$$

Invoking stationarity to set $\langle v_i(t)v_j(t-t')\rangle=\langle v_i(t')v_j(0)\rangle$ and carrying out the limit $\tau\to\infty$ due to the requirement $\tau\gg\tau_c$ yields the Green-Kubo relations

$$D_{ij}=\int_0^\infty dt\ \langle v_i(t)v_j(0)\rangle\,. \tag{2.12}$$

These relations hold independently for each component of the diffusivity tensor, including any antisymmetric part. Considering the specific form of D_{ij} in (4.39), we may contract with δ_{ij} and ϵ_{ij} to obtain

$$\begin{aligned}2D_\parallel&=\int_0^\infty dt\,\langle v_i(t)v_j(0)\rangle\delta_{ij}\\ &=\lim_{t\to\infty}\langle\Delta r_i(t)v_j(0)\rangle\delta_{ij}=\lim_{t\to\infty}\frac{1}{2t}\langle|\boldsymbol{\Delta r}(t)|^2\rangle\,,\end{aligned} \tag{2.13}$$

$$\begin{aligned}2D_\perp&=-\int_0^\infty dt\,\langle v_i(t)v_j(0)\rangle\epsilon_{ij}\\ &=-\lim_{t\to\infty}\langle\Delta r_i(t)v_j(0)\rangle\epsilon_{ij}\,.\end{aligned} \tag{2.14}$$

The first equality in equations (2.13) and (2.14) is of the usual Green-Kubo form [74, 75]. In the second equality the integral has been carried out, permitting a geometric interpretation of the two diffusion coefficients in terms of the position-velocity correlation functions (as in Figure 2.1b). The third equality in (2.13) is the well-known relationship between $D_\parallel$ and the mean squared displacement; note that no such relation exists for $D_\perp$ due to its absence from the diffusion equation (2.3).

The antisymmetric tensor ϵ_{ij} in equation (2.14) projects out the time-reversal-symmetric and even-parity part of the correlation function, indicating that whereas $D_\parallel$ is even under time reversal and parity inversion, $D_\perp$ is odd under both operations. Onsager's reciprocal relations [5, 6] similarly require that transport coefficient tensors be symmetric as a consequence of time-reversal symmetry. It should be noted however that $D_\perp$, being non-dissipative, is not compatible with entropic arguments pertaining to the reciprocal relations, an issue that was previously discussed in a Fokker-Planck context [76, 77]. The Green-Kubo relation (2.14) provides, instead, a direct statement of how time-reversal symmetry should be broken for odd diffusivity to appear.

In equilibrium systems, the diffusivity and the mobility are connected by the Einstein relation. Thus, in such systems, the Green-Kubo relation (2.14) may be shown from linear response theory [51]. The derivation above shows that equation (2.14) can be applied even to inherently nonequilibrium systems such as active matter, where the linear response relations for mobility [54–57] need no longer be interchangeable with the Green-Kubo relations for diffusion *via* an Einstein relation, except under special circumstances [78]. Consequently, odd diffusivity can arise even in cases where the antisymmetric mobility vanishes (as demonstrated in Appendix C for a chiral active Brownian particle), or where mobility has no physical meaning, as in cases of animal navigation with a documented steering bias [79–83].

2.3 Chiral random walk

To illustrate the microscopic origins of $D_\perp$ and $D_\parallel$, consider a particle which moves at a constant speed v_0 and reorients by turning left, reversing direction, or turning right at random intervals with frequency Γ_1, Γ_2 and Γ_3, respectively. Between these changes in direction, the particle moves in a straight line.

We may understand the diffusive behavior of this model by decomposing the probability density $P(x, y, t)$ of the particle sitting at coordinates (x, y) at time t into a sum of joint probabilities associated with the four possible directions of motion: $P(x, y, t) = P_\rightarrow(x, y, t) + P_\uparrow(x, y, t) + P_\leftarrow(x, y, t) + P_\downarrow(x, y, t)$. By considering the continuity of these joint probabilities,

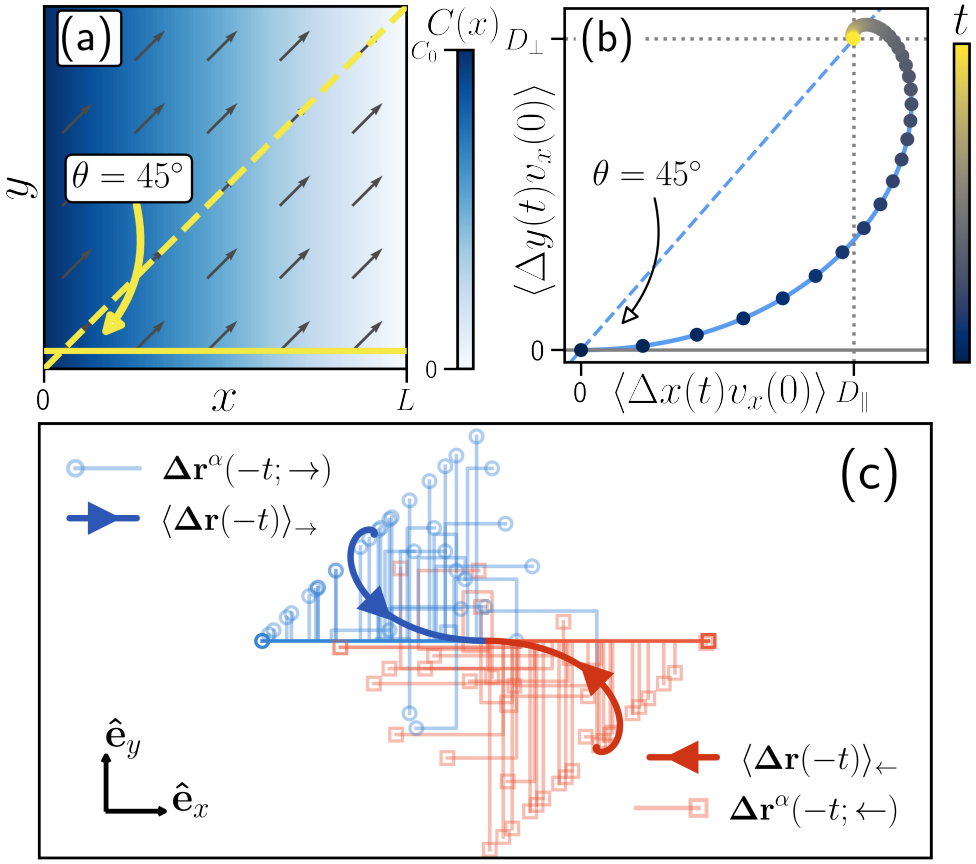

Figure 2.1: Relationship between odd diffusivity and chirality of particle trajectories in a left-turning random walk ($\Gamma_1 = 1, \Gamma_2 = \Gamma_3 = 0$). (a) A linear concentration gradient induces a uniform flux field (arrows) with a perpendicular component due to $D_\perp$. (b) Logarithmic spiral form of the position-velocity correlation functions from equations (2.25)-(2.26). The Green-Kubo relations (2.13)-(2.14) specify that the x- and y-coordinates converge to the two diffusivity coefficients as $t \to \infty$, while the angle θ is identical to that in (a), as annotated. (c) Random sample of 50 time-reversed trajectories $\boldsymbol{\Delta r}^\alpha(-t)$ satisfying either $\boldsymbol{v}^\alpha(0) = v_0 \hat{\boldsymbol{e}}_x$ (indicated by $\rightarrow$) or $\boldsymbol{v}^\alpha(0) = -v_0 \hat{\boldsymbol{e}}_x$ (indicated by $\leftarrow$) for $t \in [0, \Gamma_1^{-1}]$ together with the subensemble-averaged trajectories $\langle \boldsymbol{\Delta r}^\alpha(-t) \rangle_\rightarrow$ and $\langle \boldsymbol{\Delta r}^\alpha(-t) \rangle_\leftarrow$ for $t \in [0, \infty)$.

we arrive at the coupled master equations [84]

$$\partial_t P_\rightarrow = \Gamma_1 P_\downarrow + \Gamma_2 P_\leftarrow + \Gamma_3 P_\uparrow - \gamma P_\rightarrow - v_0 \partial_x P_\rightarrow \,, \tag{2.15}$$

$$\partial_t P_\uparrow = \Gamma_1 P_\rightarrow + \Gamma_2 P_\downarrow + \Gamma_3 P_\leftarrow - \gamma P_\uparrow - v_0 \partial_y P_\uparrow \,, \tag{2.16}$$

$$\partial_t P_\leftarrow = \Gamma_1 P_\uparrow + \Gamma_2 P_\rightarrow + \Gamma_3 P_\downarrow - \gamma P_\leftarrow + v_0 \partial_x P_\leftarrow \,, \tag{2.17}$$

$$\partial_t P_\downarrow = \Gamma_1 P_\leftarrow + \Gamma_2 P_\uparrow + \Gamma_3 P_\rightarrow - \gamma P_\downarrow + v_0 \partial_y P_\downarrow \,, \tag{2.18}$$

where $\gamma = \Gamma_1 + \Gamma_2 + \Gamma_3$. Suppose we are interested in a steady state in which concentration varies only in the x-direction. Then, from equation (2.4), we may define

$$J_x(x) = v_0\langle P_\rightarrow(x) - P_\leftarrow(x)\rangle\,, \tag{2.19}$$
$$J_y(x) = v_0\langle P_\uparrow(x) - P_\downarrow(x)\rangle\,, \tag{2.20}$$

and, upon subtracting equation (2.18) from (2.16) and averaging, obtain

$$\partial_t J_y(x) = 0 = (\Gamma_1 - \Gamma_3)J_x(x) - (\gamma + \Gamma_2)J_y(x)\,. \tag{2.21}$$

Solving for the ratio $J_y(x)/J_x(x)$, we find

$$\frac{J_y(x)}{J_x(x)} = \frac{D_\perp}{D_\parallel} = \frac{\Gamma_1 - \Gamma_3}{\gamma + \Gamma_2}\,. \tag{2.22}$$

Examining this expression we note that $D_\perp \neq 0$ whenever $\Gamma_1 \neq \Gamma_3$, indicating a preference between left and right turns, *i.e.* chirality of random motion.

We now consider the Green-Kubo relation (2.13) for this model. Recognizing that only four velocity states are possible, we expand the correlation functions as

$$\begin{aligned} D_\parallel &= \lim_{t\to\infty} \frac{1}{2}\langle \Delta r_i(t) v_j(0)\rangle \delta_{ij} \\ &= \lim_{t\to\infty} \frac{1}{8} v_0\big[\langle x(t)\rangle_\rightarrow - \langle x(t)\rangle_\leftarrow + \langle y(t)\rangle_\uparrow - \langle y(t)\rangle_\downarrow\big] \\ &= \lim_{t\to\infty} \frac{1}{2} v_0 \langle x(t)\rangle_\rightarrow\,, \end{aligned} \tag{2.23}$$

where $\langle\cdot\rangle_\rightarrow$ indicates an average conditioned on the particle initially moving to the right from the origin. The other terms $\langle\cdot\rangle_\uparrow$, $\langle\cdot\rangle_\leftarrow$ and $\langle\cdot\rangle_\downarrow$ follow the same notational convention. The simplification on the final line is due to isotropy. Likewise, from equation (2.14),

$$D_\perp = \lim_{t\to\infty} \frac{1}{2} v_0 \langle y(t)\rangle_\rightarrow\,. \tag{2.24}$$

The averages are obtained by solving equations (2.15) through (2.18) with the initial condition $P_\rightarrow(x, y, 0) = \delta(x)\delta(y)$ (see Appendix A). In doing so, we find that the mean trajectory is a logarithmic spiral, *i.e.*

$$\langle x(t)\rangle_\rightarrow = v_0 \frac{\nu - e^{-\nu t}\big(\nu\cos(\omega t) + \omega\sin(\omega t)\big)}{\nu^2 + \omega^2} \tag{2.25}$$
$$\langle y(t)\rangle_\rightarrow = v_0 \frac{\omega - e^{-\nu t}\big(\omega\cos(\omega t) - \nu\sin(\omega t)\big)}{\nu^2 + \omega^2} \tag{2.26}$$

where for compactness we have defined $\omega = \Gamma_1 - \Gamma_3$ and $\nu = \Gamma_1 + 2\Gamma_2 + \Gamma_3$. This logarithmic spiral functional form, shown in Figure 2.1b, is remarkably common, appearing in the

mean trajectories of charged particles diffusing in a magnetic field [7, 65, 85, 86], as well as those of chiral active colloids [59, 60] and certain biological systems [80, 87]. Inserting equations (2.25)-(2.26) into (2.23)-(2.24) yields

$$2D_{\parallel} = v_0^2 \frac{\nu}{\nu^2 + \omega^2}\,, \tag{2.27}$$

$$2D_{\perp} = v_0^2 \frac{\omega}{\nu^2 + \omega^2}\,, \tag{2.28}$$

in agreement with equation (2.22), showing the emergence of $D_\perp$ when chirality is present ($\omega \neq 0$).

Figure 2.1 illustrates the origins of odd diffusivity in a chiral random walk which permits only left turns ($\Gamma_1 = 1, \Gamma_2 = \Gamma_3 = 0$), for which $D_\parallel = D_\perp$, from equations (2.27)-(2.28). Figure 2.1a displays the steady-state solution to equations (4.29)-(2.3) for diffusion between two reservoirs with concentrations $C(x{=}0) = C_0$ and $C(x{=}L) = 0$, resulting in a linear concentration profile $C(x) = C_0(1 - x/L)$ and uniform flux $\boldsymbol{J} = \frac{C_0}{L}\left[D_\parallel \hat{\boldsymbol{e}}_x + D_\perp \hat{\boldsymbol{e}}_y\right]$ with a nonzero y-component due to odd diffusivity. In the presence of impermeable boundaries this solution must be modified, with $D_\perp$ affecting not only the flux but also the concentration, as shown in Appendix A. Figure 2.1b plots the position-velocity correlation functions entering into the Green-Kubo relations (2.13) and (2.14). Finally, Figure 2.1c shows a random sample from the subensembles of time-reversed trajectories $\boldsymbol{\Delta r}^\alpha(-t)$ passing through the origin at time $t = 0$ with either $\boldsymbol{v}^\alpha(0) = +v_0\hat{\boldsymbol{e}}_x$ or $\boldsymbol{v}^\alpha(0) = -v_0\hat{\boldsymbol{e}}_x$. Due to chirality, the paths in these two subensembles lead backwards in time to regions differing not only in the x- but also the y-coordinate, so that a gradient in the y-direction generates a flux in the x-direction. This is the microscopic basis of odd diffusivity.

2.4 Diffusion in a chiral active bath

Several recent studies have described novel behavior of the symmetric diffusivity $D_\parallel$ [88–91] as well as an antisymmetric mobility [35, 92–94] in active systems. In this section, we study the odd diffusivity of a passive tracer particle dissolved in a two-dimensional chiral active fluid composed of torqued dumbbells, which was found in previous studies to exhibit odd viscosity and an asymmetric hydrostatic stress [31, 95], as will be discussed further in Chapter 3. The positions $\boldsymbol{r}_i$ and velocities $\boldsymbol{v}_i$ of particle i evolve according to underdamped Langevin dynamics

$$\begin{aligned} \dot{\boldsymbol{r}}_i &= \boldsymbol{v}_i\,, \\ \dot{\boldsymbol{v}}_i &= -\frac{\partial}{\partial \boldsymbol{r}_i} U + \boldsymbol{f}_i^A - \zeta \boldsymbol{v}_i + \boldsymbol{\eta}_i\,, \end{aligned} \tag{2.29}$$

with particle masses set to one. Here, $-\frac{\partial}{\partial \boldsymbol{r}_i} U$ is the conservative force on particle i due to interactions (see Appendix B for model and simulation details). $\boldsymbol{f}_i^A$ is a nonconservative

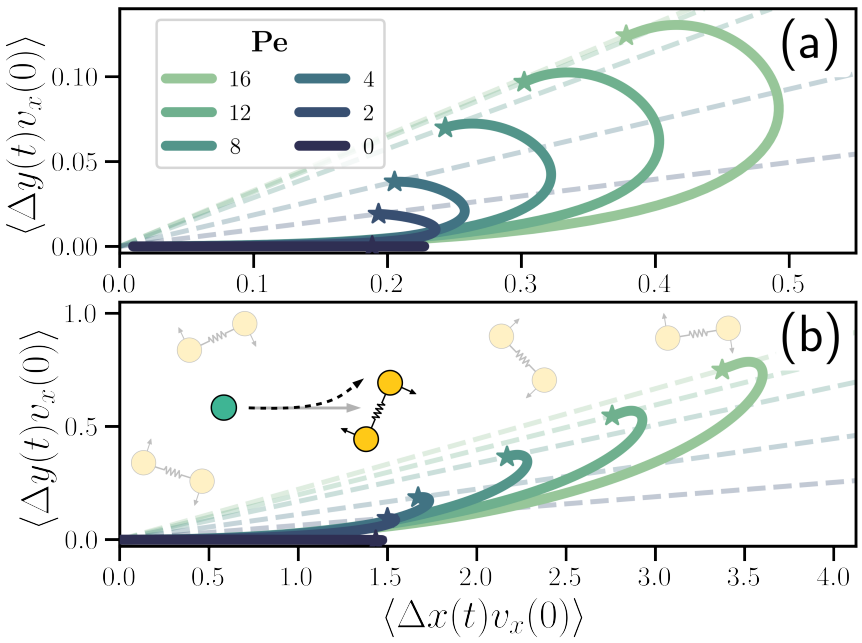

Figure 2.2: Position-velocity correlation functions computed from molecular dynamics simulations of a passive tracer in a chiral active dumbbell bath with density $\rho_{\text{bath}} = 0.4$ (a) and $\rho_{\text{bath}} = 0.1$ (b). Stars mark converged values as $t \to \infty$. Both $D_\perp$ and $D_\parallel$ increase with Pe, as does the ratio $D_\perp / D_\parallel$, as indicated by dashed lines. The inset in (b) depicts the model system.

active force inducing rotation of the dumbbell. ζ is the dissipative bath friction and $\boldsymbol{\eta}_i$ are the bath fluctuations, modeled as Gaussian white noise characterized by $\langle \boldsymbol{\eta}_i \rangle = 0$ and $\langle \boldsymbol{\eta}_i(t) \otimes \boldsymbol{\eta}_j(t') \rangle = 2 k_{\text{B}} T \zeta \delta_{ij} \delta(t - t') \mathbf{I}$, where $k_{\text{B}} T$ is the bath temperature and $\mathbf{I}$ is the identity matrix. In all simulations the density of active dumbbells, ρ_{bath}, is spatially homogeneous. The magnitude of $f^A = |\boldsymbol{f}_i^A|$ relative to thermal fluctuations is quantified by a non-dimensional Péclet number defined as $\text{Pe} = \frac{2 f^A d}{k_{\text{B}} T}$, where d is the equilibrium dumbbell bond length.

Molecular dynamics simulations [96, 97] with fully periodic boundaries allow for the measurement of the position-velocity correlation functions, which are plotted in Figure 2.2. We have taken the convention that $\text{Pe} > 0$ corresponds to clockwise rotation of the dumbbells, which induces counterclockwise motion of the passive tracer, as depicted in the inset of Figure 2.2b. When $\text{Pe} \neq 0$, an antisymmetric part of the correlation function appears, with a shape resembling the logarithmic spirals identified in the chiral random walk model (Figure 2.1b) and magnitude depending strongly on the density of the active dumbbell bath. The resulting Green-Kubo estimates of $D_\perp$ and $D_\parallel$ are plotted in Figures 2.3a and 2.3b for a range of active bath densities, where $D_\perp$ is seen to be an odd function of Pe while $D_\parallel$ is an even function of Pe.

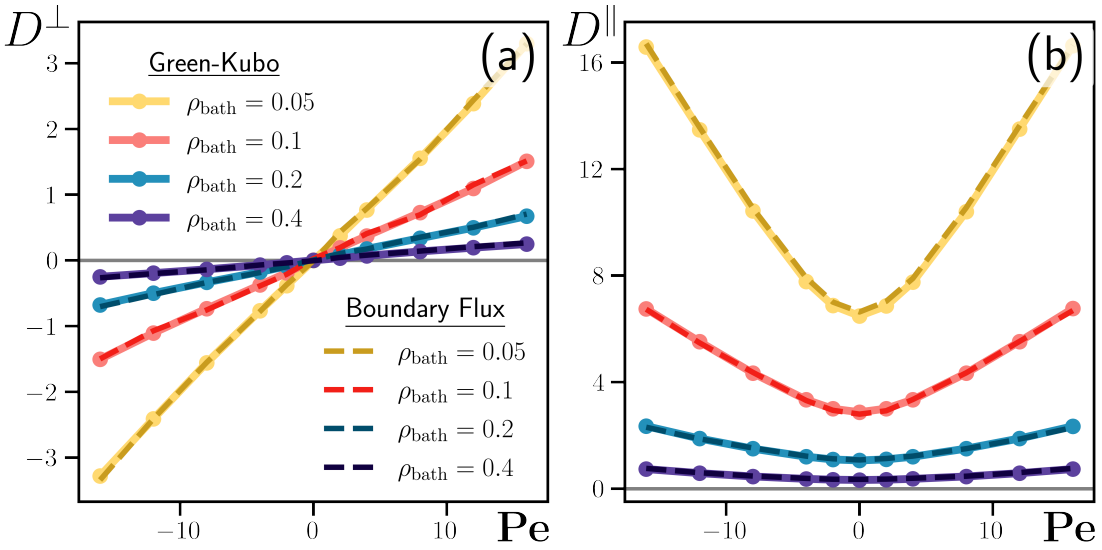

Figure 2.3: Comparison of the diffusion coefficients $D_{\perp}$ (a) and $D_{\parallel}$ (b) computed from the Green-Kubo relations (solid lines) with those measured in boundary-driven flux simulations (dashed lines) for several densities of the active dumbbell bath ρ_{bath} and values of Pe. Error bars are smaller than the symbols.

To validate the Green-Kubo relations, we independently performed boundary-driven flux simulations in which passive tracer particles at high dilution were introduced at the left boundary of the simulation box and removed from the right boundary at a constant rate, while the top and bottom boundaries remained periodic. The resulting steady state exhibits a uniform concentration gradient in the x-direction, and uniform flux with a y-component emerging for $\text{Pe} \neq 0$ (see Appendix B). The diffusion coefficients $D_{\perp}$ and $D_{\parallel}$ were then computed directly from the constitutive relations (4.29) and (4.39). The resulting values are plotted in Figure 2.3 against the Green-Kubo predictions, demonstrating good agreement. We note that this system exhibits an antisymmetric part of the mobility, but with no apparent Einstein relation connecting this quantity to the odd diffusivity (see Appendix C).

2.5 Conclusion

Ordinarily, isotropic diffusion involves fluxes parallel to concentration gradients. In general, however, there may emerge fluxes in the perpendicular direction. This behavior appears as an antisymmetric part of the diffusivity tensor, which we have termed odd diffusivity. From a first-principles consideration of the microscopic basis of the constitutive relations describing these perpendicular fluxes, we have derived a Green-Kubo relation for odd diffusivity, show-

ing it to exist only when time-reversal and parity symmetries are broken, whether in or out of equilibrium. This approach may help to characterize additional odd transport phenomena with divergence-free fluxes, such as odd heat conduction and odd couplings between viscous and diffusive transport.

Chapter 3

Odd Viscosity

I'm an ever rolling wheel, without a destination real
I'm an ever spinning top, whirling around till I drop
– "Going in Circles" by The Friends of Distinction

3.1 Introduction

In Chapter 2, odd diffusion was seen to emerge as a macroscopic consequence of microscopic chiral random motion. In an analogous fashion, this chapter will show that odd viscosity — which couples shear flow to normal stresses and extensive flow to shear stresses — arises in chiral active fluids due to the breaking of time reversal symmetry at the level of stress correlations. This draws from recent work published as *J. Chem. Phys.* 152(20), 201102 (2020), which in turn built on the theoretical analysis of Epstein and Mandadapu [30]. In that investigation, the authors derived a set of Green-Kubo relations through the application of the Onsager regression hypothesis [5, 6, 74] to non-equilibrium steady states characteristic of active matter. In this Chapter, we evaluate these Green-Kubo relations using molecular dynamics simulations of a canonical chiral active fluid composed of microscopically torqued dumbbells, finding the Green-Kubo predictions to be in good agreement with independent measurements form non-equilibrium molecular dynamics (NEMD) flow simulations across a wide range of densities and activities.

3.2 Theory

We begin by reviewing the continuum theory for two-dimensional viscous active fluids with internal spin. This provides the setting for the derivation of Green-Kubo relations for viscosity coefficients in fluids breaking time reversal symmetry. Because the chiral active dumbbell model considered in this chapter is capable of storing angular momentum in the form of internal (*i.e.* molecular) spin, we anticipate possible coupling between a velocity field v_i and a

spin field m. These satisfy balance equations for linear and angular momentum, as proposed by Dahler and Scriven [98]:

$$\rho \dot{v}_i = T_{ij,j} + \rho g_i \,, \tag{3.1}$$
$$\rho \dot{m} = C_{i,i} - \epsilon_{ij} T_{ij} + \rho G \,. \tag{3.2}$$

T_{ij} denotes the stress tensor and C_i the spin flux, which accounts for transfer of internal angular momentum across surfaces. The variables g_i and G denote body forces and body torques, respectively. Finally note that the balance of angular momentum includes a term in which the two-dimensional Levi-Civita tensor ϵ_{ij} is contracted with the stress, so that the antisymmetric component of the stress may be nontrivial. We use the notation $a_{,i} = \partial a / \partial x_i$.

The most general isotropic constitutive equations for viscous fluids relating T_{ij} and C_i to v_i, m and their derivatives up to first order in two-dimensional systems are given by

$$T_{ij} = \eta_{ijkl} v_{k,l} + \gamma_{ij} m - p \delta_{ij} + p^* \epsilon_{ij} \,, \tag{3.3}$$
$$C_i = \alpha_{ij} m_{,j} \,, \tag{3.4}$$

where η_{ijkl}, γ_{ij} and α_{ij} are the viscous transport coefficients [30]. Here, p and p^* are hydrostatic contributions and are not constitutively related to v_i and m. The forms of equations (3.3) and (3.4) follow from a general representation theorem stating that any isotropic tensor can be expressed in a basis consisting of contractions of Kronecker tensors δ_{ij} and Levi-Civita tensors ϵ_{ij} and that, consequently, there exist no isotropic tensors of odd rank in two dimensions. Thus the transport coefficients may be expressed as

$$\eta_{ijkl} = \sum_{n=1}^{6} \lambda_n s^{(n)}_{ijkl} \,, \tag{3.5}$$
$$\gamma_{ij} = \gamma_1 \delta_{ij} + \gamma_2 \epsilon_{ij} \,, \tag{3.6}$$
$$\alpha_{ij} = \alpha_1 \delta_{ij} + \alpha_2 \epsilon_{ij} \,, \tag{3.7}$$

where Table I contains the definitions of tensors $s^{(n)}_{ijkl}$.

The coefficients γ_n and α_n indicate the responses of the stress and spin flux tensors to spin and spin gradients. λ_1 and λ_2 are the typical bulk and shear viscosities. λ_3 is the rotational viscosity indicating resistance to vorticity and giving rise to an anti-symmetric stress, while λ_4 is the so-called odd viscosity quantifying response to shear with a tension or compression in the orthogonal direction. λ_5 and λ_6 correspond to an anti-symmetric pressure from compression and isotropic pressure from vorticity, respectively. Note that nonvanishing λ_3 or λ_6 violates objectivity (independence of stress from vorticity), while nonvanishing λ_3 or λ_5 violates symmetry of the stress tensor.

Using the conservation and constitutive equations (3.1)-(3.2) and (3.5)-(3.7), Epstein and Mandadapu [30] obtained a set of Green-Kubo relations for γ_n and λ_n by invoking the Onsager regression hypothesis and following the procedure of Kubo, Yokota, and Nakajima [74].

Basis Tensor	Components
$\mathbf{s}^{(1)}$	$\delta_{ij}\delta_{kl}$
$\mathbf{s}^{(2)}$	$\delta_{ik}\delta_{jl} - \epsilon_{ik}\epsilon_{jl}$
$\mathbf{s}^{(3)}$	$\epsilon_{ij}\epsilon_{kl}$
$\mathbf{s}^{(4)}$	$\epsilon_{ik}\delta_{jl} + \epsilon_{jl}\delta_{ik}$
$\mathbf{s}^{(5)}$	$\epsilon_{ik}\delta_{jl} - \epsilon_{jl}\delta_{ik} + \epsilon_{ij}\delta_{kl} + \epsilon_{kl}\delta_{ij}$
$\mathbf{s}^{(6)}$	$\epsilon_{ik}\delta_{jl} - \epsilon_{jl}\delta_{ik} - \epsilon_{ij}\delta_{kl} - \epsilon_{kl}\delta_{ij}$

Table 3.1: Basis of isotropic rank four tensors in two dimensions appearing in equation (3.5). Adapted from Ref. [30].

These are presented below, and will be derived and discussed in greater detail in Chapter 4.5

$$\gamma_1 = \frac{1}{2\rho_0\nu}\delta_{ij}\epsilon_{kl}\mathcal{T}^{ijkl}, \tag{3.8}$$

$$\gamma_2 = \frac{1}{2\rho_0\nu}\epsilon_{ij}\epsilon_{kl}\mathcal{T}^{ijkl}, \tag{3.9}$$

$$\lambda_1 + 2\lambda_2 + \lambda_3 - \frac{\gamma_1\pi}{2\mu} + \frac{\gamma_2\tau}{2\mu} = \frac{1}{2\rho_0\mu}\delta_{ik}\delta_{jl}\mathcal{T}^{ijkl}, \tag{3.10}$$

$$\lambda_4 + \lambda_5 + \lambda_6 - \frac{\gamma_1\tau}{4\mu} - \frac{\gamma_2\pi}{4\mu} = \frac{1}{4\rho_0\mu}\epsilon_{ik}\delta_{jl}\mathcal{T}^{ijkl}, \tag{3.11}$$

$$\lambda_5 - \frac{\gamma_2\pi}{4\mu} = \frac{1}{8\rho_0\mu}\epsilon_{ij}\delta_{kl}\mathcal{T}^{ijkl}, \tag{3.12}$$

$$\lambda_3 + \frac{\gamma_2\tau}{2\mu} = \frac{1}{4\rho_0\mu}\epsilon_{ij}\epsilon_{kl}\mathcal{T}^{ijkl}\,. \tag{3.13}$$

$\mathcal{T}^{ijkl}$ is the integrated stress correlation function given by

$$\mathcal{T}^{ijkl} = \frac{1}{V}\iint d\boldsymbol{r}\, d\boldsymbol{r}' \int_0^\infty dt\ \langle \delta T_{ij}(\boldsymbol{r}, t)\delta T_{kl}(\boldsymbol{r}', 0)\rangle\,. \tag{3.14}$$

Note that the stress tensor in (3.14) is defined as a spatial average, as in the following section.

μ, ν, τ, and π are static correlation functions in the non-equilibrium steady state given by

$$\mu\delta_{ij} = \frac{1}{V}\int \left\langle \delta v^i(\mathbf{x})\delta v^j(\mathbf{y})\right\rangle d^2\mathbf{x}\, d^2\mathbf{y}\,, \tag{3.15}$$

$$\pi = \frac{1}{V}\int (y^i - x^i)\left\langle \delta v^i(\mathbf{x})\delta m(\mathbf{y})\right\rangle d^2\mathbf{x}\, d^2\mathbf{y}\,, \tag{3.16}$$

$$\tau = \frac{1}{V}\int \epsilon_{kr}(y^r - x^r)\left\langle \delta m(\mathbf{x})\delta v^k(\mathbf{y})\right\rangle d^2\mathbf{x}\, d^2\mathbf{y}\,, \tag{3.17}$$

$$\nu = \frac{1}{V}\int \left\langle \delta m(\mathbf{x})\delta m(\mathbf{y})\right\rangle d^2\mathbf{x}\, d^2\mathbf{y}\,, \tag{3.18}$$

respectively, where V is the area of the system. In particular, μ and ν can be regarded as measuring the effective translation and spin temperatures in the steady state. For equilibrium systems, equipartition implies $\mu = \nu$ and $\pi = \tau = 0$. Lastly, the above Green-Kubo relations show that two of the transport coefficients, λ_3 and γ_2, are related by $2\lambda_3 = \gamma_2(\nu - \tau)/\mu$.

For the chiral active dumbbell fluid, the situation is further simplified. As we will show in the following sections the absence of alignment interactions, *i.e.* torque interactions acting at a distance between misaligned dumbbells, results in $\gamma_1 = \gamma_2 = 0$, effectively decoupling the velocity from the spin field and also setting $\lambda_3 = 0$. Moreover, symmetry and objectivity of the stress tensor sets two more of the viscosity coefficients to zero, leaving

$$\begin{aligned}\eta_{ijkl} = \lambda_1\big(\delta_{ij}\delta_{kl}\big) + \lambda_2\big(\delta_{ik}\delta_{jl} - \epsilon_{ik}\epsilon_{jl}\big) \\ + \lambda_4\big(\epsilon_{ik}\delta_{jl} + \epsilon_{jl}\delta_{ik}\big)\,.\end{aligned} \tag{3.19}$$

These simplifications also allow us to write simplified Green-Kubo expressions for the shear viscosity

$$\begin{aligned}\lambda_2 = \frac{1}{4\rho_0\mu}\int_0^\infty dt\ \big\langle (\delta T_{22}(t) - \delta T_{11}(t)) \\ (\delta T_{22}(0) - \delta T_{11}(0))\big\rangle\,,\end{aligned} \tag{3.20}$$

and the odd viscosity

$$\begin{aligned}\lambda_4 = \frac{1}{4\rho_0\mu}\int_0^\infty dt\Big[\langle \delta T_{11}(t)\delta T_{21}(0)\rangle - \langle \delta T_{11}(0)\delta T_{21}(t)\rangle \\ + \langle \delta T_{12}(t)\delta T_{22}(0)\rangle - \langle \delta T_{12}(0)\delta T_{22}(t)\rangle\Big]\,,\end{aligned} \tag{3.21}$$

(see Appendix E for details on separating the coefficient λ_2 from (3.10)). Equation (3.21) shows that nonvanishing odd viscosity, *i.e.* $\lambda_4 \neq 0$, requires breaking time reversal symmetry at the level of stress correlation functions, thus breaking the Onsager reciprocal relations [6, 30]. Note that (3.20) is not the typical Green-Kubo expression used to calculate the shear

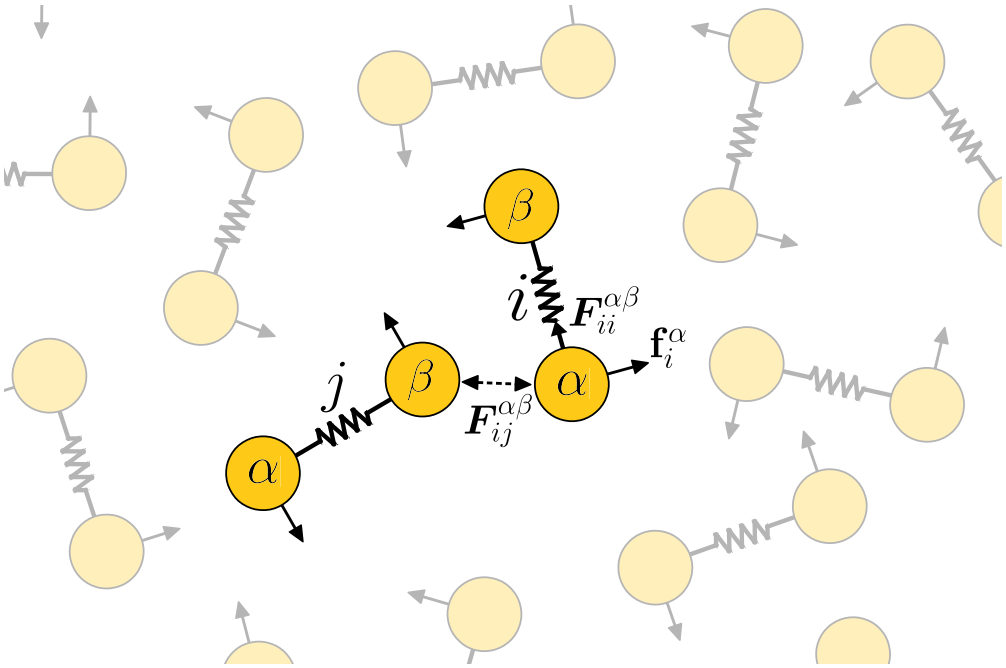

Figure 3.1: A two-dimensional fluid composed of chiral active dumbbells. In addition to interacting with its neighbors, each dumbbell is rotated counterclockwise by equal and opposite active forces $\mathbf{f}_i^{\alpha}$.

viscosity. However, it can also be rewritten for isotropic systems in the typical form, which are invariant under rotation as

$$\lambda_2 = \frac{1}{\rho_0 \mu} \int_0^{\infty} dt \, \langle \delta T'_{12}(t) \delta T'_{12}(0) \rangle \,, \tag{3.22}$$

using a transformation $\boldsymbol{T'} = \boldsymbol{R^T T R}$ corresponding to a rotation $\boldsymbol{R}$ of angle $\pi/4$, for which $T'_{12} = \frac{1}{2}(T_{22} - T_{11})$. The form in (3.20) is a result of the theory for the choice of the representation theorem for viscous transport coefficients using the basis $s^{(n)}_{ijkl}$.

In what follows, we evaluate the shear and odd viscosity Green-Kubo expressions at various densities and driving forces using molecular simulations of chiral active dumbbells in a non-equilibrium steady state (see Appendix D for simulations details). We then subject the dumbbell system to non-uniform shearing flow, and evaluate the viscosity coefficients independently. Such an analysis will provide support to both the application of Onsager's regression hypothesis to fluctuations in active non-equilibrium steady states and the ensuing Green-Kubo relations for viscous behaviors of active systems.

3.3 Microscopic model: Chiral active dumbbells.

We consider a fluid composed of dumbbells subject to active torques [95], as shown in Fig. 3.1. Each dumbbell is composed of two particles of unit mass connected by a harmonic spring. The system evolves according to underdamped Langevin dynamics

$$\begin{aligned}\dot{\boldsymbol{x}}_i^\alpha &= \boldsymbol{v}_i^\alpha\,,\\ \dot{\boldsymbol{v}}_i^\alpha &= \sum_{j\beta}\boldsymbol{F}_{ij}^{\alpha\beta}+\mathbf{f}_i^\alpha+\boldsymbol{g}_i^\alpha-\zeta\boldsymbol{v}_i^\alpha+\boldsymbol{\eta}_i^\alpha\,,\end{aligned}\tag{3.23}$$

with indices $i,j\in[1,N]$ and $\alpha,\beta\in\{1,2\}$ running over dumbbells and particles, respectively. Variables $\boldsymbol{x}_i^\alpha$ and $\boldsymbol{v}_i^\alpha$ represent atom positions and velocities. ζ is the dissipative substrate friction and T is the substrate temperature determining the variance of the random thermal force $\boldsymbol{\eta}_i^\alpha(t)$, modeled as Gaussian white noise affecting each particle independently such that $\langle\boldsymbol{\eta}_i^\alpha(t)\boldsymbol{\eta}_j^\beta(t')\rangle=2k_\mathrm{B}T\zeta\delta(t-t')\delta_{ij}\delta_{\alpha\beta}\mathbf{I}$, where $\mathbf{I}$ is the identity matrix. Particles in different dumbbells interact through a pairwise WCA potential [97], resulting in interaction forces $\boldsymbol{F}_{ij}^{\alpha\beta}$. The particles in a dumbbell are subjected to equal and opposite non-conservative active forces $\mathbf{f}_i^\alpha$, which satisfy $\mathbf{f}_i^1=-\mathbf{f}_i^2:=\mathbf{f}_i$, and are always perpendicular to the bond vector $\boldsymbol{d}_i=\boldsymbol{x}_i^1-\boldsymbol{x}_i^2$. This imposes an active torque at the level of individual dumbbells. Finally, $\boldsymbol{g}_i^\alpha=\boldsymbol{g}(\boldsymbol{x}_i^\alpha)$ is an optional externally imposed body force, and will be employed later in Poisueille flow simulations to test the Green-Kubo relations.

Previous work [95] used the Irving-Kirkwood procedure to coarse-grain the microscopic equations (3.23) and derive the equations of hydrodynamics, including balance of mass, linear momentum and angular momentum, as also employed in the context of measuring odd viscosity by [99]. This coarse-graining procedure yields expressions for the stress tensor in terms of molecular variables and active forces. In particular, it is found that applying active forces at the microscale results in an asymmetric stress tensor at the continuum scale given by

$$\boldsymbol{T}=\boldsymbol{T}^\mathrm{K}+\boldsymbol{T}^\mathrm{V}+\boldsymbol{T}^\mathrm{A}\,,\tag{3.24}$$

where

$$\boldsymbol{T}^\mathrm{K}=-\frac{1}{A}\sum_{i,\alpha}m_i^\alpha\boldsymbol{v}_i^\alpha\otimes\boldsymbol{v}_i^\alpha\,,\tag{3.25}$$

$$\boldsymbol{T}^\mathrm{V}=-\frac{1}{2A}\sum_{i,j,\alpha,\beta}\boldsymbol{F}_{ij}^{\alpha\beta}\otimes\boldsymbol{x}_{ij}^{\alpha\beta}\,,\tag{3.26}$$

$$\boldsymbol{T}^\mathrm{A}=-\frac{1}{A}\sum_i\mathbf{f}_i\otimes\boldsymbol{d}_i\,,\tag{3.27}$$

denote the kinetic, virial, and active contributions, respectively (see Appendix F)

The active force vector $\mathbf{f}_i$ is related to the unit bond vector $\hat{\boldsymbol{d}}_i$ by a rotation $\boldsymbol{R}$ of angle $\pi/2$, *i.e.,*

$$\mathbf{f}_i=\mathrm{f}\boldsymbol{R}\hat{\boldsymbol{d}}_i\tag{3.28}$$

For positive (negative) f, the dumbbells rotate counter-clockwise (clockwise). We find that the steady state time average of $\boldsymbol{T}^{\mathrm{A}}$ is

$$\begin{aligned}\langle \boldsymbol{T}^{\mathrm{A}} \rangle &= -\rho_0 \langle \mathbf{f} \otimes \boldsymbol{d} \rangle \\ &= -\rho_0 \mathrm{f} d \langle \boldsymbol{R}\hat{\boldsymbol{d}} \otimes \hat{\boldsymbol{d}} \rangle = \frac{\rho_0 \mathrm{f} d}{2} \begin{bmatrix} 0 & 1 \\ -1 & 0 \end{bmatrix} ,\end{aligned} \tag{3.29}$$

where $d = \langle |\boldsymbol{d}| \rangle$ is the average bond length. Because the dumbbells rotate with no preferred alignment, the antisymmetry of $\langle \boldsymbol{T}^{\mathrm{A}} \rangle$ follows from replacing the time average with a uniformly weighted average over angles of rotation θ. For example,

$$\langle \boldsymbol{R}\hat{\boldsymbol{d}} \otimes \hat{\boldsymbol{d}} \rangle_{21} = \langle \hat{d}_1 \hat{d}_1 \rangle = \frac{1}{2\pi} \int_0^{2\pi} d\theta \ \cos^2(\theta) = \frac{1}{2} \tag{3.30}$$

while the diagonal elements are zero. This shows that the antisymmetric hydrostatic-like term p^* introduced in (3.3) arises in a non-equilibrium steady state of the active dumbbell model due to the presence of active rotational forces, and has the magnitude $p^* = \rho_0 \mathrm{f} d/2$. We further relate p^* to a non-dimensional Péclet number describing the ratio of active rotational forces to thermal fluctuations due to the substrate bath held at temperature T

$$\mathrm{Pe} = \frac{2\mathrm{f} d}{k_{\mathrm{B}} T} = \frac{4p^*}{\rho_0 k_{\mathrm{B}} T}. \tag{3.31}$$

We use Pe as defined in (3.31) to vary the activity in the system when evaluating the transport coeffcients.

3.4 Green-Kubo calculations

Steady-state molecular dynamics simulations [96] allow direct measurement of the integrated stress correlation functions $\mathcal{T}_{ijkl}$ defined in (3.14), which are required for evaluation of the viscous transport coefficients using the Green-Kubo equations (3.8)-(3.13) [1]. We find that several of these coefficients vanish in the non-equilibrium steady states at all simulated activities and densities due to cancellations of the correlation functions (see Appendix Fig. E.1). In particular,

$$\epsilon_{ij}\epsilon_{kl}\mathcal{T}_{ijkl} = \delta_{ij}\epsilon_{kl}\mathcal{T}_{ijkl} = \epsilon_{ij}\delta_{kl}\mathcal{T}_{ijkl} = 0\,. \tag{3.32}$$

This immediately implies $\gamma_1 = \gamma_2 = \lambda_3 = \lambda_5 = \lambda_6 = 0$, so that the stress tensor is symmetric and objective. It now remains to evaluate the two non-trivial transport coefficients λ_2 and λ_4 using (3.20) and (3.21). For these coefficients, we compute the effective translation temperature as $(A\rho_0)\mu = m\langle (v_i^\alpha)^2 \rangle$, consistent with the stress tensor defined in (3.24)-(3.27).

[1] Our simulation and analysis code is publicly available at https://github.com/mandadapu-group/active-matter.

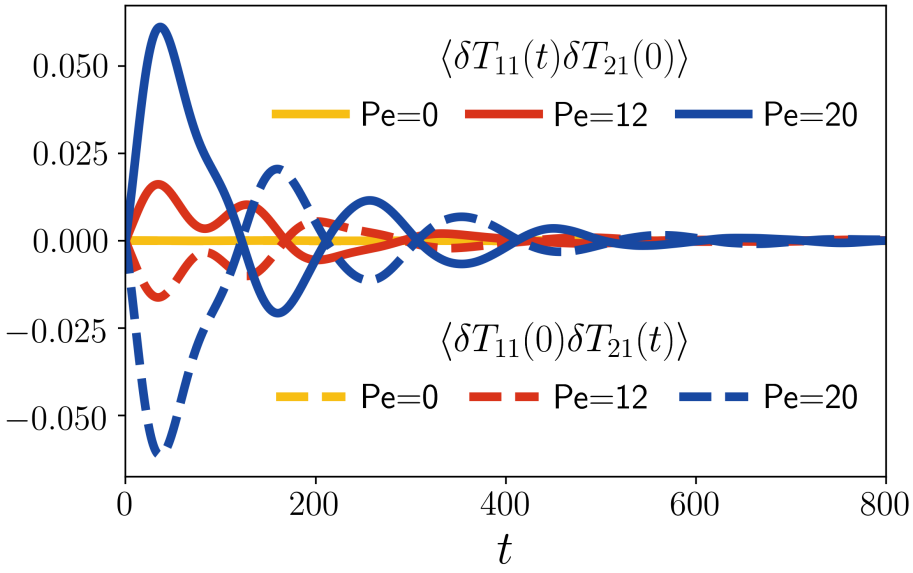

Figure 3.2: Stress correlation functions contributing to the odd viscosity ($\rho_0 = 0.4$). For Pe $\neq 0$ these correlation functions display time reversal antisymmetry, adding constructively to yield a nonzero odd viscosity.

Figure 3.2 shows the stress correlation functions $\langle \delta T_{11}(t)\delta T_{21}(0)\rangle$ and $\langle \delta T_{11}(0)\delta T_{21}(t)\rangle$ for various Pe. These are typically zero for systems in equilibrium, but become nonzero in the chiral active dumbbell fluid for Pe $\neq 0$. In general, we find

$$\begin{aligned} \langle \delta T_{11}(t)\delta T_{21}(0)\rangle &= -\langle \delta T_{11}(0)\delta T_{21}(t)\rangle \\ &= -\langle \delta T_{11}(\text{-}t)\delta T_{21}(0)\rangle \,, \end{aligned} \tag{3.33}$$

where the final equality is due to stationarity. The analogous equations are satisfied by $\langle \delta T_{12}(t)\delta T_{22}(0)\rangle$. Due to this time reversal antisymmetry these correlation functions add constructively, yielding a nonvanishing odd viscosity from the Green-Kubo relation (3.21).

Figure 3.4 shows the Green-Kubo estimates for λ_2 and λ_4 for various activities and for a range of low to high densities. We find that the shear viscosity increases with density as well as with activity. The dependence of the odd viscosity on activity, while apparently linear at low density, becomes increasingly sigmoidal at high density. Because the sign of Pe controls the direction of active rotation, the time reversal symmetry and antisymmetry, respectively, of λ_2 and λ_4 in equations (3.20) and (3.21) require that λ_2 must be an even function of Pe while λ_4 must be odd. Note that the odd viscosity, as a non-dissipative transport coefficient, may be negative without introducing an inconsistency with the second law of thermodynamics.

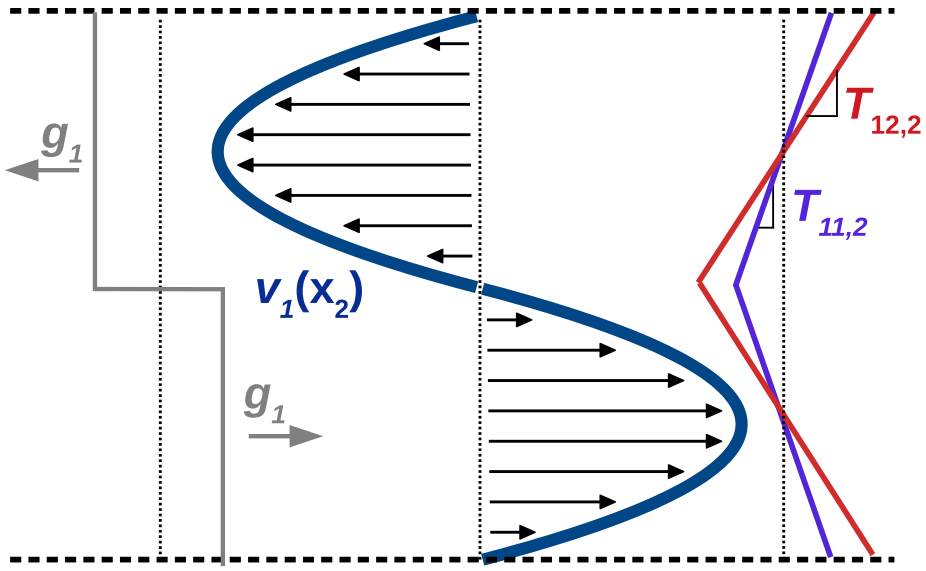

Figure 3.3: A schematic of the periodic Poiseuille non-equilibrium molecular dynamics (NEMD) simulation method. The top half of the system is subjected to a uniform body force to the left, and the bottom half to a uniform body force of equal magnitude to the right. This yields a parabolic velocity profile and, for odd viscous fluids, an atypical normal stress T_{11}.

3.5 Poiseuille flow NEMD simulations

To verify the values computed from the Green-Kubo formulas, (3.20) and (3.21), we measure λ_2 and λ_4 independently via non-equilibrium molecular dynamics simulations. To this end, we simulate plane Poiseuille-like flow via the inclusion of a nonzero body force $\boldsymbol{g}$ in (3.23) according to the periodic Poiseuille method [100]. As depicted in Fig. 3.3, we apply equal and opposite uniform body forces of magnitude g_1 in the x_1 direction across a rectangular channel of width $2L$, compatible with periodic boundary conditions. In the following analysis, we consider only the bottom half of the system depicted in Fig. 3.3, as the top half is symmetrically identical.

The setup in Fig. 3.3 represents a non-trivial boundary value problem, which not only yields non-uniform flows and non-uniform stresses, but also provides a stringent test for the expected constitutive behaviors of the active dumbbell fluid and the estimates of the transport coefficients obtained from Green-Kubo formulas. The velocity profile and pressure profile for flow driven by a small, uniform body force can be solved analytically from the continuum theory, yielding

$$v_1(x_2) = \frac{\rho_0 g_1}{2\lambda_2} x_2(L - x_2)\,, \tag{3.34}$$

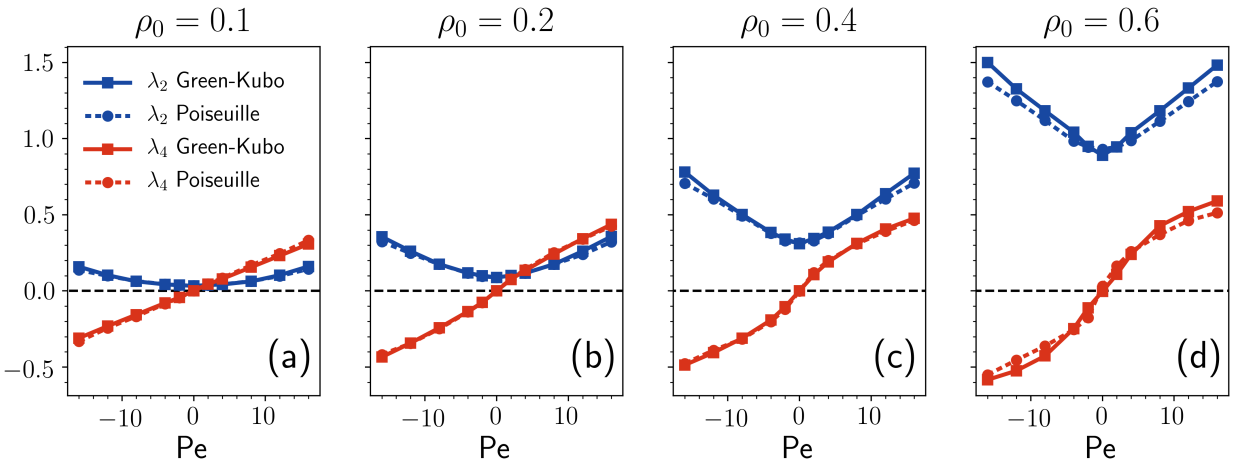

Figure 3.4: Comparison of shear viscosity (λ_2) and odd viscosity (λ_4) values obtained from the Green-Kubo relations (solid lines) with those obtained from periodic Poiseuille NEMD simulations (dashed lines). Error bars due to sampling convergence are smaller than the symbols. Figures (a)-(d) show this comparison at densities $\rho_0 \in \{0.1, 0.2, 0.4, 0.6\}$, respectively. Each figure scans over Pe $\in$ {-16, -12, -8, -4, -2, 0, 2, 4, 8, 12, 16}.

and

$$p(x_2) = \frac{\lambda_4}{\lambda_2}\rho_0 x_2 g_1 + p_0\,, \tag{3.35}$$

respectively, where p_0 is an arbitrary reference pressure (see Appendix G for the solution to the corresponding boundary value problem). Our simulations of active dumbbell fluids are consistent with these profiles for various densities and activities (see Appendix Fig. G.1). Given the velocity and pressure profiles in (3.34) and (3.35), the shear and odd viscosities can be computed from the expressions

$$\lambda_2 = \frac{\rho_0 g_1 L^2}{12\bar{v}}\,, \tag{3.36}$$

$$\lambda_4 = \frac{T_{11,2}}{2v_{1,22}} = -\frac{\lambda_2 T_{11,2}}{2\rho_0 g_1}\,, \tag{3.37}$$

respectively, where $\bar{v} = \frac{1}{L}\int_0^L dx_2\; v_1(x_2)$; see Appendix G. The slope of the stress component T_{11} can be identified in molecular simulations using the Irving-Kirkwood expression (3.24)-(3.27).

The shear and odd viscosities calculated using this NEMD approach are found to be in agreement with the Green-Kubo predictions for a wide range of densities and Péclet numbers, see Fig. 3.4.

3.6 Discussion

In this chapter, we have validated the non-equilibrium Green-Kubo formulas derived in Ref. [30], using molecular dynamics simulations of the chiral active dumbbell model system to show that odd viscosity is a direct consequence of the breaking of time reversal symmetry at the level of stress fluctuations. In doing so, we provide support for the application of the Onsager regression hypothesis to fluctuations about non-equilibrium steady states, which was used to derive these equations. Complementary work by Han *et al.* [38] measures transport coefficients including the odd viscosity in a different model system consisting of frictional granular particles, upon obtaining Green-Kubo relations identical in form to [30] using a projection operator formalism and finding similar agreement with NEMD measurements. Together with the present findings, these results suggest broad applicability of these Green-Kubo relations in active fluids. Future work entails understanding the microscopic origins of the functional dependence of the viscosities with density and activity.

Chapter 4

A General Framework for Odd Transport

You shall know the truth, and the truth shall make you odd.
– attributed to Flannery O'Connor

4.1 Introduction

In the previous two chapters, Green-Kubo relations provided the critical connection between microscopic fluctuations and macroscopic transport coefficients. In particular, odd diffusion and odd viscosity were seen to arise as macroscopic consequences of microscopic chiral dynamics, characterized by the breaking of time-reversal and parity symmetry. We saw how this is especially relevant for chiral active matter — a broad class of systems capable of breaking these symmetries by consuming energy from their environment. Indeed, even in such active matter systems, fluctuations occurring in an unperturbed steady state were seen to encode precisely the response of the system to perturbations away from steady state.

The Green-Kubo relation for the odd self-diffusion obtained in Chapter 2 emerged together with the linear constitutive behavior through a first-principles consideration of microscopic chiral random motion, following a similar logic to the pioneering work of Einstein, Smoluchowski and others [1–4]. More generally, however, linear constitutive relations are *phenomenological*. That is, given a macroscopically observed constitutive behavior, a connection to microscopic fluctuations is sought. Various approaches exist to derive Green-Kubo relations for transport coefficients governing the response of an equilibrium system to perturbations away from equilibrium [101, 102]. In the context of active matter, however, such approaches may not be appropriate; in particular, those relying on the statistical properties of thermal systems at equilibrium such as Gaussian fluctuations and linear response relationships.

In Kubo's original work on the subject, he distinguished between *mechanical* and *thermal* — or boundary-driven — transport coefficients [74, 75]. Those in the former category, such

as mobility, govern the response of the system to an external field coupling directly to the microscopic equations of motion. Those in the latter category, such as diffusivity, thermal conductivity, and viscosity, govern the response of the system to perturbation from the boundaries, *i.e.* inducing a gradient in the concentration, temperature or shear velocity through imposed boundary conditions, without modifying the microscopic dynamics. Kubo showed that the Onsager regression hypothesis — which connects microscopic fluctuations to macroscopic transport phenomena — holds rigorously in the context of mechanical transport, as required by linear response theory, while it must be considered an additional assumption when dealing with boundary-driven transport. It is also a feature of equilibrium systems that mechanical and boundary-driven transport coefficients are connected through Einstein relations. As was discussed in Chapter 1, however, such Einstein relations need not exist in the broader context of active matter.

In this chapter, we present a general framework for deriving Green-Kubo relations for odd boundary-driven transport in active matter. We build on the approach introduced by Epstein and Mandadapu [30] and discussed in Chapter 2.2. In that approach, the Onsager regression hypothesis [5, 6] was generalized beyond the original context of perturbations about equilibrium, to include perturbations about non-equilibrium steady states such as encountered in active matter, and a derivation paralleling that of Kubo, Yokota, and Nakjima [74] led to a Green-Kubo relation for the the six viscosity coefficients appearing in the rank-four viscosity tensor of a two-dimensional isotropic fluid, including the odd viscosity. The regression hypothesis approach is inapplicable, however, for rank-two transport tensors, such as the diffusion or heat conduction tensors, for which the odd part plays no role in the relaxation of the scalar variable. Thus, rather than assuming that microscopic fluctuations relax on average according to the macroscopic relaxation equation, as stated by the regression hypothesis, we shall instead assume that microscopic fluctuations of fluxes are governed on average by the macroscopic constitutive laws. We shall refer to this assumption as the *flux hypothesis*.

With the flux hypothesis as a starting point, we will derive generic Green-Kubo relation for odd transport coefficients, which reveal reciprocal relations for time-reversal symmetric systems and indicate in what context time-reversal symmetry breaking is a prerequisite for odd transport. It will be shown, moreover, that the regression hypothesis follows directly from the flux hypothesis, but that the latter contains additional content regarding the behavior of the odd fluxes. Finally, we shall show that flux hypothesis derivation recovers the previously-obtained Green-Kubo relations for odd self-diffusion and odd viscosity, and yields a new Green-Kubo relation for odd collective diffusion in concentrated solutions, which is verified in molecular dynamics simulations of a model system.

4.2 Flux hypothesis

Consider the conservation and constitutive equations governing a generic variable $\bar{A}_i(\boldsymbol{r},t)$ and its corresponding flux $\bar{\boldsymbol{J}}_i(\boldsymbol{r},t)$ in d spatial dimensions

$$\frac{d}{dt}\bar{A}_i = -\boldsymbol{\nabla}\cdot\bar{\boldsymbol{J}}_i\,, \tag{4.1}$$

$$\bar{\boldsymbol{J}}_i = -\sum_{j=1}^{m}\mathbf{M}_{ij}\boldsymbol{\nabla}\bar{A}_j\,, \tag{4.2}$$

where $\mathbf{M}_{ij}$ is the $d\times d$ matrix of transport coefficients coupling the flux $\bar{\boldsymbol{J}}_i$ to the variable $\bar{A}_j$. Here i and j run from 1 to m, where m is the total number of fluxes and corresponding gradients of interest. When examining cross-couplings of distinct fluxes and gradients, as in the Soret and Dufour effects, m will necessarily be greater than one.

The corresponding equations governing the Fourier modes $\bar{A}_i^{\boldsymbol{q}}(t)$ and $\bar{\boldsymbol{J}}_i^{\boldsymbol{q}}(t)$ are

$$\frac{d}{dt}\bar{A}_i^{\boldsymbol{q}} = \mathrm{i}\boldsymbol{q}\cdot\bar{\boldsymbol{J}}_i^{\boldsymbol{q}}\,, \tag{4.3}$$

$$\bar{\boldsymbol{J}}_i^{\boldsymbol{q}} = \sum_{j=1}^{m}\mathbf{M}_{ij}\cdot\mathrm{i}\boldsymbol{q}\bar{A}_j^{\boldsymbol{q}}\,, \tag{4.4}$$

where we have defined the Fourier transform

$$y^{\boldsymbol{q}}(t) := \int d\boldsymbol{r}\; e^{-\mathrm{i}\boldsymbol{q}\cdot\boldsymbol{r}}y(\boldsymbol{r},t)\,. \tag{4.5}$$

Combining equations (4.3)-(4.4) yields the relaxation equation for the Fourier modes of the state variables

$$\frac{d}{dt}\bar{A}_i^{\boldsymbol{q}} = -\sum_{j=1}^{m}(\boldsymbol{q}\cdot\mathbf{M}_{ij}\cdot\boldsymbol{q})\bar{A}_j^{\boldsymbol{q}}\,. \tag{4.6}$$

In this work we concern ourselves with the spatially-antisymmetric part of $\mathbf{M}_{ij}$, which we denote $\mathbf{M}_{ij}^{\mathrm{odd}} = \frac{1}{2}(\mathbf{M}_{ij}-\mathbf{M}_{ij}^T)$ and contrast with $\mathbf{M}_{ij}^{\mathrm{even}} = \frac{1}{2}(\mathbf{M}_{ij}+\mathbf{M}_{ij}^T)$. We seek to derive general Green-Kubo relations for $\mathbf{M}_{ij}^{\mathrm{odd}}$ which encompass transport coefficients governing the response of a system to perturbation about non-equilibrium steady states, such as those encountered in active matter; consequently we avoid relying on any linear-response assumptions. To obtain a relationship between the transport coefficients $\mathbf{M}_{ij}$ and microscopic fluctuations, Kubo, Yokota and Nakajima [74] first invoke Onsager's regression hypothesis (RH), which presumes that microscopic fluctuations in $A^{\boldsymbol{q}}$ on average relax according to equation (4.6). That is,

$$\frac{1}{\Delta t}\big[\langle A_i^{\boldsymbol{q}}(t+\Delta t)\rangle_{\mathcal{A}^{\boldsymbol{q}}(t)} - A_i^{\boldsymbol{q}}(t)\big] = -\sum_{j=1}^{m}(\boldsymbol{q}\cdot\mathbf{M}_{ij}\cdot\boldsymbol{q})A_j^{\boldsymbol{q}}(t)\,. \tag{4.7}$$

Here, the variables $A_i^{\boldsymbol{q}}(t)$ indicate fluctuating microscopic state variables corresponding to the macroscopic variables $\bar{A}_i$. $\langle A_i^{\boldsymbol{q}}(t+\Delta t)\rangle_{\mathcal{A}^{\boldsymbol{q}}(t)}$ indicates the expectation value of $A^{\boldsymbol{q}}$ at time $t+\Delta t$ conditioned on the vector of all observables $\mathcal{A}^{\boldsymbol{q}}$ having assumed the specified values at time t. Multiplying equation (4.7) through by the state variable $A_k^{-\boldsymbol{q}}$ [in doing so, we have assumed isotropy] and averaging over the steady-state distribution of the initial values $\mathcal{A}^{\boldsymbol{q}}(t)$ yields

$$\frac{1}{\Delta t}\big[\langle A_i^{\boldsymbol{q}}(\Delta t)A_k^{-\boldsymbol{q}}(0)\rangle - \langle A_i^{\boldsymbol{q}}A_k^{-\boldsymbol{q}}\rangle\big] = -\sum_{j=1}^{m}(\boldsymbol{q}\cdot\mathbf{M}_{ij}\cdot\boldsymbol{q})\langle A_j^{\boldsymbol{q}}A_k^{-\boldsymbol{q}}\rangle\,, \tag{4.8}$$

where stationarity has been invoked to set $t=0$.

The left-hand side of equations (4.7)-(4.8) is formulated as a finite-difference time derivative, valid for $\Delta t \ll \tau_{\mathrm{r}}$, where τ_{r} is the characteristic relaxation time of $A^{\boldsymbol{q}}$. At the same time, for equations (4.7)-(4.8) to reproduce the Markovian behavior of equation (4.6), in which the rate of relaxation is determined instantaneously and without memory effects by the values of the state variables, it is necessary that we set $\Delta t \gg \tau_c$, where τ_c is the correlation time above which the increment $A_i^{\boldsymbol{q}}(t+\Delta t) - A_i^{\boldsymbol{q}}(t)$ may be considered to be independent of the preceding increment $A_i^{\boldsymbol{q}}(t) - A_i^{\boldsymbol{q}}(t-\Delta t)$ for all i. Thus, it is assumed that an intermediate timescale Δt exists satisfying the separation of timescales

$$\tau_c \ll \Delta t \ll \tau_r\,. \tag{4.9}$$

In the present work, we will place similar conditions on the timescales. Because of its antisymmetry, however, $\mathbf{M}_{ij}^{\mathrm{odd}}$ does not contribute to the relaxation equation (4.6), and thus cannot be examined from the perspective of the regression hypothesis (4.7). We shall instead apply the conceptual content of Onsager's hypothesis at the level of the constitutive relation (4.4), by asserting that microscopic fluctuations should on average behave according to the macroscopic constitutive equations. We formulate this flux hypothesis as

$$\langle \boldsymbol{J}_i^{\boldsymbol{q}}(t+\Delta t)\rangle_{\mathcal{A}^{\boldsymbol{q}}(t)} = \sum_{j=1}^{m}\mathbf{M}_{ij}\cdot \mathrm{i}\boldsymbol{q}A_j^{\boldsymbol{q}}(t)\,. \tag{4.10}$$

Note that the right-hand side, while similar to that of equation (4.7), preserves all information about $\mathbf{M}_{ij}^{\mathrm{odd}}$, since the equality must hold for all orientations of $\boldsymbol{q}$. Paralleling equation (4.7), $\langle \boldsymbol{J}_i^{\boldsymbol{q}}(t+\Delta t)\rangle_{\mathcal{A}^{\boldsymbol{q}}(t)}$ indicates a conditional expectation of the fluctuating flux $\boldsymbol{J}_i^{\boldsymbol{q}}$ after a lag time Δt, conditioned on an initial specification $\mathcal{A}^{\boldsymbol{q}}(t)$ of the state variables. Multiplying equation (4.10) through by $A_k^{-\boldsymbol{q}}$ and averaging yields

$$\langle \boldsymbol{J}_i^{\boldsymbol{q}}(\Delta t)A_k^{-\boldsymbol{q}}(0)\rangle = \sum_{j=1}^{m}\mathbf{M}_{ij}\cdot \mathrm{i}\boldsymbol{q}\langle A_j^{\boldsymbol{q}}A_k^{-\boldsymbol{q}}\rangle\,. \tag{4.11}$$

As with the regression hypothesis (4.7), the flux hypothesis (4.10) is expected to hold in the macroscopic limit $\boldsymbol{q}\to 0$ and when Δt satisfies the separation of timescales (4.9).

The motivation for the upper bound $\Delta t \ll \tau_r$ is straightforward: as gradients relax on long timescales of the order τ_r, fluxes lose their memory of past gradients. The motivation for choosing the lower bound $\Delta t \gg \tau_c$, however, merits greater discussion. Why not require, for instance, that gradients instantaneously determine fluxes, as in the macroscopic equation (4.4), by setting $\Delta t = 0$? The answer is that Markovian constitutive behavior (that is, an instantaneous relationship between fluxes and gradients) is only ever obtained on observation timescales much greater than the correlation time τ_c. Indeed, as will be shown in the next section, it is precisely the dynamics occurring on timescales of the order τ_c that determine the macroscopic constitutive behavior, as exemplified by Green-Kubo relations. To illustrate this point, consider taking the inner product of equation (4.11) with $\mathrm{i}\boldsymbol{q}$. The left-hand side becomes

$$\mathrm{i}\boldsymbol{q} \cdot \langle \boldsymbol{J}_i^{\boldsymbol{q}}(\Delta t) A_k^{-\boldsymbol{q}}(0) \rangle = \langle \dot{A}_i^{\boldsymbol{q}}(\Delta t) A_k^{-\boldsymbol{q}}(0) \rangle = -\langle A_i^{\boldsymbol{q}}(\Delta t) \dot{A}_k^{-\boldsymbol{q}}(0) \rangle \,, \tag{4.12}$$

where the final equality follows from the assumption of stationarity. In the case where $i = k$, setting $\Delta t = 0$ yields $\langle \dot{A}_i^{\boldsymbol{q}} A_i^{-\boldsymbol{q}} \rangle = -\langle A_i^{\boldsymbol{q}} \dot{A}_i^{-\boldsymbol{q}} \rangle = 0$. However the right-hand side of equation (4.11) becomes $\sum_{j=1}^{m} \mathbf{M}_{ij} \cdot \mathrm{i}\boldsymbol{q} \langle A_j^{\boldsymbol{q}}(0) A_i^{-\boldsymbol{q}}(0) \rangle$, which is in general nonzero. Thus, the choice of $\Delta t = 0$ leads to an apparent contradiction which, as has been pointed out [101, 103], is resolved by recognizing the Markovian constitutive behavior in equation (4.4) as an approximation or limiting form of the more generally non-Markovian behavior.

Finally, we note that while the constitutive equation (4.4) holds *on average* for microscopic fluctuating variables as expressed in equation (4.10), the conservation equation (4.3) must hold *exactly* for any realization of the microscopic fluctuating variables; that is,

$$\dot{A}_i^{\boldsymbol{q}}(t) = \mathrm{i}\boldsymbol{q} \cdot \boldsymbol{J}_i^{\boldsymbol{q}}(t) \,. \tag{4.13}$$

Now, averaging over the subensemble specified by $\mathcal{A}^{\boldsymbol{q}}(t)$ yields

$$\begin{aligned} \langle \dot{A}_i^{\boldsymbol{q}}(t + \Delta t) \rangle_{\mathcal{A}^{\boldsymbol{q}}(t)} &\approx \frac{1}{\Delta t} \big[\langle A_i^{\boldsymbol{q}}(t + \Delta t) \rangle_{\mathcal{A}^{\boldsymbol{q}}(t)} - A_i^{\boldsymbol{q}}(t) \big] \\ &= \mathrm{i}\boldsymbol{q} \cdot \langle \boldsymbol{J}_i^{\boldsymbol{q}}(t + \Delta t) \rangle_{\mathcal{A}^{\boldsymbol{q}}(t)} = -\sum_{j=1}^{m} (\boldsymbol{q} \cdot \mathbf{M}_{ij} \cdot \boldsymbol{q}) A_j^{\boldsymbol{q}}(t) \,, \end{aligned} \tag{4.14}$$

where the first equality holds due to the requirement $\Delta t \ll \tau_r$. Thus, the Onsager regression hypothesis (4.7) follows directly from the flux hypothesis (4.10), but the latter contains additional information regarding the odd transport coefficients $\mathbf{M}_{ij}^{\mathrm{odd}}$.

4.3 Green-Kubo relations

The left-hand side of equation (4.11) may be expanded into a time integral as

$$\begin{aligned}\langle \boldsymbol{J}_i^{\boldsymbol{q}}(\Delta t) A_k^{-\boldsymbol{q}}(0)\rangle &= \int_0^{\Delta t} dt\ \langle \dot{\boldsymbol{J}}_i^{\boldsymbol{q}}(t) A_k^{-\boldsymbol{q}}(0)\rangle \\ &= -\int_0^{\Delta t} dt\ \langle \boldsymbol{J}_i^{\boldsymbol{q}}(t) \dot{A}_k^{-\boldsymbol{q}}(0)\rangle \\ &= \int_0^{\Delta t} dt\ \langle \boldsymbol{J}_i^{\boldsymbol{q}}(t) \boldsymbol{J}_k^{-\boldsymbol{q}}(0)\rangle \cdot \mathrm{i}\boldsymbol{q}\,,\end{aligned} \tag{4.15}$$

where the second equality follows from stationarity and the third from equation (4.13). Comparison with the right-hand side of equation (4.11) yields

$$\int_0^{\Delta t} dt\ \langle \boldsymbol{J}_i^{\boldsymbol{q}}(t) \boldsymbol{J}_k^{-\boldsymbol{q}}(0)\rangle = \sum_{j=1}^{m} \mathbf{M}_{ij} \langle A_j^{\boldsymbol{q}} A_k^{-\boldsymbol{q}}\rangle\,, \tag{4.16}$$

since equations (4.11) and (4.15) must hold for all orientations of $\boldsymbol{q}$. Thus, we obtain the Green-Kubo relation

$$\mathbf{M}_{ij} = \sum_{k=1}^{m} g_{ik}(\boldsymbol{q}) \mathbf{L}_{kj}(\boldsymbol{q}, \Delta t)\,, \tag{4.17}$$

where we have defined the static correlation function and time-integrated dynamic correlation functions as, respectively

$$g_{ij}(\boldsymbol{q}) = \langle A_i^{\boldsymbol{q}} A_j^{-\boldsymbol{q}}\rangle^{-1} \tag{4.18}$$

$$\mathbf{L}_{ij}(\boldsymbol{q}, \Delta t) = \int_0^{\Delta t} dt\ \langle \boldsymbol{J}_i^{\boldsymbol{q}}(t) \boldsymbol{J}_j^{-\boldsymbol{q}}(0)\rangle\,. \tag{4.19}$$

Equation (4.17) is expected to hold in the limit of $\boldsymbol{q} \to 0$. However, there remains the ambiguity of identifying an intermediate timescale Δt satisfying the separation of timescales (4.9). Setting $\boldsymbol{q} = 0$ identically yields the Green-Kubo relation

$$\mathbf{M}_{ij} = \sum_{k=1}^{m} g^{\circ}_{ik} \mathbf{L}^{\circ}_{kj}\,, \tag{4.20}$$

where

$$g^{\circ}_{ij} = \langle A_i^{\boldsymbol{q}} A_j^{-\boldsymbol{q}}\rangle^{-1}\big|_{\boldsymbol{q}=0} = \left\{ \iint d\boldsymbol{r}\, d\boldsymbol{r'} \langle A_i(\boldsymbol{r}) A_j(\boldsymbol{r'})\rangle \right\}^{-1} \tag{4.21}$$

$$\mathbf{L}^{\circ}_{ij} = \int_0^{\infty} dt\ \langle \boldsymbol{J}_i^{\boldsymbol{q}}(t) \boldsymbol{J}_j^{-\boldsymbol{q}}(0)\rangle\big|_{\boldsymbol{q}=0} = \int_0^{\infty} dt \iint d\boldsymbol{r}\, d\boldsymbol{r'} \langle \boldsymbol{J}_i(\boldsymbol{r}, t) \boldsymbol{J}_j(\boldsymbol{r'}, 0)\rangle\,. \tag{4.22}$$

Note that the timescale Δt appearing in the integral of equation (4.19) has been replaced in (4.22) by ∞, since at $\boldsymbol{q} = 0$, the relaxation time $\tau_r \to \infty$. Strictly speaking, however, all fluctuations vanish at $\boldsymbol{q} = 0$; thus for both conceptual and practical reasons, it is more generally appropriate to consider the $\boldsymbol{q} \to 0$ limit of equation (4.17).

This observation motivates an alternative means of specifying the intermediate timescale Δt, following from recognizing the self-similarity of the correlation functions in the $\boldsymbol{q} \to 0$ limit. In this limit, and for Δt satisfying the separation of timescales (4.9), it follows from the flux hypothesis (4.11) that, for any $t \geq 0$,

$$\langle \mathcal{J}^{\boldsymbol{q}}(t + \Delta t)\mathcal{A}^{\boldsymbol{q}}(0)\rangle = \exp(-q^2\mathcal{M}t)\langle \mathcal{J}^{\boldsymbol{q}}(\Delta t)\mathcal{A}^{\boldsymbol{q}}(0)\rangle \,, \tag{4.23}$$

and thus, the time-integrated flux correlation functions obey the scaling relation

$$\mathcal{L}(\boldsymbol{q}, t + \Delta t)/q = \mathcal{L}(\lambda\boldsymbol{q}, \frac{t}{\lambda^2} + \Delta t)/\lambda q \,. \tag{4.24}$$

where λ is a scaling parameter and where $\mathcal{A}^{\boldsymbol{q}}$, $\mathcal{J}^{\boldsymbol{q}}$, $\mathcal{M}$, and $\mathcal{L}$ denote the tensor quantities previously specified in index notation as $A_i^{\boldsymbol{q}}$, $\boldsymbol{J}_i^{\boldsymbol{q}}$, $\mathbf{M}_{ij}$, and $\mathbf{L}_{ij}$, respectively. The macroscopic limit can then be obtained as $\lambda \to 0$, which simultaneously ensures that Markovian time-dependence is recovered as Δt becomes negligible

$$\lim_{\lambda\to 0} \mathcal{L}(\lambda\boldsymbol{q}, \frac{t}{\lambda^2} + \Delta t)/\lambda q = \lim_{\lambda\to 0} \mathcal{L}(\lambda\boldsymbol{q}, \frac{t}{\lambda^2})/\lambda q \,. \tag{4.25}$$

In this way, recognizing self-similarity allows the Green-Kubo relations to be restated in the limit form

$$\mathbf{M}_{ij} = \lim_{t\to 0}\lim_{\lambda\to 0} \sum_{k=1}^{m} g_{ik}(\lambda\boldsymbol{q})\mathbf{L}_{kj}(\lambda\boldsymbol{q}, t/\lambda^2) \,, \tag{4.26}$$

which, unlike equation (4.17), encapsulates the requirements that $\boldsymbol{q} \to 0$ and that Δt must satisfy the separation of timescales (4.9). Note that the limits in equation (4.26) do not commute. It is only after taking $\lambda \to 0$ that Δt is rescaled to a discontinuity at the time origin, and thus the flux correlation function $\mathcal{L}(\lambda\boldsymbol{q}, \frac{t}{\lambda^2})/\lambda q$ yields the correct (nonzero) transport coefficient in the limit $t \to 0$. This non-commutativity of the limits is illustrated in Figure 4.1c, where it is seen that evaluating $\lim_{t\to 0} \mathcal{L}(\lambda\boldsymbol{q}, \frac{t}{\lambda^2})/\lambda q = 0$ for any finite λ. To summarize, self-similarity provides a means of reconciling the apparent contradiction between microscopically non-Markovian dynamics and macroscopically Markovian constitutive laws.

The Green-Kubo relations (4.17), (4.20), and (4.26), by providing a quantitative connection between microscopic fluctuations and macroscopic transport, also reveal the microscopic symmetries involved in odd transport. In particular, in equations (4.19) and (4.22) time-reversal symmetry leads to the reciprocal relations

$$\mathbf{L}_{ij} = \mathbf{L}_{ji}^T \,. \tag{4.27}$$

In the case where $m = 1$, *i.e.* where only one transported quantity is of interest, we find that for dynamics obeying time-reversal symmetry,

$$\mathbf{M}_{11}^{\text{odd}} = \frac{1}{2}(\mathbf{M}_{11} - \mathbf{M}_{11}^{T}) = 0\,. \tag{4.28}$$

Therefore, in this common case time-reversal symmetry breaking (at the level of the flux correlations) is indeed a prerequisite for odd transport. On the other hand, for cross-coupling coefficients $\mathbf{M}_{ij}$ where $i \neq j$, it is in principle possible to have $\mathbf{M}_{ij}^{\text{odd}} \neq 0$ without breaking time-reversal symmetry.

4.4 Odd diffusion in concentrated solutions

The general constitutive equation governing the flux of a species $\boldsymbol{J}$ that arises in response to gradients in density ρ is Fick's Law

$$\boldsymbol{J}(\boldsymbol{r}, t) = -\mathbf{D}(\rho)\boldsymbol{\nabla}\rho(\boldsymbol{r}, t) \tag{4.29}$$

where $\rho(\boldsymbol{r}, t) \in \mathbb{R}$ is the density field, $\boldsymbol{J}(\boldsymbol{r}, t) \in \mathbb{R}^d$ is the flux and $\mathbf{D} \in \mathbb{R}^{d\times d}$ is the diffusivity. Any non-linearity in the constitutive relation (4.29) is accounted for through the density dependence of $\mathbf{D}(\rho)$. For small perturbations $\delta\rho(\boldsymbol{r}, t)$ about the constant and homogeneous density $\bar{\rho}$, equation (4.29) obtains the linear form of (4.2) as

$$\boldsymbol{J}(\boldsymbol{r}, t) = -\mathbf{D}(\bar{\rho})\boldsymbol{\nabla}\delta\rho(\boldsymbol{r}, t) \tag{4.30}$$

For concentrated solutions, $\mathbf{D}$ is sometimes called the collective (or down-gradient) diffusivity. In the dilute limit $\bar{\rho} \to 0$, as interactions between particles of the diffusing species become negligible, the collective diffusivity and the self-diffusivity are identical.

The flux hypothesis (4.10) corresponding to equations (4.29)-(4.30) is

$$\langle \boldsymbol{J}^{\boldsymbol{q}}(\Delta t)\rho^{-\boldsymbol{q}}(0)\rangle = \mathbf{D}\cdot \mathrm{i}\boldsymbol{q}\langle \rho^{\boldsymbol{q}}\rho^{-\boldsymbol{q}}\rangle\,. \tag{4.31}$$

The flux and density fields may be expressed as phase variables for an N-particle system as

$$\rho(\boldsymbol{r}, t) = \sum_{i=1}^{N} \delta(\boldsymbol{r} - \boldsymbol{r}_i)\,, \tag{4.32}$$

$$\boldsymbol{J}(\boldsymbol{r}, t) = \sum_{i=1}^{N} v_i\delta(\boldsymbol{r} - \boldsymbol{r}_i)\,. \tag{4.33}$$

The corresponding Fourier modes follow from equation (4.5) as

$$\rho^{\boldsymbol{q}}(t) = \sum_{i=1}^{N} e^{-\mathrm{i}\boldsymbol{q}\cdot\boldsymbol{r}_i(t)} \tag{4.34}$$

$$\boldsymbol{J}^{\boldsymbol{q}}(t) = \sum_{i=1}^{N} \boldsymbol{v}_i(t)e^{-\mathrm{i}\boldsymbol{q}\cdot\boldsymbol{r}_i(t)}\,. \tag{4.35}$$

The correlation function appearing in equation (4.31) may then be expressed as

$$\langle \boldsymbol{J}^{\boldsymbol{q}}(t)\rho^{-\boldsymbol{q}}(0)\rangle = \sum_{i,j=1}^{N} \langle \boldsymbol{v}_i(t) e^{-\mathrm{i}\boldsymbol{q}\cdot(\boldsymbol{r}_i(t)-\boldsymbol{r}_j(0))}\rangle \,. \tag{4.36}$$

Recalling that $\mathbf{D}$ is real, we can reexpress equation (4.31) as

$$\begin{aligned} \mathbf{D}\cdot\boldsymbol{q} &= \Im\big[\langle\rho^{\boldsymbol{q}}\rho^{-\boldsymbol{q}}\rangle^{-1}\langle \boldsymbol{J}^{\boldsymbol{q}}(\Delta t)\rho^{-\boldsymbol{q}}(0)\rangle\big] \\ &= \frac{\sum_{ij}\langle \boldsymbol{v}_i(t)\sin\big(\boldsymbol{q}\cdot(\boldsymbol{r}_i(t)-\boldsymbol{r}_j(0))\big)\rangle}{\sum_{ij}\langle\sin^2\big(\boldsymbol{q}\cdot\boldsymbol{r}_i-\boldsymbol{r}_j\big)\big)\rangle + \langle\cos^2\big(\boldsymbol{q}\cdot(\boldsymbol{r}_i-\boldsymbol{r}_j)\big)\big)\rangle} \end{aligned} \tag{4.37}$$

where $\Im[\boldsymbol{y}]$ denotes the imaginary part of $\boldsymbol{y}\in\mathbb{C}^d$. Here he have used that $\langle\rho^{\boldsymbol{q}}\rho^{-\boldsymbol{q}}\rangle$ is real, since all particles are indistinguishable and thus the system is identical under exchange of particles i and j.

In the dilute limit, the off-diagonal ($i\neq j$) terms in the sums vanish, reducing equation (4.37) to

$$\mathbf{D}\cdot\boldsymbol{q} \overset{\text{dilute}}{=} \Im[\langle \boldsymbol{v}(\Delta t)e^{\mathrm{i}\boldsymbol{q}\cdot\boldsymbol{\Delta r}(\Delta t)}\rangle] = \langle \boldsymbol{v}(\Delta t)\sin\big(\boldsymbol{q}\cdot\boldsymbol{\Delta r}(\Delta t)\big)\rangle \,, \tag{4.38}$$

where $\boldsymbol{\Delta r}(\Delta t) = \boldsymbol{r}(\Delta t)-\boldsymbol{r}(0)$.

Considering the case of two-dimensional isotropic diffusion

$$D_{ij} = D_\parallel\delta_{ij} - D_\perp\epsilon_{ij} = \begin{bmatrix} D_\parallel & -D_\perp \\ D_\perp & D_\parallel \end{bmatrix} \tag{4.39}$$

and setting $\boldsymbol{q} = q\hat{\boldsymbol{e}}_x$ for simplicity, equation (4.38) yields the Green-Kubo relations

$$\begin{aligned} D_\parallel &\overset{\text{dilute}}{=} \langle v_x(\Delta t)\sin\big(q\Delta x(\Delta t)\big)\rangle/q && (4.40)\\ &= \langle v_x(0)\sin\big(q\Delta x(\Delta t)\big)\rangle/q \,, && (4.41)\\ D_\perp &\overset{\text{dilute}}{=} \langle v_y(\Delta t)\sin\big(q\Delta x(\Delta t)\big)\rangle/q && (4.42)\\ &= -\langle v_y(0)\sin\big(q\Delta x(\Delta t)\big)\rangle/q \,. && (4.43) \end{aligned}$$

The second equality in each of equations (4.40) and (4.42) follows from the even and odd time-dependence of the respective time-correlation functions. In the limit form of equation (4.26), these relations become

$$D_\parallel \overset{\text{dilute}}{=} \lim_{t\to0}\lim_{\lambda\to0}\langle v_x(0)\sin\big(\lambda q\Delta x(\Delta t/\lambda^2)\big)\rangle/\lambda q \,, \tag{4.44}$$

$$D_\perp \overset{\text{dilute}}{=} \lim_{t\to0}\lim_{\lambda\to0}\langle v_y(0)\sin\big(\lambda q\Delta x(\Delta t/\lambda^2)\big)\rangle/\lambda q \,. \tag{4.45}$$

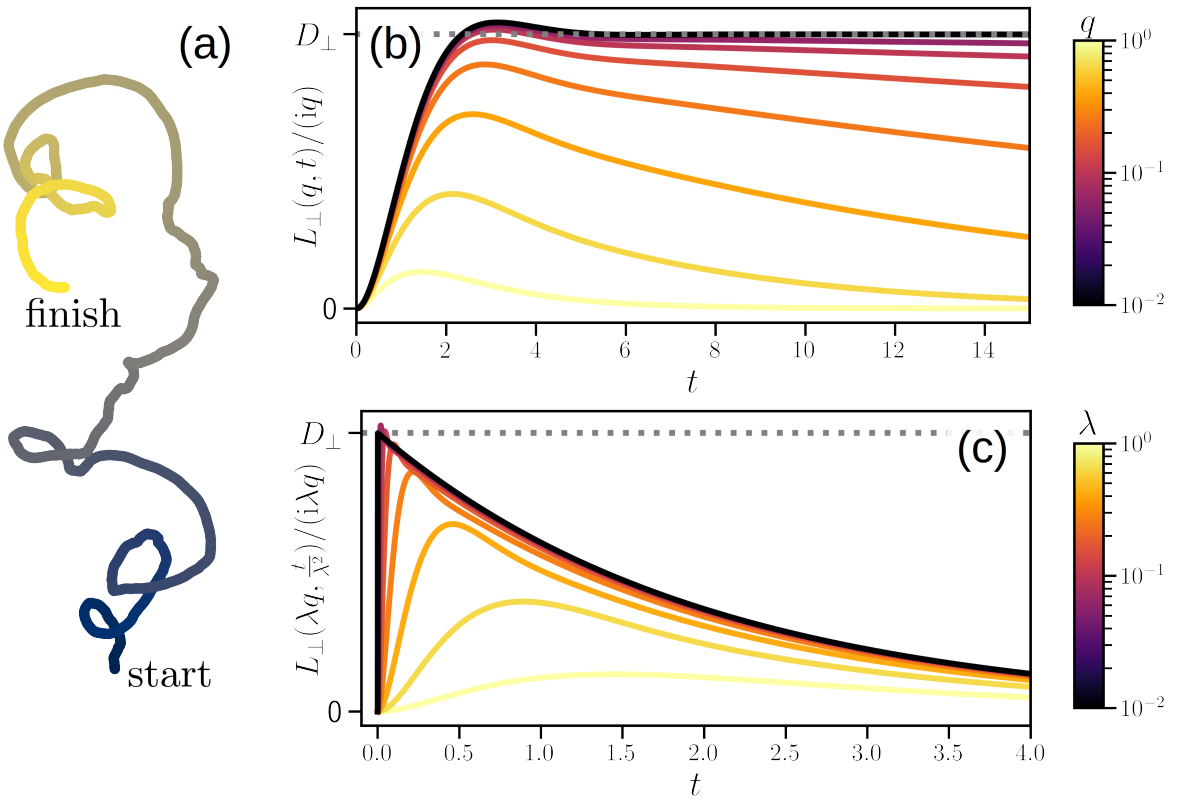

Figure 4.1: (a) A representative trajectory of chiral Langevin dynamics from equation (4.46). The particle displays counterclockwise chirality ($\gamma_\perp > 0$) as it moves from blue (dark) to yellow (light). (b) The time-correlation function $L_\perp(q,t) = \langle v_y(0)e^{iqx(t)}\rangle$ for the dilute chiral Langevin solution. For sufficiently small wave vector q, there exists an intermediate timescale Δt satisfying the separation of timescales (4.9), on which $L_\perp(q,t)$ converges to the exact value of the odd diffusivity (dotted line). (c) Rescaling the time-correlation function as $L_\perp(\lambda q, t/\lambda^2)$ causes the various curves to collapse in the macroscopic limit $\lambda \to 0$ and compresses the correlation time to a discontinuity at the origin. The exact value of the odd diffusivity (dotted line) is obtained by first taking the limit $\lambda \to 0$ and then $t \to 0$, as described in equation (4.45).

Chiral Langevin diffusion

In this section we solve for the exact correlation functions appearing in equations (4.40)-(4.42) in a simple model system exhibiting odd diffusion. We then show that carrying out the limits in equations (4.44)-(4.45) yields the correct result, for both the symmetric (even) and antisymmetric (odd) diffusion.

In particular, we consider a dilute solution of particles subject to underdamped Langevin

dynamics in two dimensions

$$\dot{\boldsymbol{v}}(t) = -\boldsymbol{\gamma}\boldsymbol{v}(t) + \boldsymbol{\eta}(t)\,, \tag{4.46}$$

where

$$\boldsymbol{\gamma} = \gamma_{\parallel}\boldsymbol{\delta} + \gamma_{\perp}\boldsymbol{\epsilon} \tag{4.47}$$

is the isotropic friction on the particle due to interactions with its environment. The antisymmetric friction $\gamma_\perp$ plays an identical role to the Lorentz force in a system of particles with charge q moving in the plane normal to a magnetic field B, in which case $\gamma_\perp = qB$. In a very different context, equation (4.46) with asymmetric friction was recently used to describe the stochastic dynamics of the hair bundle found in vertebrate ears [104]. More generally, the presence of antisymmetric friction can be a consequence of chiral dynamics occurring at the level of the bath, as was shown in Chapter 2.4 for a tracer particle diffusing in a bath of chiral active dumbbells. A typical particle trajectory for the dynamics in equation (4.46) is shown in Figure 4.1a, where $\gamma_\perp > 0$ results in counterclockwise chirality of the particle.

The noise $\boldsymbol{\eta}$ is assumed to be delta-correlated, such that $\langle \boldsymbol{\eta}(t)\boldsymbol{\eta}(t')\rangle = \mathbf{Q}\delta(t-t')$. Equation (4.46) admits the solution

$$\boldsymbol{v}(t) = e^{-\boldsymbol{\gamma}t}\boldsymbol{v}(0) + \int_0^t dt'\; e^{-\boldsymbol{\gamma}(t-t')}\boldsymbol{\eta}(t')\,, \tag{4.48}$$

where $\boldsymbol{v}(0)$ is the initial velocity. The same-time velocity correlation tensor is then

$$\langle \boldsymbol{v}(t)\boldsymbol{v}^T(t)\rangle = e^{-\boldsymbol{\gamma}t}\langle \boldsymbol{v}(0)\boldsymbol{v}^T(0)\rangle e^{-\boldsymbol{\gamma}^T t} + \int_0^t dt' \int_0^t dt''\; e^{-\boldsymbol{\gamma}(t-t')}\mathbf{Q}\delta(t'-t'')e^{-\boldsymbol{\gamma}^T(t-t'')} \tag{4.49}$$

We require that after starting from any initial velocity, the particle should reach a steady state exhibiting Maxwell-Boltzmann statistics, such that

$$\lim_{t\to\infty}\langle \boldsymbol{v}(t)\boldsymbol{v}^T(t)\rangle = k_{\mathrm{B}}T\boldsymbol{\delta}\,. \tag{4.50}$$

Together with equation (4.49), this leads to the fluctuation-dissipation relation

$$\mathbf{Q} = 2\gamma_{\parallel}k_{\mathrm{B}}T\boldsymbol{\delta}\,, \tag{4.51}$$

where it is seen that the noise, unlike the friction, is symmetric, and moreover independent of $\gamma_\perp$.

The time-correlation function from equation (4.38) can be expressed as

$$\langle \boldsymbol{v}(0)e^{\mathrm{i}\boldsymbol{q}\cdot\boldsymbol{r}(t))}\rangle = \int d\boldsymbol{v}_0\, d\boldsymbol{r}\, P(\boldsymbol{r},t|\boldsymbol{v}_0,0)W_{ss}(\boldsymbol{v}_0)\boldsymbol{v}_0 e^{-\mathrm{i}\boldsymbol{q}\cdot\boldsymbol{r}}\,, \tag{4.52}$$

where $P(\boldsymbol{r},t|\boldsymbol{v}_0,0)$ denotes the transition probability of observing the undergoing a displacement $\boldsymbol{r}$ in the time interval t conditioned on beginning with velocity $\boldsymbol{v}_0$, which is distributed in the steady state according to the Maxwell-Boltzmann distribution

$$W_{ss}(\boldsymbol{v}_0) = \frac{1}{2\pi k_{\mathrm{B}}T}\exp\big[-\frac{|\boldsymbol{v}_0|^2}{2k_{\mathrm{B}}T}\big]\,. \tag{4.53}$$

Following the original derivation of S. Chandrasekhar [105], the transition probability is seen to be Gaussian-distributed:

$$P(\boldsymbol{r},t|\boldsymbol{v}_0,0) = \frac{1}{2\pi\sigma_r(t)}\exp\big[-\frac{|\boldsymbol{r}-\mathbf{G}(t)\boldsymbol{v}_0|^2}{2\sigma_r^2(t)}\big]\,, \tag{4.54}$$

$$\mathbf{G}(t) = -\boldsymbol{\gamma}^{-1}\big[e^{-\boldsymbol{\gamma}t}-\boldsymbol{\delta}\big]\,, \tag{4.55}$$

$$\sigma_r^2(t) = \frac{2k_\mathrm{B}T\gamma_\parallel}{\gamma_\parallel^2+\gamma_\perp^2}\Bigg[t+\frac{1}{2\gamma_\parallel(1-e^{-2\gamma_\parallel t})} \tag{4.56}$$

$$-\big\{e^{-\boldsymbol{\gamma}t}\boldsymbol{\gamma}^{-1}(e^{\boldsymbol{\gamma}t}-\boldsymbol{\delta})+e^{-\boldsymbol{\gamma}^T t}(\boldsymbol{\gamma}^T)^{-1}(e^{\boldsymbol{\gamma}^T t}-\boldsymbol{\delta})\big\}:\boldsymbol{\delta}/2\Bigg]\,. \tag{4.57}$$

Inserting equations (4.50) and (4.54) into equation (4.52) and evaluating using a Gaussian integral identity yields

$$\langle\boldsymbol{v}(0)e^{\mathrm{i}\boldsymbol{q}\cdot\boldsymbol{r}(t)}\rangle = k_\mathrm{B}T\exp\Bigg[-\frac{1}{2}\sigma_r^2(t)|\boldsymbol{q}|^2\Bigg]\exp\Bigg[-\frac{k_\mathrm{B}T}{2}\boldsymbol{q}^T\cdot\mathbf{G}(t)\mathbf{G}^T(t)\cdot\boldsymbol{q}\Bigg]\mathbf{G}(t)\cdot\mathrm{i}\boldsymbol{q}\,. \tag{4.58}$$

From isotropy, the orientation of $\boldsymbol{q}$ may be chosen arbitrarily. Setting $\boldsymbol{q}=q\hat{\boldsymbol{e}}_x$, the odd part of the correlation function is then

$$L_\perp(q,t) = \langle v_y(0)e^{iqx(t)}\rangle\,, \tag{4.59}$$

and the Green-Kubo relation (4.42) becomes

$$D_\perp = L_\perp(q,\Delta t)/iq\,. \tag{4.60}$$

$L_\perp(q,t)$ is plotted in Figure 4.1b, where it is seen that for sufficiently small q, there indeed exists an intermediate timescale Δt where the Green-Kubo relation (4.42) holds, supporting the validity of the flux hypothesis. Moreover, the limit form of the Green-Kubo relation (4.45) yields the exact result

$$\begin{aligned} D_\perp &= \lim_{t\to0}\lim_{\lambda\to0} L_\perp(\lambda q, t/\lambda^2)/i\lambda q \\ &= \lim_{t\to0}\lim_{\lambda\to0} k_\mathrm{B}TG_{xy}(t/\lambda^2) \\ &= k_\mathrm{B}T\frac{\gamma_\perp}{\gamma_\parallel^2+\gamma_\perp^2}\,. \end{aligned} \tag{4.61}$$

This is seen graphically in Figure 4.1c, where taking $\lambda\to0$ rescales the correlation time to a discontinuity at $t=0$, such that the correct diffusion coefficient is obtained upon subsequently evaluating the limit $t\to0$.

Finally, as noted before, the collective- and self-diffusivity are identical in the dilute limit. Thus, the result in equation (4.61) can be compared with the Green-Kubo relation for odd

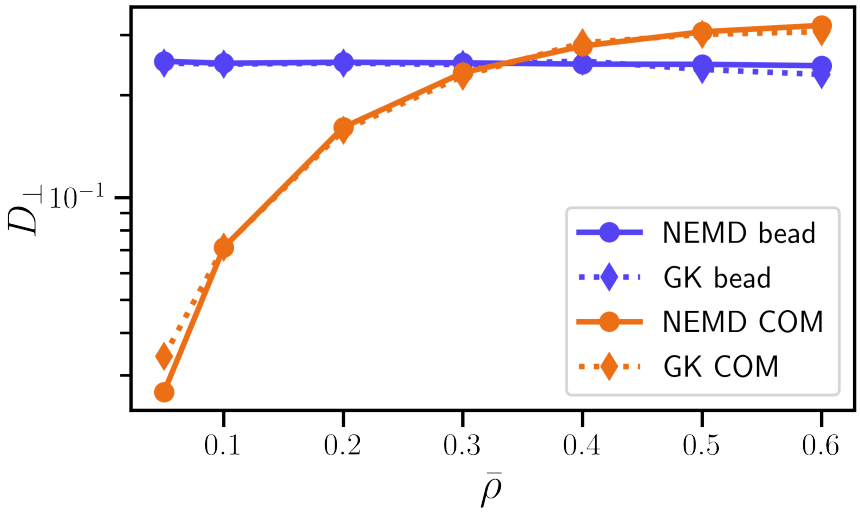

Figure 4.2: The odd collective diffusivity (see equation (4.30)) of a solution of chiral active dumbbells at different reference concentrations $\bar{\rho}$, computed from the Green-Kubo relation (4.37) (solid lines) and independent non-equilibrium molecular dynamics simulations (dashed lines). The choice between coarse-graining on the dumbbell beads versus the center-of-mass (COM) results in two equivalent but distinct continuum-level descriptions.

self-diffusion, as presented in Chapter 2. Using equation (4.48) and (4.53), the self-diffusion tensor evaluates to

$$\mathbf{D} = \int_0^\infty dt\ \langle \boldsymbol{v}(t)\boldsymbol{v}^T(0)\rangle = \int_0^\infty dt\ k_\mathrm{B}T e^{-\boldsymbol{\gamma}t} = k_\mathrm{B}T\boldsymbol{\gamma}^{-1}\,, \tag{4.62}$$

which, for the isotropic friction tensor in equation (4.47), matches the result obtained for collective diffusion from the flux hypothesis in equation (4.61).

Collective diffusion of chiral active dumbbells

As described in the beginning of this section, the collective (or down-gradient) diffusivity governs the flux arising in response to density (i.e. concentration) gradients of the diffusing species. The collective- and self-diffusivity are identical in the dilute limit, but in concentrated solutions, interactions among particles of the diffusing species cannot be neglected. Repulsive interactions, for example, will generally lead to a collective diffusivity which is larger in magnitude than the self-diffusivity.

As a final validation of the flux hypothesis, we now turn to the case of odd collective diffusion in a concentrated solution. We revisit the chiral active dumbbell model system depicted in Figure 3.1 and described by equation (3.23). The collective odd diffusion for this system at $\mathrm{Pe} = 1$ is plotted in Figure 4.2 for two possible coarse-grained descriptions,

as computed through the Green-Kubo relation (4.37). In the first, each of the two beads composing a dumbbell are included individually in the definition of the density and flux

$$\begin{aligned}\rho^{\text{bead}}(\boldsymbol{r},t) &= \sum_{i=1}^{N}\sum_{\alpha=1}^{2}\delta\big(\boldsymbol{r}-\boldsymbol{r}_i^{\alpha}(t)\big)\,,\\ \boldsymbol{J}^{\text{bead}}(\boldsymbol{r},t) &= \sum_{i=1}^{N}\sum_{\alpha=1}^{2}\boldsymbol{v}_i^{\alpha}(t)\delta\big(\boldsymbol{r}-\boldsymbol{r}_i^{\alpha}(t)\big)\,.\end{aligned} \tag{4.63}$$

The index i runs over the N dumbbells in the system and α runs over the two beads in each dumbbell. In the second description, only the dumbbell center-of-mass (COM) is included

$$\begin{aligned}\rho^{\text{COM}}(\boldsymbol{r},t) &= 2\sum_{i=1}^{N}\delta\big(\boldsymbol{r}-\boldsymbol{r}_i^{\text{COM}}(t)\big)\,,\\ \boldsymbol{J}^{\text{COM}}(\boldsymbol{r},t) &= 2\sum_{i=1}^{N}\boldsymbol{v}_i^{\text{COM}}(t)\delta\big(\boldsymbol{r}-\boldsymbol{r}_i^{\text{COM}}(t)\big)\,,\end{aligned} \tag{4.64}$$

where $\boldsymbol{r}_i^{\text{COM}} = \frac{1}{2}(\boldsymbol{r}_i^1 + \boldsymbol{r}_i^2)$ and $\boldsymbol{v}_i^{\text{COM}} = \frac{1}{2}(\boldsymbol{v}_i^1 + \boldsymbol{v}_i^2)$. Odd transport coefficients are remarkable in that the choice of coarse-graining procedure, for instance the choice between equations (4.63) and (4.64), can dramatically affect the transport coefficients emerging in the continuum description [106]. This is illustrated in Figure 4.2, where the bead odd collective diffusion is a constant function of density, while the COM odd collective diffusion vanishes in the dilute limit. This can be understood by recognizing that the dumbbell center of mass obtains chirality in its dynamics only through collisions with other dumbbells. Finally, Figure 4.2 shows good agreement between measurements of the odd collective diffusivity obtained through non-equilibrium molecular dynamics (NEMD) simulations (see Appendix H) and those predicted from the equation (4.37). This result provides further validation of the flux hypothesis as a starting point for deriving Green-Kubo relations for odd transport coefficients in a broad class of systems extending beyond equilibrium.

4.5 Odd viscosity

As a final application of the flux hypothesis, we now derive the Green-Kubo relations for the six viscosity coefficients of an isotropic, two-dimensional fluid, including the odd viscosity, as originally obtained by Epstein and Mandadapu [30] and discussed in Chapter 3.4. For simplicity, we treat a fluid without internal spin, but which nonetheless can exhibit odd viscosity due to breaking of time-reversal symmetry. The Newtonian constitutive relation (3.3) then becomes

$$\delta T_{ij}(\boldsymbol{r},t) = \eta_{ijkl}\partial_l v_k(\boldsymbol{r},t)\,, \tag{4.65}$$

where again δT_{ij} is the deviatoric stress tensor (which excludes hydrostatic contributions), η_{ijkl} is the viscosity tensor, and $v_{k,l}$ is the velocity gradient. We can rewrite this constitutive

relation in the form of equation (4.2) as

$$\boldsymbol{t}_i = \sum_{j\in\{x,y\}} \mathbf{H}_{ij} \boldsymbol{\nabla} v_j \,, \tag{4.66}$$

where we have defined

$$\begin{aligned} \boldsymbol{t}_i &= \begin{bmatrix} \delta T_{ix} \\ \delta T_{iy} \end{bmatrix} \,, \; \boldsymbol{\nabla} v_j = \begin{bmatrix} v_{j,x} \\ v_{j,y} \end{bmatrix} \,, \\ \mathbf{H}_{ij} &= \begin{bmatrix} \eta_{ixjx} & \eta_{ixjy} \\ \eta_{iyjx} & \eta_{iyjy} \end{bmatrix} \,, \end{aligned} \tag{4.67}$$

for i and j indexing over the spatial components x and y. Making the appropriate identifications with equation (4.20) yields

$$\mathbf{H}_{ij} = \sum_{k\in\{x,y\}} g^{\circ}_{ik} \mathbf{L}^{\circ}_{kj} \,, \tag{4.68}$$

where

$$\mathbf{L}^{\circ}_{kj} = \frac{1}{V} \iint d\boldsymbol{r}\, d\boldsymbol{r}' \int_0^{\infty} dt \; \langle \boldsymbol{t}_k(\boldsymbol{r}, t) \boldsymbol{t}_j(\boldsymbol{r}', 0) \rangle \,, \tag{4.69}$$

and

$$g^{\circ}_{ik} = \frac{1}{V} \iint d\boldsymbol{r}\, d\boldsymbol{r}' \; \langle v_i(\boldsymbol{r}) v_k(\boldsymbol{r}') \rangle = \rho k_{\mathrm{B}} T_{\mathrm{eff}} \delta_{ik} \,. \tag{4.70}$$

The final equality in equation (4.70) defines an effective kinetic temperature $k_{\mathrm{B}}T_{\mathrm{eff}}$ and follows from isotropy, which specifies the form $g^{\circ}_{ik} = g^{\circ}_{\parallel}\delta_{ik} + g^{\circ}_{\perp}\epsilon_{ik}$, where we have defined $g_{\parallel} = \rho k_{\mathrm{B}} T_{\mathrm{eff}}$ and where the symmetry under exchange of $\boldsymbol{r}$ and $\boldsymbol{r}'$ sets $g^{\circ}_{\perp} = 0$.

Thus, equation (4.68) simplifies to

$$\mathbf{H}_{ij} = \frac{1}{\rho k_{\mathrm{B}} T_{\mathrm{eff}}} \frac{1}{V} \iint d\boldsymbol{r}\, d\boldsymbol{r}' \int_0^{\infty} dt \; \langle \boldsymbol{t}_i(\boldsymbol{r}, t) \boldsymbol{t}_j(\boldsymbol{r}', 0) \rangle \,. \tag{4.71}$$

Re-expanding the tensorial quantities into indicial notation through equation (4.67) yields

$$\eta_{ijkl} = \frac{1}{\rho k_{\mathrm{B}} T_{\mathrm{eff}}} \frac{1}{V} \iint d\boldsymbol{r}\, d\boldsymbol{r}' \int_0^{\infty} dt \; \langle \delta T_{ij}(\boldsymbol{r}, t) \delta T_{kl}(\boldsymbol{r}', 0) \rangle \,. \tag{4.72}$$

Finally, contracting both sides of this general Green-Kubo relation on both sides with the basis tensors defined in Table 3.1 yields Green-Kubo relations in agreement with those in

equations (3.8)-(3.13) for the case of no internal spin:

$$\lambda_1 = \frac{1}{4\rho k_{\mathrm{B}} T_{\mathrm{eff}}} \delta_{ij}\delta_{kl}\mathcal{T}^{ijkl}\,, \tag{4.73}$$

$$\lambda_2 = \frac{1}{4\rho k_{\mathrm{B}} T_{\mathrm{eff}}} (\delta_{ik}\delta_{jl} - \epsilon_{ik}\epsilon_{jl})\mathcal{T}^{ijkl}\,, \tag{4.74}$$

$$\lambda_3 = \frac{1}{4\rho k_{\mathrm{B}} T_{\mathrm{eff}}} \epsilon_{ij}\epsilon_{kl}\mathcal{T}^{ijkl}\,, \tag{4.75}$$

$$\lambda_4 = \frac{1}{4\rho k_{\mathrm{B}} T_{\mathrm{eff}}} (\epsilon_{ik}\delta_{jl} + \epsilon_{jl}\delta_{ik})\mathcal{T}^{ijkl}\,, \tag{4.76}$$

$$\lambda_5 = \frac{1}{4\rho k_{\mathrm{B}} T_{\mathrm{eff}}} (\epsilon_{ik}\delta_{jl} - \epsilon_{jl}\delta_{ik} + \epsilon_{ij}\delta_{kl} + \epsilon_{kl}\delta_{ij})\mathcal{T}^{ijkl}\,, \tag{4.77}$$

$$\lambda_6 = \frac{1}{4\rho k_{\mathrm{B}} T_{\mathrm{eff}}} (\epsilon_{ik}\delta_{jl} - \epsilon_{jl}\delta_{ik} - \epsilon_{ij}\delta_{kl} - \epsilon_{kl}\delta_{ij})\mathcal{T}^{ijkl}\,. \tag{4.78}$$

As in Chapter 3.4, we have defined

$$\mathcal{T}^{ijkl} = \frac{1}{V}\iint d\boldsymbol{r}\, d\boldsymbol{r}' \int_0^\infty dt\ \langle \delta T_{ij}(\boldsymbol{r}, t)\delta T_{kl}(\boldsymbol{r}', 0)\rangle\,. \tag{4.79}$$

Note that equations (4.73)-(4.78), which follow from the flux hypothesis, exhibit clean separation of the six viscosity coefficients, in contrast to equations (3.8)-(3.13), which follow from the regression hypothesis.

4.6 Conclusion

In this final chapter, we have proposed a general framework describing the statistical mechanics of boundary-driven odd transport phenomena. We began by introducing the flux hypothesis, a re-application of Onsager's regression hypothesis — namely, that microscopic averages should reproduce macroscopic transport phenomena — at the level of linear constitutive relations. The flux hypothesis provides a small but meaningful generalization Onsager's regression hypothesis, by connecting odd fluxes to microscopic fluctuations. From this starting point, we obtained Green-Kubo relations following a derivation paralleling that of Kubo, Yokota and Nakajima [74] and, more recently, that of Epstein and Mandadapu [30].

These Green-Kubo relations generalize to any odd transport phenomena, reproducing the existing formulas known to govern odd self-diffusion and odd viscosity, and moreover suggesting extensions to new areas of odd transport phenomena. Self-similarity of the correlation functions allowed the Green-Kubo relations to be posed in a limit form which simultaneously encapsulates the requirements for macroscopic (*i.e.* small wave vector) gradients and separation of timescales. Examination of the Green-Kubo relations reveals the conditions under which time-reversal symmetry breaking is a prerequisite for odd transport, and leads to a generalization of Onsager's reciprocal relations for odd boundary-driven transport coefficients.

Appendix A

Chiral random walk

In this appendix, we present derivations of the analytical expressions in the main text concerning the chiral random walk model. We begin by considering the balance equations for the joint probability densities of the particle occupying coordinates (x, y) at time t while moving in one of the four available directions indicated by $\{\rightarrow, \uparrow, \leftarrow, \downarrow\}$ with fixed speed v_0. For instance,

$$\begin{aligned} P_{\rightarrow}(x, y, t+\delta t) = P_{\rightarrow}(x-\delta x, y, t) + \delta t\big[&\Gamma_1 P_{\downarrow}(x, y, t) + \Gamma_2 P_{\leftarrow}(x, y, t) \\ &+\Gamma_3 P_{\uparrow}(x, y, t) - \gamma P_{\rightarrow}(x, y, t)\big]\,, \end{aligned} \tag{A.1}$$

where $\delta x = v_0 \delta t$ and $\gamma = \Gamma_1 + \Gamma_2 + \Gamma_3$ is the total turning frequency. Taking the limit $\delta t \to 0$ and repeating the process for the other directions yields the coupled master equations (2.15)-(2.18). We can solve the master equations by applying Fourier and Laplace transforms in space and time, respectively:

$$(s+\gamma)\tilde{P}_{\rightarrow}(\boldsymbol{k}, s) + \mathrm{i}k_x v_0 \tilde{P}_{\rightarrow}(\boldsymbol{k}, s) - \Gamma_1 \tilde{P}_{\downarrow}(\boldsymbol{k}, s) - \Gamma_2 \tilde{P}_{\leftarrow}(\boldsymbol{k}, s) - \Gamma_3 \tilde{P}_{\uparrow}(\boldsymbol{k}, s) = P_{\rightarrow}(\boldsymbol{k}, 0)\,, \tag{A.2}$$

$$(s+\gamma)\tilde{P}_{\uparrow}(\boldsymbol{k}, s) + \mathrm{i}k_y v_0 \tilde{P}_{\uparrow}(\boldsymbol{k}, s) - \Gamma_1 \tilde{P}_{\rightarrow}(\boldsymbol{k}, s) - \Gamma_2 \tilde{P}_{\downarrow}(\boldsymbol{k}, s) - \Gamma_3 \tilde{P}_{\leftarrow}(\boldsymbol{k}, s) = P_{\uparrow}(\boldsymbol{k}, 0)\,, \tag{A.3}$$

$$(s+\gamma)\tilde{P}_{\leftarrow}(\boldsymbol{k}, s) - \mathrm{i}k_x v_0 \tilde{P}_{\leftarrow}(\boldsymbol{k}, s) - \Gamma_1 \tilde{P}_{\uparrow}(\boldsymbol{k}, s) - \Gamma_2 \tilde{P}_{\rightarrow}(\boldsymbol{k}, s) - \Gamma_3 \tilde{P}_{\downarrow}(\boldsymbol{k}, s) = P_{\leftarrow}(\boldsymbol{k}, 0)\,, \tag{A.4}$$

$$(s+\gamma)\tilde{P}_{\downarrow}(\boldsymbol{k}, s) - \mathrm{i}k_y v_0 \tilde{P}_{\downarrow}(\boldsymbol{k}, s) - \Gamma_1 \tilde{P}_{\leftarrow}(\boldsymbol{k}, s) - \Gamma_2 \tilde{P}_{\uparrow}(\boldsymbol{k}, s) - \Gamma_3 \tilde{P}_{\rightarrow}(\boldsymbol{k}, s) = P_{\downarrow}(\boldsymbol{k}, 0)\,, \tag{A.5}$$

where the transforms are defined as

$$f(\boldsymbol{x}, t) = \frac{1}{2\pi} \int_{-\infty}^{\infty} d\boldsymbol{k}\ f(\boldsymbol{k}, t) e^{\mathrm{i}\boldsymbol{k}\cdot\boldsymbol{x}}\,, \tag{A.6}$$

$$f(\boldsymbol{x}, t) = \int_{0}^{\infty} ds\ \tilde{f}(\boldsymbol{x}, s) e^{st}\,. \tag{A.7}$$

To quantify $D_{\parallel}$, we ask how the total probability density $\tilde{P}(\boldsymbol{k}, s) = \tilde{P}_{\rightarrow}(\boldsymbol{k}, s) + \tilde{P}_{\uparrow}(\boldsymbol{k}, s) + \tilde{P}_{\leftarrow}(\boldsymbol{k}, s) + \tilde{P}_{\downarrow}(\boldsymbol{k}, s)$ spreads out in time from a point, allowing us to calculate the mean-squared displacement. To this end, we specify the isotropic initial conditions $P_{\rightarrow}(\boldsymbol{k}, 0) =$

$P_\uparrow(\boldsymbol{k},0) = P_\leftarrow(\boldsymbol{k},0) = P_\downarrow(\boldsymbol{k},0) = 1/4$ and consequently are free to choose any direction for $\boldsymbol{k}$. Arbitrarily setting $\boldsymbol{k} = k_x\hat{\boldsymbol{e}}_{\boldsymbol{x}}$ and solving algebraically yields

$$\tilde{P}(k_x,s) = \frac{2(2\gamma - 2\Gamma_2 + s)\big[(\Gamma_1-\Gamma_3)^2 + (\gamma+\Gamma_2+s)^2\big] + k_x^2 v_0^2(\gamma+\Gamma_2+s)}{2s(2\gamma-2\Gamma_2+s)\big[(\Gamma_1-\Gamma_3)^2+(\gamma+\Gamma_2+s)^2\big] + 2k_x^2v_0^2\big[(\gamma+s)^2-\Gamma_2^2\big]}\,. \tag{A.8}$$

We may then obtain the second moment of the probability density as

$$\langle \Delta\tilde{x}(s)^2\rangle = -\partial_{k_x}^2\tilde{P}(k_x,s)\big|_{k_x=0} = \frac{v_0^2(\gamma+\Gamma_2+s)}{s^2\big[(\Gamma_1-\Gamma_3)^2+(\gamma+\Gamma_2+s)^2\big]}\,. \tag{A.9}$$

Taking the diffusive limit $s\to 0$ and performing the inverse Laplace transform (A.7) yields an expression for the diffusion coefficient $D_\parallel$ from the mean-squared displacement relation in the third equality of (2.13) in the main text:

$$\lim_{t\to\infty}\langle \Delta x(t)^2\rangle = 2D_\parallel t = \left(\frac{v_0^2(\gamma+\Gamma_2)}{(\Gamma_1-\Gamma_3)^2+(\gamma+\Gamma_2)^2}\right)t\,. \tag{A.10}$$

As noted in the main text, because the diffusion equation (2.3) does not involve $D_\perp$, the second moment of $P(x,y,t)$ does not contain any direct information about $D_\perp$. Instead, from the expansion described in (2.23)-(2.24), we may consider the first moment when specifying both the initial position and initial velocity in equations (A.2)-(A.5). For example, to obtain $\langle x(t)\rangle_\rightarrow$ we set $P_\rightarrow(\boldsymbol{k},0) = 1$ and $P_\uparrow(\boldsymbol{k},0) = P_\leftarrow(\boldsymbol{k},0) = P_\downarrow(\boldsymbol{k},0) = 0$, and choose $\boldsymbol{k} = k_x\hat{\boldsymbol{e}}_{\boldsymbol{x}}$. Solving equations (A.2)-(A.5) as before and adding to obtain the total probability density yields

$$\tilde{P}(k_x,s) = \frac{(2\gamma-2\Gamma_2+s)\big[-\mathrm{i}k_xv_0(\gamma+\Gamma_2+s) + (\Gamma_1-\Gamma_3)^2+(\gamma+\Gamma_2+s)^2\big]}{s(2\gamma-2\Gamma_2+s)\big[(\Gamma_1-\Gamma_3)^2+(\gamma+\Gamma_2+s)^2\big] + k_x^2v_0^2\big[(\gamma+s)^2-\Gamma_2^2\big]}\,. \tag{A.11}$$

Note that, unlike in equation (A.8), $\tilde{P}(k_x,s)$ now has an imaginary part due to the asymmetry of the initial conditions. Differentiating in k_x obtains the first moment

$$\langle \tilde{x}(s)\rangle_\rightarrow = \mathrm{i}\partial_{k_x}\tilde{P}(k_x,s)\big|_{k_x=0} = \frac{v_0(s+\gamma+\Gamma_2)}{s\big[(s+\gamma+\Gamma_2)^2+(\Gamma_1-\Gamma_3)^2\big]}\,. \tag{A.12}$$

Taking the same approach but choosing instead $\boldsymbol{k} = k_y\hat{\boldsymbol{e}}_{\boldsymbol{y}}$, we find

$$\langle \tilde{y}(s)\rangle_\rightarrow = \mathrm{i}\partial_{k_y}\tilde{P}(k_y,s)\big|_{k_y=0} = \frac{v_0(\Gamma_1-\Gamma_3)}{s\big[(s+\gamma+\Gamma_2)^2+(\Gamma_1-\Gamma_3)^2\big]}\,. \tag{A.13}$$

Finally, introducing the notation $\omega = \Gamma_1 - \Gamma_3$ and $\nu = \Gamma_1 + 2\Gamma_2 + \Gamma_3$, and performing the inverse Laplace transform (A.7) on equations (A.12)-(A.13) leads to the logarithmic spiral form given in (2.25)-(2.26). The diffusion coefficients $D_\parallel$ and $D_\perp$ given in equations (2.27)-(2.28) then follow directly from the long-time response as $t\to\infty$.

One can understand the effect odd diffusivity may have on the concentration by constructing a boundary value problem. Let us consider a channel of length L whose top and bottom boundaries are impermeable and separated by a distance W, and to which particles are added at the left boundary and removed from the right boundary at a constant rate $J_0 W$. These boundary conditions suggest the ansatz $\boldsymbol{J}(x,y) = J_0 \hat{\boldsymbol{e}}_x$ for all (x,y). Then, from the constitutive relations of (4.29) and (4.39), we have

$$J_0 = -D_\parallel \partial_x C + D_\perp \partial_y C \,, \tag{A.14}$$

$$0 = -D_\parallel \partial_y C - D_\perp \partial_x C \,. \tag{A.15}$$

Upon defining the average concentration $C_0 = \frac{1}{LW}\int_0^L dx \int_0^W dy \; C(x,y) = C(0,0)$, equations (A.14)-(A.15) permit the solution

$$\begin{aligned} C^{\text{ss}}(x,y) &= C_0 + \frac{J_0}{D_\parallel^2 + D_\perp^2}\big(- D_\parallel x + D_\perp y\big) \\ &= C_0 + \frac{J_0}{v_0^2}\big(- \nu x + \omega y\big) \,. \end{aligned} \tag{A.16}$$

When $D_\perp \neq 0$, as seen from equation (A.16), asymmetric accumulation occurs along the impermeable channel walls giving rise to a linear concentration profile not only in the x-direction but in the y-direction as well.

We check this solution by running numerical simulations of the chiral random walk model with corresponding boundary conditions, where the probability density P is interpreted

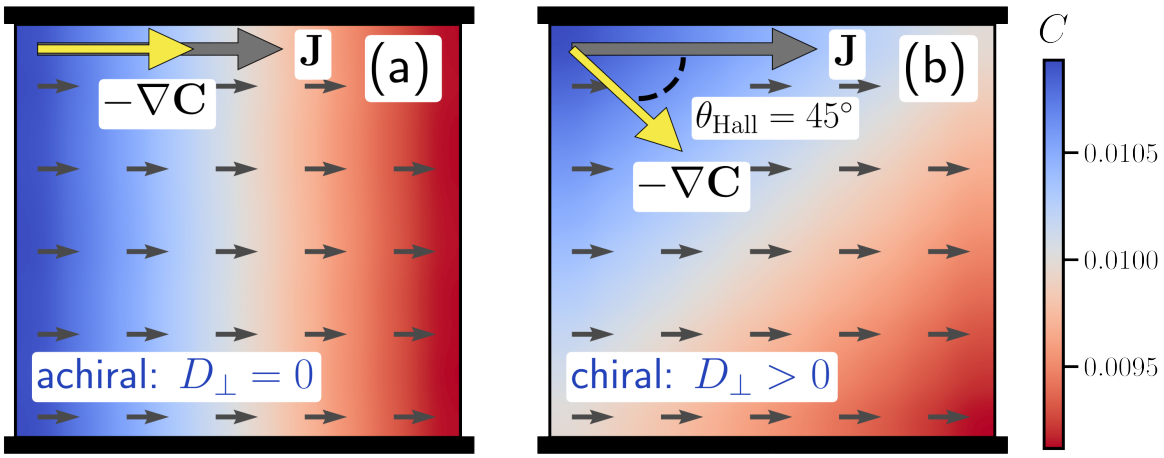

Figure A.1: Steady-state concentration profile for diffusive flux through a channel with impermeable walls obtained from numerical simulation of the chiral random walk model without odd diffusivity (a; achiral, $\Gamma_1 = 1, \Gamma_2 = 0, \Gamma_3 = 1$) and with odd diffusivity (b; chiral, $\Gamma_1 = 1, \Gamma_2 = 0, \Gamma_3 = 0$).

as the concentration C. Specifically, we simulate the dynamics of a particle governed by equations (2.15)-(2.18) with either $\Gamma_1 = 1, \Gamma_2 = 0, \Gamma_3 = 1$ (left- and right-turning) or $\Gamma_1 = 1, \Gamma_2 = 0, \Gamma_3 = 0$ (left-turning only) for a single particle in a box of dimensions $L = 10$, $W = 10$, advancing the dynamics in timesteps of $\delta t = 0.01$. Whenever the particle crosses the boundary at $x = L$, it is replaced at $x = 0$ on the next timestep. In Figure A.1 we plot the steady-state simulation average, finding the resulting flux field to be uniform while the concentration field depends linearly on x and y, in agreement with equation (A.16) where $C_0 = 0.01$ and $J_0 = 0.0001$.

Appendix B

Odd diffusion simulation details

Molecular dynamics simulations of a passive tracer particle diffusing in a chiral active bath composed of self-spinning dumbbells were performed in LAMMPS [96] with custom modifications[1] implementing the microscopic active forces and constant-flux boundary conditions. The nonconservative active force $\boldsymbol{f}_i^A$ in equation (2.29) affects only the dumbbell particles, with constant magnitude $|\boldsymbol{f}_i^A| = f^A$. The orientation of $\boldsymbol{f}_i^A$ is perpendicular to the bond vector $\boldsymbol{r}_i - \boldsymbol{r}_j$ for the bonded pair i and j, and directed oppositely ($\boldsymbol{f}_i^A = -\boldsymbol{f}_j^A$), inducing rotation of the dumbbell. Chiral active dumbbells are composed of two particles held together by a harmonic potential $U^{\mathrm{Harm}}(r) = \frac{1}{2}k(r - r_0)^2$, where r is the separation distance. We set the spring constant $k = 100$ and the reference bond length $r_0 = 1$. All particles (including the passive tracer) interact with non-bonded neighbors through a Weeks-Chandler-Andersen [97] potential defined by

$$U^{\mathrm{WCA}}(r) = \begin{cases} 4\epsilon\left[\left(\sigma/r\right)^{12} - \left(\sigma/r\right)^{6}\right] + \epsilon & r < 2^{1/6}\sigma \\ 0 & r \geq 2^{1/6}\sigma\,, \end{cases} \tag{B.1}$$

such that $U = U^{\mathrm{Harm}} + U^{\mathrm{WCA}}$ in equation (2.29). Here, m, σ and ϵ are the particle mass, diameter and interaction energy, providing characteristic mass, length and energy scales which define the Lennard-Jones units system. All simulation results are reported in Lennard-Jones units. The Langevin dynamics described in equation (2.29) were discretized with a velocity Verlet scheme with time step $\delta t = 0.005$ and bath temperature $k_{\mathrm{B}}T = 1.0$. The friction coefficient was set to $\zeta = 2.0$ for dumbbell particles and $\zeta = 0$ for the passive tracer particles, such that the tracers move ballistically between collisions. Simulations were performed at high dilution of the passive solute particles, where all simulations contained at least twenty times the number of active dumbbell solvent particles as passive tracer solute particles.

Calculation of the velocity autocorrelation tensor entering the Green-Kubo relations (2.13) and (2.14) was performed in a fully periodic system in a non-equilibrium steady state exhibit-

[1] Our simulation and analysis code is publicly available at https://github.com/mandadapu-group/active-matter.

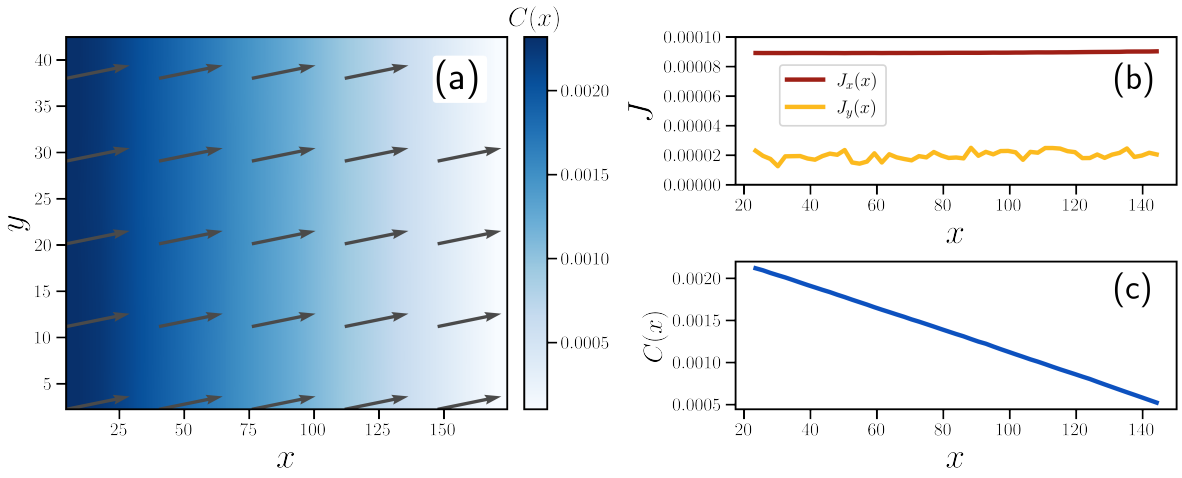

Figure B.1: Results of a typical boundary-driven flux simulation of diffusion of a passive tracer particle in a chiral active bath. Parameters $\rho_{\text{active}} = 0.1$ and $\text{Pe} = 16$ have been chosen arbitrarily. (a) The flux field (arrows) is spatially homogeneous with a component in the y-direction due to odd diffusivity, while the concentration $C(x)$ varies linearly in the x-direction. The profiles of the flux and the concentration along the x-direction are plotted in (b) and (c), respectively. All quantities are averaged over 2×10^8 timesteps.

ing stationarity and spatial homogeneity of all observables. Boundary-driven flux simulations were performed in a rectangular simulation box with special boundary conditions affecting the diffusing passive solute particles but not the active bath particles. A passive solute particle passing out of the simulation box through the right boundary behaves periodically, reappearing at the left boundary. A passive solute particle particle passing through the left boundary is reflected back into the simulation box. All interactions across the boundaries remain fully periodic. These conditions ensure a constant flux of particles across the simulation box, with the concentration varying linearly in x, as shown in Figure B.1 for a particular simulation with $\rho_{\text{active}} = 0.1$ and $\text{Pe} = 16$.

Appendix C

Linear response mobility tensor

The mobility tensor $\boldsymbol{\mu}$ provides a linear relation between a particle's drift velocity $\boldsymbol{u}$ and an applied body force $\boldsymbol{g}$ which, within the context of linear response theory, is expected to be valid for sufficiently small $\boldsymbol{g}$

$$u_i = \mu_{ij} g_j \,. \tag{C.1}$$

For passive systems, the mobility and diffusivity are ordinarily connected by the Einstein relation

$$D_{ij} = k_\mathrm{B} T \mu_{ij} \,. \tag{C.2}$$

Active matter systems need not obey such a relation. Indeed, one of the hallmarks of many active matter models is the "enhancement" of the diffusivity, due to the presence of active driving forces, over its value in the absence of such forces. When such behavior is present, the

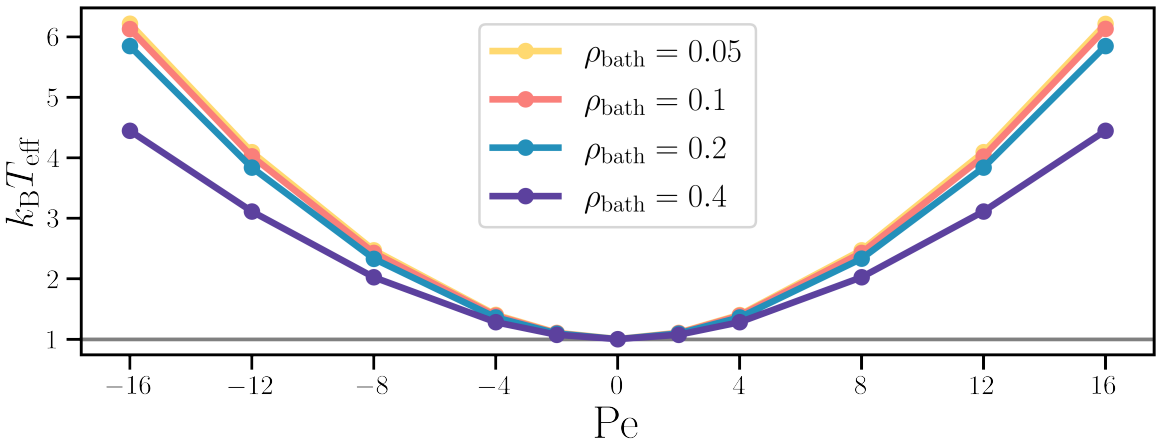

Figure C.1: Effective kinetic temperature of the passive tracer particle across all values of ρ_bath and Pe corresponding to the simulation results displayed in Figure 2.3 of the main text.

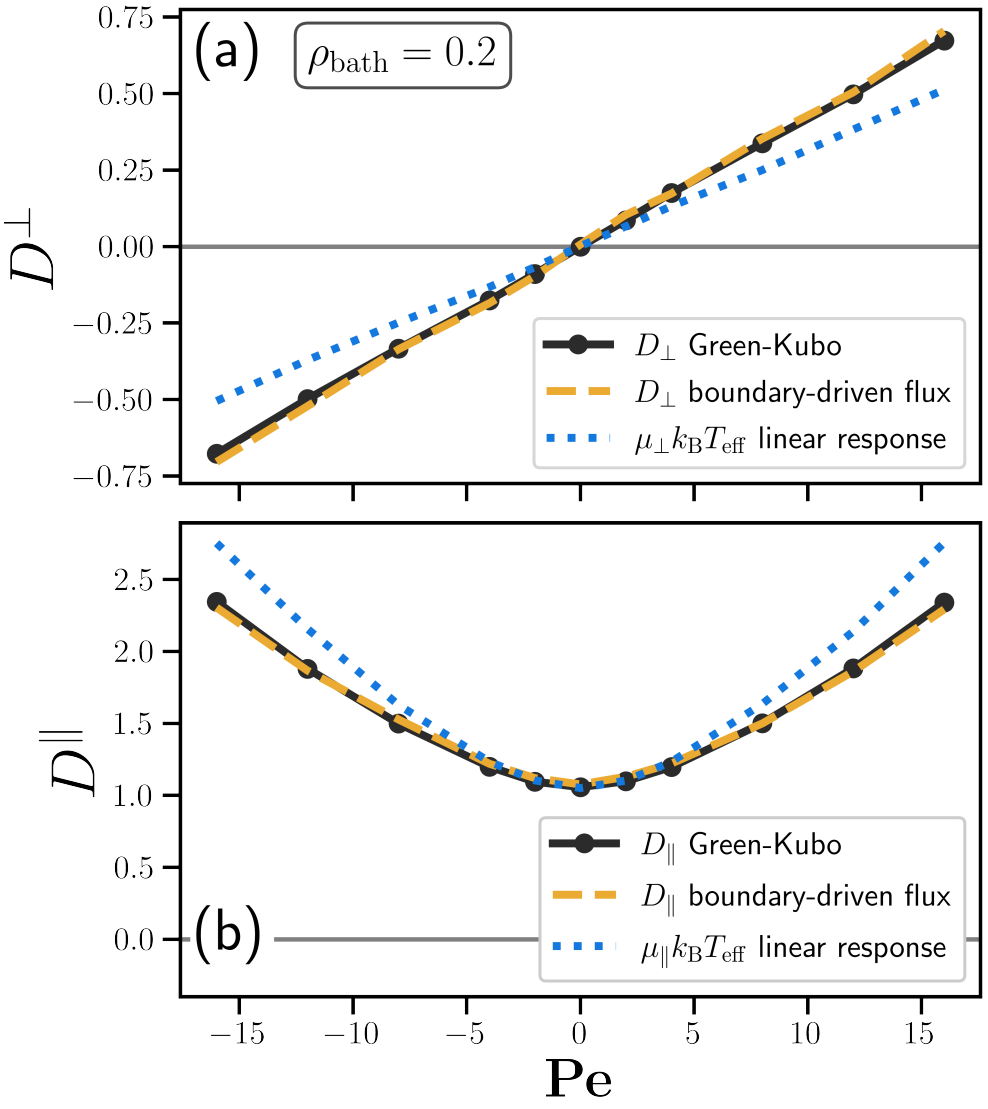

Figure C.2: Comparison of the diffusion coefficients for a passive tracer particle in an active dumbbell bath with $\rho_{\text{bath}} = 0.2$ obtained from Green-Kubo and boundary-driven flux calculations (solid lines and dashed lines, respectively) against those predicted from the from the mobility using the Einstein relation with an effective kinetic temperature.

Green-Kubo relations for the diffusivity coefficients in equations (2.13)-(2.14) are expected to remain valid while predictions of the diffusivity coefficients from linear response theory *via* the Einstein relation (C.2) cease to be applicable.

To illustrate this, let us briefly consider a simple model system which exhibits nonzero

odd diffusivity but whose mobility tensor contains no antisymmetric part. Namely, we consider an active Brownian particle in two dimensions in the overdamped regime, driven by internally-generated forces oriented along a director $\hat{\boldsymbol{u}}(t) = \big(\cos\theta(t),\ \sin\theta(t)\big)$, where $\theta(t)$ is the polar angle of the director. We consider the case where the evolution of the director has both a random part, due to interactions with the environment or internal noise, as well as a deterministic bias, due to an internally generated torque. This setup has been suggested as a minimal model for zooplankton such as *Daphnia*, which tend to steer either left or right as they swim in-plane [79, 83]. The Langevin equations for such a system are

$$\dot{\boldsymbol{r}} = v_0\hat{\boldsymbol{u}}\,, \tag{C.3}$$

$$\dot{\theta} = \omega_0 + \sqrt{2D_r}\xi_r(t)\,, \tag{C.4}$$

where $\xi_r(t)$ is Gaussian white noise characterized by $\langle\xi_r(t)\rangle = 0$ and $\langle\xi_r(t)\xi_r(t')\rangle = \delta(t-t')$.

The velocity correlation functions for this isotropic system are

$$\langle v_x(t)v_x(0)\rangle = \langle v_y(t)v_y(0)\rangle = v_0^2\langle\cos\theta(t)\cos\theta(0)\rangle \tag{C.5}$$

$$\langle v_x(t)v_y(0)\rangle = -\langle v_y(t)v_x(0)\rangle = v_0^2\langle\cos\theta(t)\sin\theta(0)\rangle \tag{C.6}$$

Using trigonometric product identities, one may show that

$$\langle\cos\theta(t)\cos\theta(0)\rangle = \frac{1}{2}\langle\cos\big(\theta(t)-\theta(0)\big) + \cos\big(\theta(t)+\theta(0)\big)\rangle = \frac{1}{2}\langle\cos\phi(t)\rangle \tag{C.7}$$

$$\langle\cos\theta(t)\sin\theta(0)\rangle = \frac{1}{2}\langle\sin\big(\theta(t)+\theta(0)\big) - \sin\big(\theta(t)-\theta(0)\big)\rangle = -\frac{1}{2}\langle\sin\phi(t)\rangle \tag{C.8}$$

where the second equality in both equations follows from isotropy and $\phi(t) = \theta(t) - \theta(0)$ is the displacement at time t of the angle from its initial value.

The Fokker-Planck equation corresponding to the Langevin equation (C.4) is [84]

$$\frac{\partial}{\partial t}f(\phi,t) = \omega_0\frac{\partial}{\partial\phi}f(\phi,t) + D_r\frac{\partial^2}{\partial\phi^2}f(\phi,t)\,, \tag{C.9}$$

where $f(\phi,t)$ is the probability density of the director angle. Defining the characteristic function of the angle distribution as

$$\tilde{f}(k,t) = \langle e^{\mathrm{i}k\phi}\rangle = \int_{-\infty}^{\infty} d\phi\ e^{\mathrm{i}k\phi}f(\phi,t)\,, \tag{C.10}$$

Equation (C.9) can be solved in Fourier space resulting in

$$\tilde{f}(k,t) = \exp\left[(\mathrm{i}k\omega_0 - k^2D_r)t\right]. \tag{C.11}$$

Thus,

$$\langle\cos\phi(t)\rangle = \mathrm{Re}\,\tilde{f}(1,t) = \cos(\omega_0 t)e^{-D_r t}\,, \tag{C.12}$$

$$\langle\sin\phi(t)\rangle = \mathrm{Im}\,\tilde{f}(1,t) = \sin(\omega_0 t)e^{-D_r t} \tag{C.13}$$

Finally, inserting equations (C.7)-(C.8) and (C.12)-(C.13) into the Green-Kubo relations (2.13)-(2.14) yields

$$D_{\parallel} = \frac{v_0^2}{2} \frac{D_r}{D_r^2 + \omega_0^2} \,, \tag{C.14}$$

$$D_{\perp} = \frac{v_0^2}{2} \frac{\omega_0}{D_r^2 + \omega_0^2} \,. \tag{C.15}$$

Note that the functional form is identical to that of the chiral random walk model in equations (2.27)-(2.28), elucidating the merits of this model in capturing the essential features of the odd diffusivity. Now, as the mechanisms generating active propulsive forces and steering torques were assumed to be "internal", *i.e.* not resulting from external interactions, the mobility tensor in this idealized model will be symmetric and independent of the values of v_0 and ω_0, for instance following Stokes' Law.

We now evaluate the applicability of an effective Einstein relation for the chiral active dumbbell bath model discussed in the main text, upon defining an effective temperature computed from the mean kinetic energy of the diffusing passive tracer particle (C.2):

$$k_{\mathrm{B}} T_{\mathrm{eff}} = \frac{1}{2} \langle |\boldsymbol{v}_{\mathrm{tracer}}|^2 \rangle \,. \tag{C.16}$$

The dependence of this temperature on Pe is plotted for all densities of the dumbbell bath in Figure C.1, corresponding to the simulation results plotted in Figure 2.3 of the main text. The temperature of the nonequilibrium stationary state is determined by the competition between active forces and dissipative Langevin forces and, more noticeably at higher dumbbell densities, collisions occurring between dumbbells.

The resulting relationship is plotted in Figure C.2, where we have defined the isotropic mobility tensor analogously to the diffusivity as $\mu_{ij} = \mu_{\parallel} \delta_{ij} - \mu_{\perp} \epsilon_{ij}$. We observe that the linear response prediction captures only the qualitative behavior of $D_{\perp}$ and $D_{\parallel}$, with the disagreement most pronounced at high Pe. Note, finally, that because the sign of the linear response error differs for $D_{\perp}$ and $D_{\parallel}$ in Figure C.2, no single choice of T_{eff} could simultaneously reconcile the disagreement for both diffusion coefficients.

Appendix D

Odd viscosity simulation details

To investigate the viscous behavior of a fluid composed of self-spinning dumbbells, we perform molecular dynamics simulations in LAMMPS [96], implementing our own modifications [1] to impose microscopic driving forces and compute the active stress $\boldsymbol{T}^{\mathrm{A}}$. All measured quantities in both the Green-Kubo and NEMD calculations are converged with respect to timestep and system size.

Particles interact with their non-bonded neighbors through a Weeks-Chandler-Andersen [97] potential defined by

$$V_{ij}^{\mathrm{WCA}}(r) = \begin{cases} 4\epsilon\left[\left(\sigma/r\right)^{12} - \left(\sigma/r\right)^{6}\right] + \epsilon & r < 2^{1/6}\sigma \\ 0 & r \geq 2^{1/6}\sigma\,. \end{cases} \tag{D.1}$$

Here, σ, ϵ and particle mass m are the characteristic length, energy, and mass scales, which are used to define the Lennard-Jones units system. All numerical settings and results in this Communication are reported in Lennard-Jones units. The two particles in a single dumbbell are held together by a harmonic potential $V(r) = \frac{1}{2}k(r - r_0)^2$ with spring constant $k = 100$ and reference length $r_0 = 1$.

Dynamics are evolved according to underdamped Langevin dynamics (3.23) with bath temperature $T = 1.0$ and friction $\zeta = 2.0$. We apply the Langevin bath interactions only along the x_2 direction, so as not to impede flow in the x_1 direction, and employ these conditions in both Green-Kubo and periodic Poiseuille simulations. We note that imposing bath interactions selectively along x_2 may lead to a violation of isotropy by aligning dumbbells along a preferred axis. In all simulations, however, we check that dumbbells have no preferred alignment by measuring the departure of the bond angle of a dumbbell projected onto $[0, \pi/2]$ from the reference value of $\pi/4$:

$$\delta\theta_i^{+} = \arctan\left(\frac{|\mathbf{d}_i \cdot \mathbf{e}_2|}{|\mathbf{d}_i \cdot \mathbf{e}_1|}\right) - \frac{\pi}{4}\,. \tag{D.2}$$

[1] We have published our simulation and analysis code at https://github.com/mandadapu-group/active-matter.

We find that in all simulations, $\max(|\langle \delta\theta_i^+ \rangle|) < 0.01$ radians, where angle brackets indicate averaging in time and maximization is in space. We also confirm that the density is indeed uniform in all periodic Poiseuille calculations. The relative spatial variation in the density is bounded in all simulations by $\left(\langle(\delta\rho)^2\rangle/\langle\rho^2\rangle\right)^{1/2} < 0.1\%$.

Appendix E

Green-Kubo formula for the shear viscosity

We also perform a derivation to obtain separate expressions for the shear and bulk viscosities. To this end, we begin with the following equation (also equation (127) in the SI of [30] in the absence of internal spin):

$$k^j k^l \eta_{ijkl} = \frac{1}{\rho_0 \mu} k^j k^l \int_0^\infty dt \ \langle \delta T^{ij}_{\mathbf{k}}(t) \delta T^{kl}_{-\mathbf{k}}(0) \rangle = \frac{1}{\rho_0 \mu} k^j k^l \mathcal{T}^{\mathbf{k}}_{ijkl} \,, \tag{E.1}$$

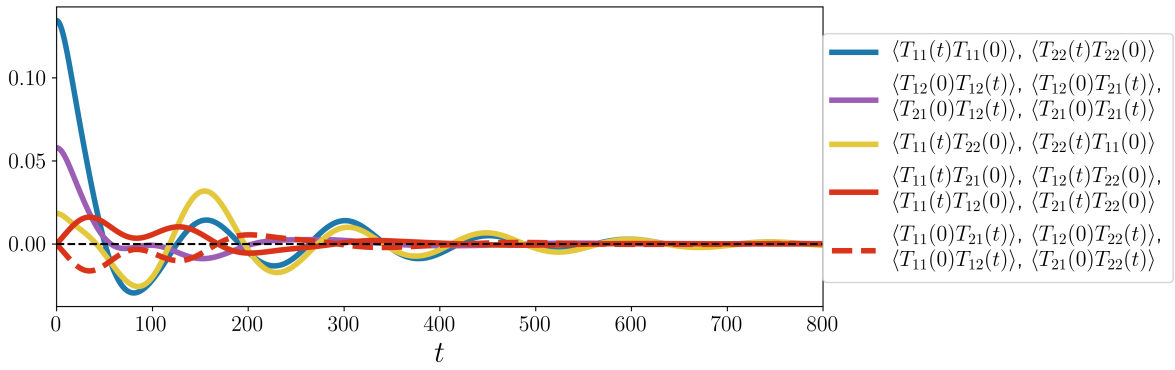

Figure E.1: The sixteen stress correlation functions computed at $\rho_0 = 0.4$, Pe $= 12$. Due to symmetries present in the chiral active dumbbell model, many of the correlation functions are identical, and are grouped as such. From this grouping, it is possible to ascertain that certain viscosity coefficients defined in (3.8)-(3.13) will vanish. For example, λ_3 depends on a sum of the correlation functions $\mathcal{T}_{1212} - \mathcal{T}_{1221} - \mathcal{T}_{2112} + \mathcal{T}_{2121}$. Here we see that these four correlation functions are identical, hence their sum will be zero. We further observe that the correlation functions contributing to the odd viscosity λ_4 go to zero in the static limit $t \to 0$, a consequence of the antisymmetry identified in (3.33).

where

$$\mathcal{T}^{\mathbf{k}}_{ijkl} = \int_0^\infty dt\ \langle \delta T^{ij}_{\mathbf{k}}(t) \delta T^{kl}_{-\mathbf{k}}(0) \rangle \,. \tag{E.2}$$

Following [30], we can obtain an equation for λ_1 and λ_2

$$\lambda_1 + 2\lambda_2 = \frac{1}{2\rho_0 \mu} \delta_{ik}\delta_{jk} \mathcal{T}^{\mathbf{k}}_{ijkl} \,, \tag{E.3}$$

in the limit of $\mathbf{k} \to \mathbf{0}$.

To separate λ_1 from λ_2 we return to (E.1) and contract both sides with $k^i k^k$ to obtain

$$k^i k^j k^k k^l \eta_{ijkl} = \frac{1}{\rho_0 \mu} k^i k^j k^k k^l \mathcal{T}^{\mathbf{k}}_{ijkl} \,. \tag{E.4}$$

The resulting equation holds independently for any choice of $\mathbf{k}$ in the limit $\mathbf{k} \to 0$. Now, we set $\mathbf{k} = k(\mathbf{e}_1 + \mathbf{e}_2)$ and $\mathbf{k} = k(\mathbf{e}_1 - \mathbf{e}_2)$ in (E.4) and sum the resulting equations to obtain

$$4\lambda_1 + 4\lambda_2 = \frac{1}{\rho_0 \mu} \big(\mathcal{T}^{\mathbf{k}}_{1111} + \mathcal{T}^{\mathbf{k}}_{1122} + \mathcal{T}^{\mathbf{k}}_{1212} + \mathcal{T}^{\mathbf{k}}_{1221} + \mathcal{T}^{\mathbf{k}}_{2112} + \mathcal{T}^{\mathbf{k}}_{2121} + \mathcal{T}^{\mathbf{k}}_{2211} + \mathcal{T}^{\mathbf{k}}_{2222} \big) \,, \tag{E.5}$$

which cannot be written in compact form as a contraction of Kronecker and Levi-Civita tensors with $\mathcal{T}^{\mathbf{k}}_{ijkl}$. Subtracting (E.5) from twice (E.3) and invoking the symmetry of the stress fluctuations gives

$$\begin{aligned} \lambda_2 &= \frac{1}{4\rho_0 \mu} (\mathcal{T}^{\mathbf{k}}_{1111} - \mathcal{T}^{\mathbf{k}}_{1122} - \mathcal{T}^{\mathbf{k}}_{2211} + \mathcal{T}^{\mathbf{k}}_{2222} + \mathcal{T}^{\mathbf{k}}_{1212} - \mathcal{T}^{\mathbf{k}}_{1221} - \mathcal{T}^{\mathbf{k}}_{2112} + \mathcal{T}^{\mathbf{k}}_{2121}) \\ &= \frac{1}{4\rho_0 \mu} (\mathcal{T}^{\mathbf{k}}_{1111} - \mathcal{T}^{\mathbf{k}}_{1122} - \mathcal{T}^{\mathbf{k}}_{2211} + \mathcal{T}^{\mathbf{k}}_{2222}) \,. \end{aligned} \tag{E.6}$$

Finally, returning to the definition of $\mathcal{T}^{\mathbf{k}}_{ijkl}$ in (E.1), and taking the zero wavevector limit $\mathbf{k} \to 0$ yields

$$\begin{aligned} \lambda_2 &= \frac{1}{4\rho_0 \mu} \int_0^\infty dt\ \langle (\delta T_{22}(t) - \delta T_{11}(t))(\delta T_{22}(0) - \delta T_{11}(0)) \rangle \\ &= \frac{1}{\rho_0 \mu} \int_0^\infty dt\ \langle \delta T_{12}(t) \delta T_{12}(0) \rangle \,, \end{aligned} \tag{E.7}$$

where, in obtaining the last equality, we use material isotropy to make the stress transformation $\boldsymbol{T'} = \boldsymbol{R^T T R}$ corresponding to a two-dimensional rotation $\boldsymbol{R}$ of angle $\pi/4$, for which $T'_{12} = \frac{1}{2}(T_{22} - T_{11})$. The last equality in (E.7) is the standard Green-Kubo relation for the shear viscosity. One may evaluate either of these expressions to compute the shear viscosity λ_2.

Appendix F

Decomposed contributions to the viscosity coefficients from the Irving-Kirkwood stress tensor

The Irving-Kirkwood procedure provides a natural decomposition of the stress tensor into kinetic, virial, and active molecular contributions (3.24). In Fig. F.1, we examine the component-wise stress contributions to the shear and odd viscosity in both Green-Kubo and periodic Poiseuille calculations. The stress appears twice in the correlation functions entering the Green-Kubo equations *via* (3.14), thus there are nine components contributing to the Green-Kubo viscosity coefficients, which we label λ^{KK}, λ^{KV}, λ^{KA}, λ^{VK}, λ^{VV}, λ^{VA}, λ^{AK}, λ^{AV} and λ^{AA}.

From (3.22), we define a decomposed shear viscosity as

$$\lambda_2^{XY} = \frac{1}{\rho_0 \mu} \int_0^\infty dt \ \langle \delta T_{12}^X(t) \delta T_{12}^Y(0) \rangle \,, \tag{F.1}$$

where $X, Y \in \{\mathrm{K}, \mathrm{V}, \mathrm{A}\}$ indicate the kinetic, virial and active parts. Similarly, the odd viscosity from (3.21) may be decomposed as

$$\lambda_4^{XY} = \frac{1}{4\rho_0 \mu} \int_0^\infty dt \ \langle \delta T_{ij}^X(t) \delta T_{kl}^Y(0) \rangle \epsilon_{ik} \delta_{jl} \,. \tag{F.2}$$

For periodic Poiseuille calculations, the decompositions contributing to the viscous coefficients simply involve the choice of whether to use $\boldsymbol{T}^{\mathrm{K}}$, $\boldsymbol{T}^{\mathrm{V}}$, or $\boldsymbol{T}^{\mathrm{A}}$ in (3.36) and (3.37), corresponding to λ^{K}, λ^{V}, and λ^{A}, respectively. We observe that the active stress $\boldsymbol{T}^{\mathrm{A}}$ plays a small but not insignificant role in both λ_2 and λ_4 at $\mathrm{Pe} \neq 0$. Notably, the dominant Green-Kubo contributions to λ_2 are λ^{KK} and λ^{VV} while the cross correlations λ^{KV} and λ^{VK} are dominant in λ_4.

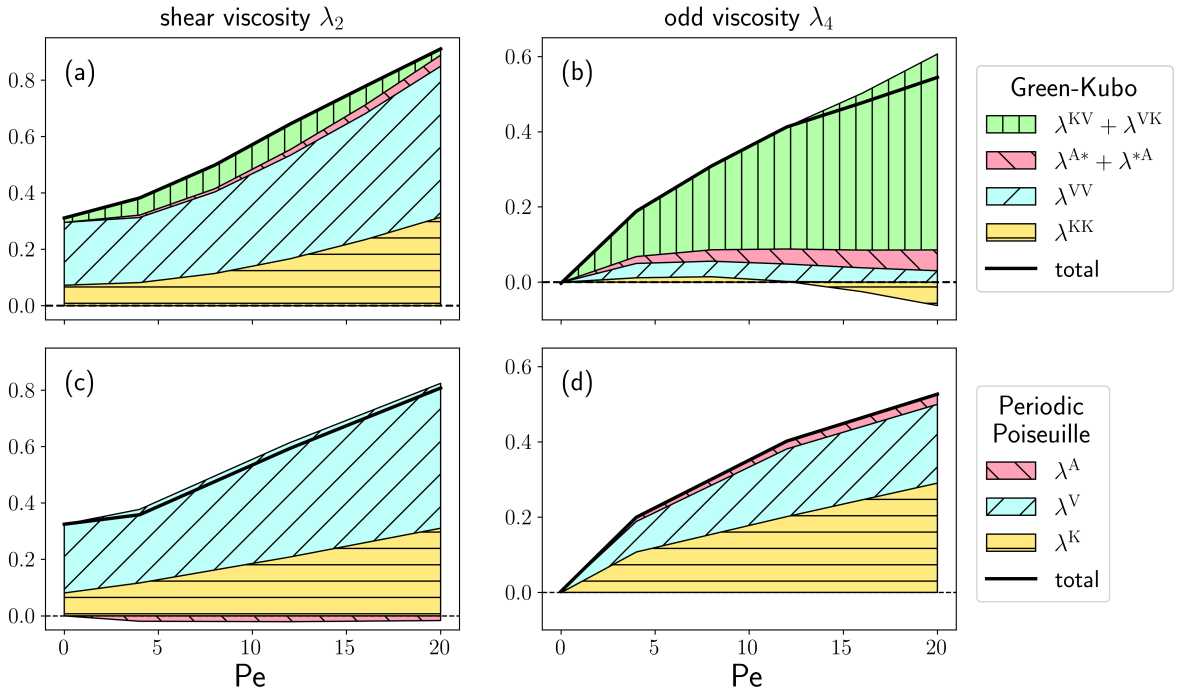

Figure F.1: Components of the stress contributing to Green-Kubo and Poiseuille calculations of the shear and odd viscosity at $\rho_0 = 0.4$ as a function of Pe. Figures (a) and (b) are the component-wise contributions to λ_2 and λ_4, respectively, from Green-Kubo calculations according to the decompositions in (F.1) and (F.2). Here, $\lambda^{A*}+\lambda^{*A} = \lambda^{AK}+\lambda^{AV}+\lambda^{KA}+\lambda^{VA}+\lambda^{AA}$. Figures (c) and (d) are the component-wise contributions to the λ_2 and λ_4, respectively, in periodic Poiseuille calculations. The solid black line indicates the total viscosity coefficient, obtained by adding the shaded areas above $y = 0$ and subtracting those below $y = 0$.

Appendix G

Periodic Poiseuille measurements

Non-equilibrium molecular dynamics simulations allow measurement of viscosity coefficients in direct analogy to experimental viscometry. For the chiral active dumbbell fluid, $\gamma_1 = \gamma_2 = \lambda_3 = \lambda_5 = \lambda_6 = 0$, resulting in decoupling of the linear and angular momentum balances and leading to modified Navier-Stokes equations

$$\rho \dot{v}_i = \lambda_1 v_{k,ki} + \lambda_2 v_{i,jj} + \lambda_4 \epsilon_{ik} v_{k,jj} - p_{,i} + \epsilon_{ij} p^*_{,j} + \rho g_i \,, \tag{G.1}$$

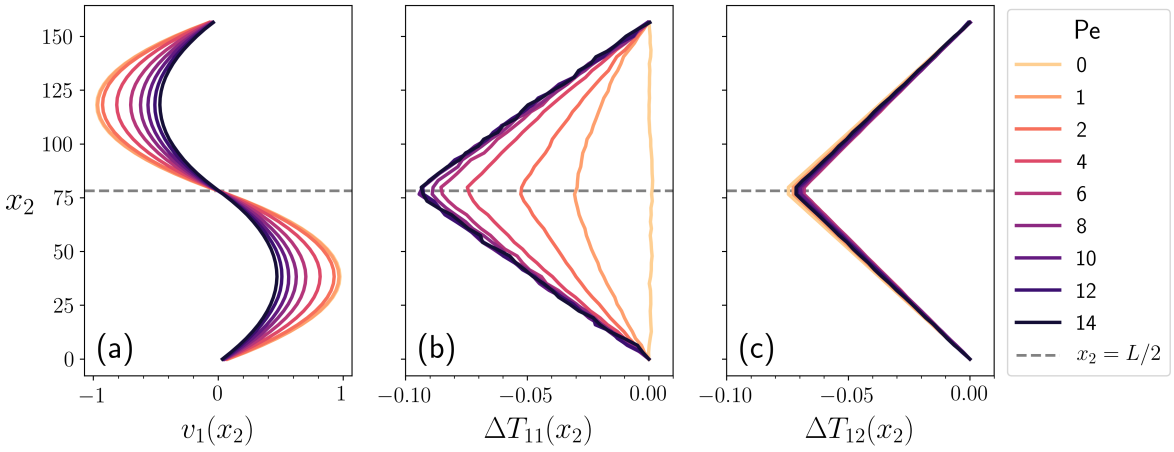

Figure G.1: Time-averaged velocity and stress profiles from periodic Poiseuille simulations at $\rho_0 = 0.4$ over a range of Pe. Axes are chosen to be consistent with the schematic in Fig. 3.3. Figure (a) shows the velocity profile $v_1(x_2)$, where the increase in shear viscosity with increasing Pe is apparent, as described in (G.7), in the decrease of the average velocity with increasing Pe. Figures (b) and (c) show $\Delta T_{11}(x_2) = T_{11}(x_2) - \Delta T_{11}(0)$ and $\Delta T_{12}(x_2) = T_{12}(x_2) - \Delta T_{12}(0)$, respectively. Spatial variation in T_{11} is seen to arise due to odd viscosity at Pe $\neq 0$ as in (G.11), while the slope of T_{12} is unaffected by Pe, supporting the ansatz of constant p^* used in (G.5) and (G.6).

with bulk viscosity λ_1, shear viscosity λ_2, odd viscosity λ_4, pressure p, and body force g_i.

In the periodic Poiseuille simulations, we subject the system to equal and opposite body forces in the x_1 direction across a rectangular channel of width $2L$, as depicted in Fig. 3.3. In general, the non-uniform normal stress $\Delta T_{11}(x_2)$, due to the odd viscosity, may cause compression and extension of the fluid such that the steady state density is non-uniform in the x_2 direction. Accordingly, we ensure that the body force g_1 driving the flow is sufficiently small in all simulations so that the density ρ is well-approximated as constant, as described in Appendix D. Therefore, we consider a steady state exhibiting incompressible flow, *i.e.,*

$$v_{i,i} = 0\,, \tag{G.2}$$

and obtain the simplified constitutive and Navier-Stokes equations:

$$T_{ij} = \lambda_2\big(v_{i,j} + v_{j,i}\big) + \lambda_4\big(\epsilon_{ik}v_{k,j} + \epsilon_{jk}v_{i,k}\big) - p\delta_{ij} + p^*\epsilon_{ij}\,, \tag{G.3}$$

and

$$\rho_0 v_{i,j}v_j = \lambda_2 v_{i,jj} + \lambda_4\epsilon_{ik}v_{k,jj} - p_{,i} + \epsilon_{ij}p^*_{,j} + \rho_0 g_i\,. \tag{G.4}$$

where ρ_0 is the uniform reference density.

We now seek a steady state analytical solution for the velocity and pressure profiles of a fluid between two plates separated by a distance L, subjected to a body force $\mathbf{g} = (g_1, 0)$, where g_1 is uniform in space. The solution is analogous to that of a planar Poiseuille flow, with boundary conditions $v_i = 0$ at $x_2 = 0$ and $x_2 = L$. Using the ansatz $v_1 = v_1(x_2)$, $v_2 = 0$, $p = p(x_2)$, and $p^* = \text{const}$, conditions which are observed in all non-equilibrium simulations considered in this study, one may find the steady state solution to be

$$v_1(x_2) = \frac{\rho_0 g_1}{2\lambda_2}x_2(L - x_2)\,, \tag{G.5}$$

and

$$p(x_2) = \frac{\lambda_4}{\lambda_2}\rho_0 g_1 x_2 + p_0\,, \tag{G.6}$$

where p_0 is an arbitrary reference pressure.

We see that the steady state velocity profile is identical to the usual solution for planar Poiseuille flow, remaining unaffected by odd viscosity. In fact it is always true that odd viscosity does not appear in the velocity profile in incompressible flows with no-slip boundary conditions [107]. The odd viscosity does appear, however, in a pressure gradient arising in the x_2-direction to maintain the no-penetration condition at the walls, *i.e.* to prevent flow in the x_2-direction. Our active dumbbell fluid simulations show parabolic velocity profiles consistent with (G.5) and (G.6) when subjected to equal and opposite body forces as shown in Fig. 3.3.

Integrating the velocity profile to get an average velocity $\bar{v} = \dfrac{1}{L}\int_0^L v_1(x_2)dx_2$, we obtain a convenient expression for computing the shear viscosity λ_2 in molecular simulations:

$$\lambda_2 = \frac{\rho_0 g_1 L^2}{12\bar{v}}\,. \tag{G.7}$$

As noted above, λ_4 does not appear in the velocity but in the stress (G.3). For the velocity profile (G.5),

$$T_{11} = -p + \lambda_4 v_{1,2}\,, \tag{G.8}$$

which results in

$$T_{11,2} = -p_{,2} + \lambda_4 v_{1,22}\,. \tag{G.9}$$

Using (G.4) in the x_2-direction, one may reduce (G.9) to

$$T_{11,2} = 2\lambda_4 v_{1,22} = -2\lambda_4 \frac{\rho_0 g_1}{\lambda_2}\,. \tag{G.10}$$

Finally, rearranging (G.10), λ_4 is obtained in terms of the slope of T_{11} as

$$\lambda_4 = \frac{T_{11,2}}{2v_{1,22}} = -\frac{\lambda_2 T_{11,2}}{2\rho_0 g_1}\,. \tag{G.11}$$

where T_{11} can be calculated using the Irving-Kirkwood formula (3.24) for the active dumbbell fluid.

Appendix H

Sinusoidal forcing NEMD measurement of odd collective diffusivity

To compute the odd collective diffusivity in periodic molecular dynamics simulations of the chiral active dumbbell fluid, we impose a sinusoidal perturbing force in the x-direction according to

$$\delta F(x) = \delta F_0 \sin\left(\frac{2\pi x}{L}\right)\hat{\boldsymbol{e}}_x \,, \tag{H.1}$$

where L is the total length of the simulation box. Periodic boundaries are imposed such that $\rho(x=0) = \rho(x=L)$ and $\rho(y=0) = \rho(y=W)$, where ρ is determined from the particle positions by the coarse-graining convention in either equation (4.63) or (4.64).

We may solve for the steady-state behavior using the ansatze $\rho(\boldsymbol{r}) = \rho(x)$ and $\boldsymbol{J} = J_y\hat{\boldsymbol{e}}_y$. Thus, in steady state the fluxes in the x-direction due to diffusion and the perturbative force cancel

$$J_x = 0 = -D_\parallel \frac{\partial \rho}{\partial x} + \frac{\rho \delta F(x)}{\gamma} \,, \tag{H.2}$$

where γ is the friction due to the Langevin bath. Expanding the density to perturbative order $\rho(x) = \bar{\rho} + \delta\rho(x)$, equation (H.2) admits the solution

$$\delta\rho(x) = -\frac{\delta F_0 \bar{\rho} L}{2\pi\gamma D_\parallel}\cos\left(\frac{2\pi x}{L}\right). \tag{H.3}$$

The flux in the y-direction is nonvanishing even in steady state, due to the odd diffusion. We measure the odd diffusivity as

$$D_\perp = -\frac{1}{\delta\rho}\int_0^{L/4} dx\ \langle J_y(x)\rangle \,, \tag{H.4}$$

where both $\delta\rho$ and the integrated flux are measured using the definitions in equation (4.63) or (4.64).

Bibliography

[1] Albert Einstein. "Investigations on the Theory of the Brownian Movement". In: *Annals of physics* 322 (1905), p. 549. ISSN: 0031-9112.

[2] Albert Einstein. *Investigations on the theory of the Brownian movement*. Edited with notes by R. Fürth, Translated by A. D. Cowper. 1956, pp. vi + 122. ISBN: 0-486-60304-0.

[3] Marian Smoluchowski. "On the Kinetic Theory of the Brownian Molecular Motion and of Suspensions". In: *Annals of physics* 326 (1906), p. 756.

[4] Paul Langevin. "On the Theory of Brownian Motion". In: *C. R. Acad. Sci.* 146 (1908).

[5] L. Onsager. "Reciprocal relations in irreversible processes. I." In: *Physical review* 37.4 (1931), pp. 405–426.

[6] L. Onsager. "Reciprocal relations in irreversible processes. II." In: *Physical review* 38.12 (1931), pp. 2265–2279.

[7] John S. Townsend. "The diffusion and mobility of ions in a magnetic field". In: *Proceedings of the royal society of London. Series A, Containing Papers of a Mathematical and Physical Character* 86.590 (1912), pp. 571–577. ISSN: 0950-1207.

[8] Rolf Landauer and John Swanson. "Diffusion Currents in the Semiconductor Hall Effect". In: *Physical Review* 91.3 (1953), pp. 555–560. ISSN: 0036-8075. DOI: 10.1126/science.201.4362.1217.

[9] J. E. Avron, Ruedi Seiler, and Petr G Zograf. "Viscosity of quantum Hall fluids". In: *Physical review letters* 75.4 (1995), p. 697.

[10] M. C. Marchetti et al. "Hydrodynamics of soft active matter". In: *Rev. Mod. Phys.* 85.3 (2013), p. 1143.

[11] J Prost, F Jülicher, and J-f Joanny. "Active gel physics". In: *Nature Physics* 11.February (2015).

[12] Masatoshi Nishikawa et al. "Controlling contractile instabilities in the actomyosin cortex". In: *Elife* 6 (2017), e19595.

[13] M. E. Cates et al. "Arrested phase separation in reproducing bacteria creates a generic route to pattern formation". In: *Proceedings of the National Academy of Sciences* 107.26 (2010), pp. 11715–11720.

[14] Andrey Sokolov and Igor S. Aranson. "Physical properties of collective motion in suspensions of bacteria". In: *Physical Review Letters* 109.24 (2012), pp. 1–5. ISSN: 00319007. DOI: 10.1103/PhysRevLett.109.248109.

[15] Amin Doostmohammadi, Sumesh P Thampi, and Julia M Yeomans. "Defect-mediated morphologies in growing cell colonies". In: *Physical review letters* 117.4 (2016), p. 048102.

[16] Tamás Vicsek et al. "Novel type of phase transition in a system of self-driven particles". In: *Physical review letters* 75.6 (1995), p. 1226.

[17] Andrea Cavagna and Irene Giardina. "Bird flocks as condensed matter". In: *Annual Review of Condensed Matter Physics* 5.1 (2014), pp. 183–207. ISSN: 19475462.

[18] J. Palacci et al. "Living crystals of light-activated colloidal surfers". In: *Science* (2013), p. 1230020.

[19] I. Buttinoni et al. "Dynamical clustering and phase separation in suspensions of self-propelled colloidal particles". In: *Phys. Rev. Lett.* 110.23 (2013), p. 238301.

[20] G. S. Redner, M. F. Hagan, and A. Baskaran. "Structure and dynamics of a phase-separating active colloidal fluid". In: *Physical review letters* 110.5 (2013), p. 055701.

[21] F. Ginot et al. "Nonequilibrium equation of state in suspensions of active colloids". In: *Phys. Rev. X* 5.1 (2015), p. 011004.

[22] Amélie Chardac et al. "Emergence of dynamic vortex glasses in disordered polar active fluids". In: *Proceedings of the National Academy of Sciences of the United States of America* 118.10 (2021), pp. 1–9. ISSN: 10916490. DOI: 10.1073/pnas.2018218118. arXiv: 2002.12893.

[23] V. Narayan, S. Ramaswamy, and N. Menon. "Long-lived giant number fluctuations in a swarming granular nematic". In: *Science* 317.5834 (2007), pp. 105–108.

[24] Nitin Kumar et al. "Flocking at a distance in active granular matter". In: *Nature communications* 5 (2014). ISSN: 20411723.

[25] M. E. Cates and J. Tailleur. "Motility-induced phase separation". In: *Annual reviews of condense matter physics* 6.1 (2015), pp. 219–244.

[26] Alexandre P. Solon, Hugues Chaté, and Julien Tailleur. "From phase to microphase separation in flocking models: The essential role of nonequilibrium fluctuations". In: *Physical Review Letters* 114.6 (2015), pp. 1–5. ISSN: 10797114. DOI: 10.1103/PhysRevLett.114.068101. eprint: 1406.6088.

[27] Debarghya Banerjee et al. "Odd viscosity in chiral active fluids". In: *Nature Communications* 8.1 (2017), pp. 1–12. ISSN: 20411723.

[28] Vishal Soni et al. "The odd free surface flows of a colloidal chiral fluid". In: *Nature physics* 15 (2019), pp. 1188–1194. ISSN: 1745-2473.

[29] Anton Souslov et al. "Topological waves in fluids with odd viscosity". In: *Physical review letters* 122.12 (2019), p. 128001.

[30] Jeffrey M. Epstein and Kranthi K. Mandadapu. "Time-reversal symmetry breaking in two-dimensional nonequilibrium viscous fluids". In: *Physical review E* 101.5 (2020), p. 052614. ISSN: 24700053.

[31] Cory Hargus et al. "Time reversal symmetry breaking and odd viscosity in active fluids: Green-Kubo and NEMD results". In: *The journal of chemical physics* 152 (2020).

[32] Tomer Markovich and Tom C. Lubensky. "Odd viscosity in active matter: microscopic origin and 3D effects". In: *Physical Review Letters* 127.4 (2020), p. 48001. ISSN: 1079-7114. DOI: 10.1103/PhysRevLett.127.048001. arXiv: 2006.05662. URL: http://arxiv.org/abs/2006.05662.

[33] Anton Souslov, Andrey Gromov, and Vincenzo Vitelli. "Anisotropic odd viscosity via a time-modulated drive". In: *Physical Review E* 101.5 (Sept. 2020). ISSN: 24700053. DOI: 10.1103/PhysRevE.101.052606. arXiv: 1909.08505. URL: https://arxiv.org/abs/1909.08505.

[34] Cory Hargus, Jeffrey M. Epstein, and Kranthi K. Mandadapu. "Odd Diffusivity of Chiral Random Motion". In: *Physical Review Letters* 127.17 (2021), p. 178001. ISSN: 10797114. DOI: 10.1103/PhysRevLett.127.178001. eprint: 2103.09958. URL: https://journals.aps.org/prl/abstract/10.1103/PhysRevLett.127.178001.

[35] Yuto Hosaka, Shigeyuki Komura, and David Andelman. "Non-reciprocal response of a two-dimensional fluid with odd viscosity". In: *Physical review E* 103.1 (2021), p. 042610.

[36] Qing Yang et al. "Topologically Protected Transport of Cargo in a Chiral Active Fluid Aided by Odd-Viscosity-Enhanced Depletion Interactions". In: *Physical Review Letters* 126.19 (2021), p. 198001. ISSN: 0031-9007. DOI: 10.1103/physrevlett.126.198001. URL: https://doi.org/10.1103/PhysRevLett.126.198001.

[37] David T. Limmer, Chloe Y. Gao, and Anthony R. Poggioli. "A large deviation theory perspective on nanoscale transport phenomena". In: *European Physical Journal B* 94.7 (2021), pp. 1–16. ISSN: 14346036. DOI: 10.1140/epjb/s10051-021-00164-1. arXiv: 2104.05194. URL: https://doi.org/10.1140/epjb/s10051-021-00164-1.

[38] Ming Han et al. "Fluctuating hydrodynamics of chiral active fluids". In: *Nature Physics* 17.November (2021), pp. 1260–1269. DOI: 10.1038/s41567-021-01360-7.

[39] Michel Fruchart et al. "The odd ideal gas: Hall viscosity and thermal conductivity from non-Hermitian kinetic theory". In: (2022), pp. 1–26. arXiv: 2202.02037. URL: http://arxiv.org/abs/2202.02037.

[40] Anthony R. Poggioli and David T. Limmer. "Odd mobility of a passive tracer in a chiral active fluid". In: (2022), pp. 1–5. arXiv: 2211.07003. URL: https://arxiv.org/abs/2211.07003v1.

[41] Carlos Floyd, Aaron R. Dinner, and Suriyanarayanan Vaikuntanathan. "Signatures of odd dynamics in viscoelastic systems: from spatiotemporal pattern formation to odd rheology". In: (2022). arXiv: 2210.01159. URL: http://arxiv.org/abs/2210.01159.

[42] Erik Kalz et al. "Collisions Enhance Self-Diffusion in Odd-Diffusive Systems". In: *Physical Review Letters* 129.9 (2022), p. 90601. ISSN: 10797114. DOI: 10.1103/PhysRevLett.129.090601. arXiv: 2206.13566. URL: https://doi.org/10.1103/PhysRevLett.129.090601.

[43] Hidde D. Vuijk et al. "Active Colloidal Molecules in Activity Gradients". In: *Physical Review E* 106.1 (2022), p. 014617. DOI: 10.1103/PhysRevE.106.014617. arXiv: 2205.07678. URL: http://arxiv.org/abs/2205.07678.

[44] Pietro Luigi Muzzeddu et al. "Active chiral molecules in activity gradients". In: *Journal of Chemical Physics* 157.13 (2022). ISSN: 10897690. DOI: 10.1063/5.0109817. arXiv: 2207.00315. URL: https://doi.org/10.1063/5.0109817.

[45] Kento Yasuda et al. "Time-correlation functions for odd Langevin systems". In: *Journal of Chemical Physics* 157.9 (2022). ISSN: 10897690. DOI: 10.1063/5.0095969. arXiv: 2202.03225. URL: https://doi.org/10.1063/5.0095969.

[46] Francisco Vega Reyes, Miguel A. López-Castaño, and Álvaro Rodríguez-Rivas. "Diffusive regimes in a two-dimensional chiral fluid". In: *Communications Physics* 5.1 (2022), pp. 1–7. ISSN: 23993650. DOI: 10.1038/s42005-022-01032-9. arXiv: 2202.08920.

[47] S. R. de Groot. *Thermodynamics of Irreversible Processes*. New York: Interscience Publishers Inc., 1951.

[48] S. R. de Groot and P. Mazur. *Non-Equilibrium Thermodynamics*. New York: Dover, 1984.

[49] I. Prigogine. *Introduction to Thermodynamics of Irreversible Processes*. John Wiley and Sons, New York, 1967.

[50] R. Kubo. *Statistical Mechanics*. New York: Interscience Publishers, 1965.

[51] Denis J. Evans and Gary P. Morriss. *Statistical Mechanics of Nonequilibrium Liquids*. 2008. ISBN: 9781921313226.

[52] T. Speck and U. Seifert. "Restoring a fluctuation-dissipation theorem in a nonequilibrium steady state". In: *Europhysics Letters* 74.3 (2006), pp. 391–396. ISSN: 02955075. DOI: 10.1209/epl/i2005-10549-4. arXiv: 0511696 [cond-mat].

[53] U. Seifert and T. Speck. "Fluctuation-dissipation theorem in nonequilibrium steady states". In: *Europhysics Letters* 89.1 (2010). ISSN: 02955075. DOI: 10.1209/0295-5075/89/10007. arXiv: 0907.5478.

[54] Marco Baiesi, Christian Maes, and Bram Wynants. "Fluctuations and response of nonequilibrium states". In: *Physical Review Letters* 103.1 (2009), p. 010602. ISSN: 00319007. DOI: 10.1103/PhysRevLett.103.010602. arXiv: 0902.3955.

[55] M. Baiesi and C. Maes. "An update on the nonequilibrium linear response". In: *New Journal of Physics* 15 (2013). ISSN: 13672630. DOI: 10.1088/1367-2630/15/1/013004. arXiv: 1205.4157.

[56] Christian Maes, Karel Netočný, and Bram Wynants. "Monotonic return to steady nonequilibrium". In: *Physical Review Letters* 107.1 (2011), p. 010601. ISSN: 00319007. DOI: 10.1103/PhysRevLett.107.010601.

[57] Sara Dal Cengio, Demian Levis, and Ignacio Pagonabarraga. "Linear Response Theory and Green-Kubo Relations for Active Matter". In: *Physical Review Letters* 123.23 (2019), p. 238003. ISSN: 10797114. DOI: 10.1103/PhysRevLett.123.238003. arXiv: 1907.02560. URL: https://doi.org/10.1103/PhysRevLett.123.238003.

[58] Hyun Myung Chun, Qi Gao, and Jordan M. Horowitz. "Nonequilibrium Green-Kubo relations for hydrodynamic transport from an equilibrium-like fluctuation-response equality". In: *Physical Review Research* 3.4 (2021). ISSN: 26431564. DOI: 10.1103/PhysRevResearch.3.043172. arXiv: 2103.09288.

[59] Felix Kummel et al. "Circular motion of asymmetric self-propelling particles". In: *Physical review letters* 110.19 (2013), p. 198302. ISSN: 00319007.

[60] Amir Nourhani et al. "Spiral diffusion of rotating self-propellers with stochastic perturbation". In: *Physical review E* 94.3 (2016), 030601(R). ISSN: 24700053.

[61] Thomas A. Witten and Haim Diamant. "A review of shaped colloidal particles in fluids: Anisotropy and chirality". In: *Reports on progress in physics* 83.11 (2020), p. 116601. ISSN: 13616633.

[62] Willow R Diluzio et al. "Escherichia coli swim on the right-hand side". In: *Nature* 435.June (2005), pp. 1271–1274.

[63] Knut Drescher et al. "Dancing Volvox : Hydrodynamic Bound States of Swimming Algae". In: *Physical review letters* 102.16 (2009), p. 168101.

[64] Ingmar H Riedel, Karsten Kruse, and Jonathon Howard. "Biophysics: A self-organized vortex array of hydrodynamically entrained sperm cells". In: *Science* 309.5732 (2005), pp. 300–303. ISSN: 00368075.

[65] Lyman Jr. Spitzer. *Physics of Fully Ionized Gases*. 2nd Edition. Interscience Publishers Inc., 1956.

[66] John W Bieber and William H Matthaeus. "Perpendicular diffusion and drift at intermediate cosmic-ray energies". In: *The astrophysical journal* 485 (1997), pp. 655–659.

[67] J. Giacalone and J. R. Jokipii. "The Transport of Cosmic Rays across a Turbulent Magnetic Field". In: *The astrophysical journal* 520.1 (1999), pp. 204–214. ISSN: 0004-637X.

[68] Iman Abdoli et al. "Correlations in multithermostat Brownian systems with Lorentz force". In: *New journal of physics* 22.9 (2020), p. 093057.

[69] Sara Bonella et al. "Time-reversal symmetry for systems in a constant external magnetic field". In: *Physical Review E* 96.1 (2017), p. 012160. DOI: 10.1103/PhysRevE.96.012160.

[70] Alessandro Coretti et al. "Time reversal and symmetries of time correlation functions". In: *Molecular Physics* 116.21-22 (2018), pp. 3097–3103. DOI: 10.1080/00268976.2018.1464674. URL: https://doi.org/10.1080/00268976.2018.1464674.

[71] H. Larralde. "Transport properties of a two-dimensional fffdfffdfffdchiralfffdfffdfffd persistent random walk". In: *Physical review E* 56.5 (1997), pp. 5004–5010. ISSN: 1063651X.

[72] Kosuke Hijikata, Ihor Lubashevsky, and Alexander Vazhenin. "Markovian Random Walks on Square Lattice with Constant Non-Symmetric Diffusion Coefficients". In: *Proceedings of the ISCIE International Symposium on Stochastic Systems Theory and its Applications* 2015 (2015), pp. 213–218. ISSN: 2188-4730.

[73] Donald L. Koch and John F. Brady. "The symmetry properties of the effective diffusivity tensor in anisotropic porous media". In: *Physics of fluids* 30.3 (1987), p. 642. ISSN: 00319171.

[74] R. Kubo, M. Yokota, and S. Nakajima. "Statistical-mechanical theory of irreversible processes. II. Response to Thermal Disturbance". In: *Journal of physical society of Japan* 12 (1957), pp. 1203–1211.

[75] R. Kubo. "Statistical-mechanical theory of irreversible processes. 1. General Theory and Simple Applications to Magnetic and Conduction Problems". In: *Journal of physical society of Japan* 12 (1957), pp. 570–586.

[76] K. Tomita and H. Tomita. "Irreversible circulation of fluctuation". In: *Progress of theoretical physics* 51.6 (1974), pp. 1731–1749. ISSN: 03759601.

[77] K. Tomita and H. Tomita. "Irreversible circulation of fluctuation". In: *Progress of theoretical physics* 53.5 (1975), p. 1546.

[78] Alireza Shakerpoor, Elijah Flener, and Grzegorz Szamel. "The Einstein effective temperature can predict the tagged active particle density". In: *The Journal of chemical physics* 154.184901 (2021). DOI: 10.1063/5.0049239. URL: https://doi.org/10.1063/5.0049239.

[79] Niko Komin, Udo Erdmann, and Lutz Schimansky-Geier. "Random walk theory applied to daphnia motion". In: *Fluctuation and Noise Letters* 4.1 (2004), pp. 151–160. ISSN: 02194775. DOI: 10.1142/S0219477504001756.

[80] Edward A. Codling, Michael J. Plank, and Simon Benhamou. "Random walk models in biology". In: *Journal of the royal society interface* 5.25 (2008), pp. 813–834. ISSN: 17425662.

[81] Jan L. Souman et al. "Walking Straight into Circles". In: *Current Biology* 19.18 (2009), pp. 1538–1542. ISSN: 09609822.

[82] Emma Bestaven, Etienne Guillaud, and Jean René Cazalets. "Is "Circling" Behavior in Humans Related to Postural Asymmetry?" In: *PLoS ONE* 7.9 (2012). ISSN: 19326203.

[83] P. Romanczuk et al. "Active brownian particles". In: *Eur. Phys. J. S.T.* 202.1 (2012), pp. 1–162.

[84] Hannes Risken. *The Fokker-Planck Equation*. 2nd Edition. Springer, 1989.

[85] I. Abdoli et al. "Nondiffusive fluxes in a Brownian system with Lorentz force". In: *Physical review E* 101.1 (2020), p. 012120. ISSN: 24700053.

[86] H. D. Vuijk et al. "Lorentz forces induce inhomogeneity and flux in active systems". In: *Physical Review Research* 2 (2020), p. 013320. DOI: 10.1103/physrevresearch.2.013320. arXiv: 1908.02577.

[87] Sven van Teeffelen and Hartmut Lowen. "Dynamics of a Brownian circle swimmer". In: *Physical review E* 78.2 (2008), 020101(R). ISSN: 15393755.

[88] Christian Weber et al. "Active motion assisted by correlated stochastic torques". In: *Physical review E* 84.1 (2011), p. 011132. ISSN: 15393755.

[89] Giorgio Volpe, Sylvain Gigan, and Giovanni Volpe. "Simulation of the active Brownian motion of a microswimmer". In: *American journal of physics* 82.7 (2014), pp. 659–664. ISSN: 0002-9505.

[90] Francisco J. Sevilla. "Diffusion of active chiral particles". In: *Physical review E* 94.6 (2016), p. 062120. ISSN: 24700053.

[91] Kiyoshi Kanazawa et al. "Loopy Lévy flights enhance tracer diffusion in active suspensions". In: *Nature* 579.7799 (2020), pp. 364–367. ISSN: 14764687.

[92] Amir Nourhani et al. "Chiral diffusion of rotary nanomotors". In: *Physical Review E* 87.5 (2013), 050301(R).

[93] E Kogan. "Lift force due to odd Hall viscosity". In: *Physical review E* 94.4 (2016), p. 043111.

[94] C. Reichhardt and C. J. O. Reichhardt. "Active microrheology, Hall effect, and jamming in chiral fluids". In: *Physical review E* 100.1 (2019), p. 012604. ISSN: 2470-0045.

[95] Katherine Klymko, Dibyendu Mandal, and Kranthi K Mandadapu. "Statistical mechanics of transport processes in active fluids: Equations of hydrodynamics". In: *The journal of chemical physics* 147.19 (2017), p. 194109.

[96] S. J. Plimpton. "Fast Parallel Algorithms for Short-Range Molecular Dynamics". In: *Journal of computational physics* 117 (1995). See also http://lammps.sandia.gov/, pp. 1–19.

[97] John D. Weeks, David Chandler, and Hans C. Andersen. "Role of Repulsive Forces in Determining the Equilibrium Structure of Simple Liquids". In: *The journal of chemical physics* 54.12 (1971), pp. 5237–5247.

[98] JS Dahler and LE Scriven. "Angular momentum of continua". In: *Nature* 192.4797 (1961), p. 36.

[99] Zhenghan Liao et al. "A mechanism for anomalous transport in chiral active liquids". In: *The Journal of chemical physics* 151.19 (2019), p. 194108.

[100] J. A. Backer et al. "Poiseuille flow to measure the viscosity of particle model fluids". In: *The journal of chemical physics* 122.15 (2005). ISSN: 00219606.

[101] R. Zwanzig. "Elementary derivations of time-correlation formulas for transport coefficients". In: *J. Chem. Phys.* 40 (1964), pp. 2527–2533.

[102] R Zwanzig. "Time-Correlation Functions and Transport Coefficients in Statistical Mechanics". In: *Annual Review of Physical Chemistry* 16.1 (1965), pp. 67–102. ISSN: 0066-426X.

[103] P. Mazur. "Onsagers's reciprocal relations and thermodynamics of irreversible processes". In: *Periodica Polytechnica Chemical Engineering* 41.2 (1997), pp. 197–204. ISSN: 15873765.

[104] L. Dinis et al. "Fluctuation-response theorem for the active noisy oscillator of the hair-cell bundle". In: *Physical Review Letters* 109.16 (2012), pp. 1–5. ISSN: 00319007. DOI: 10.1103/PhysRevLett.109.160602.

[105] S. Chandrasekhar. "Stochastic problems in physics and astronomy". In: *Reviews of Modern Physics* 15.1 (1943), pp. 1–89. ISSN: 00346861. DOI: 10.1103/RevModPhys.15.1.

[106] Tomer Markovich, Elsen Tjhung, and Michael E. Cates. "Chiral active matter: microscopic 'torque dipoles' have more than one hydrodynamic description". In: *New Journal of Physics* 21 (2019), p. 112001. eprint: 1908.00079. URL: http://arxiv.org/abs/1908.00079.

[107] Sriram Ganeshan and Alexander G Abanov. "Odd viscosity in two-dimensional incompressible fluids". In: *Physical review fluids* 2.9 (2017), p. 094101.